RAY TRACING AT VERY LOW FREQUENCIES WHEN THE EFFECTS OF HEAVY IONS ARE CONSIDERED.

A Thesis submitted for the Degree
of Master of Science of Rhodes University

by

P. D. TERRY.

September 1968.

Except where it is clear from the text that I am describing the work of others, or where it is obvious that I am making a survey of existing knowledge on the subject of the present study, the work described in this thesis is my own.

P. D. Terry

4/9/1968

C O N T E N T S.

PART 2.

MATHEMATICAL METHODS AND MODELS

PART 3.

RESULTS OF COMPUTATIONS

Acknowledgements.

Completion of projects of this nature is always accompanied by a deep feeling of gratitude towards those who, consciously or otherwise, have provided stimuli and help, without which the task could never have been accomplished.

In this case there has been no exception to the above sentiment. In particular I must express my deep thanks to my Research Director, Dr. A.D.M. Walker, who provided not only the original ideas, but also more than enough subsequent help and encouragement.

I must also thank the Directors of the Rhodes University Computing Centre, Professor R.N. Braae and Professor J.A. Gledhill for permission to use the university's digital computer. I am not altogether sure that my thanks are not also due to the large body of workers at Rhodes who have not discovered the potential of the machine, and who by their absence have provided practically unlimited access to the "great brain". In which connection also I must single out Mr. M.A. Lawrie, who has given frequently and freely of his time to helping me master the arts of programming languages and computing efficiency.

/I....

I have also to thank the University for the award of a Research Scholarship throughout the project; and the C.S.I.R. for a research grant during the first part of the work. Last, but by no means least, I must thank Mrs. van der Vyver for her sterling work in successfully typing as Physics that must have appeared deceptively like Greek.

ERRATA

p 35: The first line of the last paragraph should read "At oblique incidence, for the isotropic case, taking ....."

p 123; lines 3 to 5: Delete "which is outside ..... guiding. (STOREY (5))."

p 137: After the last sentence in 9.1 insert "The magnetic field is ignored in this chapter. Nevertheless, since the calculations are only order of magnitude calculations, the results obtained give an idea of the validity of the ray tracing approximations."

Introduction

The behaviour of very low frequency (V.L.F.) radio waves propagating in an ionized medium, such as the ionosphere and exosphere, may exhibit markedly different characteristics from those of frequencies such as are used for communication in the short-wave bands. The anisotropy introduced into the medium by the presence of the earth's magnetic field has a significant effect, while at frequencies below about 5KHz the presence of heavy positive ions may further affect propagation. In particular it is found that, under suitable conditions, V.L.F. signals may propagate along paths closely following the lines of force of the earth's magnetic field. The study of such signals has a practical interest in that, from consideration of their propagation times and dispersion properties, they can provide an inexpensive method of determining electron densities at levels well beyond the range of satellite investigation. For this reason, if for no other, theoretical investigation of the paths traced in a model exosphere may indicate how closely the model exosphere approximates the true one.

A powerful method of tracing out these paths is by the use of "ray-tracing", provided the

/properties...

properties of the medium very slowly in space, a condition not always fulfilled in practice. It has been the subject of this thesis to carry out ray-tracing studies, in particular noting the effects of the positive ions in the exosphere; effects which have not received much notice before, as they were thought to be unimportant.

Part I deals with the theoretical background to the concept of ray-tracing; with the development of the equations whose solution gives the path of the ray; and with the conditions which must be fulfilled if the analysis is to be valid.

Part 2 describes the methods used to perform the numerical computations, and outlines the models of the exosphere used in this case.

Part 3 describes the results of these computations, and examines the validity of the ray-tracing techniques as applied to the ionosphere, a test which previous workers do not seem to have performed.

It should be pointed out at the outset that the use of ray-tracing techniques such as we are about to describe is not original. However the effects of heavy ions have not usually been considered; the notable exception being in the study of the so-called "Subprotonospheric Whistler" by KIMURA[1],

/confined...

confined to regions both of the electromagnetic spectrum and of the ionosphere where it is felt that ray-tracing may not always be justifiable.

PART I.

THE THEORETICAL BACKGROUND

Chapter I.

The Physical Characteristics of V.L.F. Propagation through the Exosphere.

Since the early decades of this century, several interesting phenomena have been encountered by ionospheric researchers working with frequencies centred in the a.f. end of the radio spectrum, known as the v.l.f. (very low frequency) region. The most widely investigated of these phenomena, and historically the first to arouse interest, are the signals known as "whistlers". BARKHAUSEN[2] is generally credited as being the first to pay any scientific attention to peculiar whistling noises sometimes heard on telephone lines at the Front in the Great War. Investigations were carried further by ECKERSLEY[3]; by BURTON and BOARDMAN[4], who first put the signals onto magnetic tape; and were first carried out on a comprehensive scale by STOREY[5] in 1953.

Whistlers are now known to have their origin in atmospheric lightening flashes. The white noise electromagnetic energy generated by these "sferics" may penetrate the lower ionosphere, and then be guided accurately along the lines of force of the earth's field until it reaches the opposite

/hemisphere;....

hemisphere; where some of it may penetrate the ionosphere and reach the earth, while some may be reflected back along the field lines; this may occur several times, resulting in a train of echoes being received in each hemisphere. There is found to be an upper limit to the frequency which may be guided in this way, of the order of a few kiloherz, so that if the signals are detected they generally fall within the a.f. range.

The fact that the propagation takes place along the field lines was first concluded by STOREY(5), although electron density measurements of the day did not make the idea generally acceptable. His theory showed that guiding took place, due mainly to the anisotropy in the exosphere caused by the magnetic field. Experimental observations at conjugate points, involving the simultaneous recording of signals in both hemispheres at opposite ends of a field line, and subsequent identification in some cases of the causative sferics, have borne out that the propagation is very accurately along the lines of force.

As a result of the highly dispersive properties of the exosphere, the spectral distribution at the receiver is such that, aurally, whistlers sound like

/a...

a whistle, the frequency of which drops by a few kiloherz in the space of one or two seconds. The actual frequency-time spectrum of whistlers follows the form of Figure I, which shows an example of a "nose" whistler, which has both rising and falling components. All whistlers are, in fact, of this kind, but in practice the "nose" frequency is often above the upper cut-off frequency of the equipment used for detection. The detected spectrum then appears as in Figure 2, when it is found to be fairly well described by the relation

$$T = Df^{\frac{1}{2}} \qquad 1.1$$

where D is known as the Eckersley dispersion constant.

Besides whistlers, other forms of natural v.l.f. noise are detectable. These have intensities comparable with those of whistlers, and often exhibit spectral distributions closely related to those of whistlers, indicating that they have probably followed the same or similar paths. These "V.L.F. emissions" are thought to originate in the interaction of small clouds of plasma with the geophysical environment, producing radiation by such mechanisms as cyclotron radiation. A few of the more common spectral distributions are depicted in Figure 3.

/There...

Figure 1. Typical whistler spectrogram.

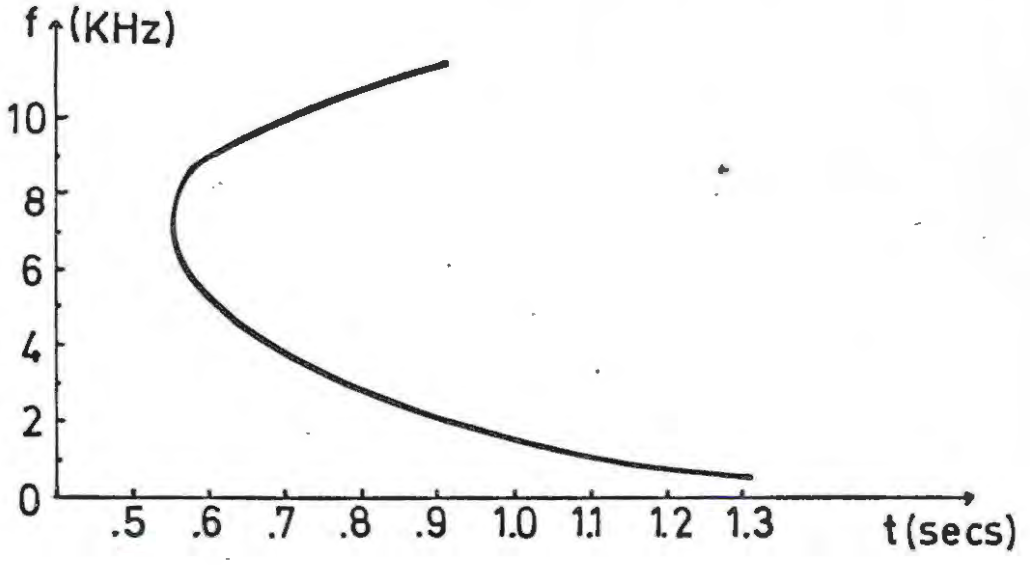

Figure 2. Whistler as usually detected.

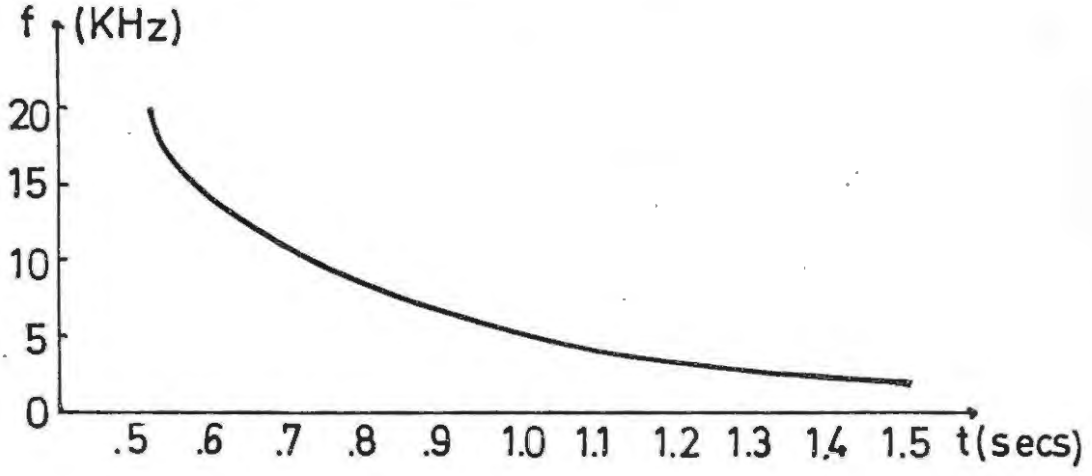

These diagrams are not accurately to scale.

Figure 3. Typical spectrograms of V.L.F. Emissions.

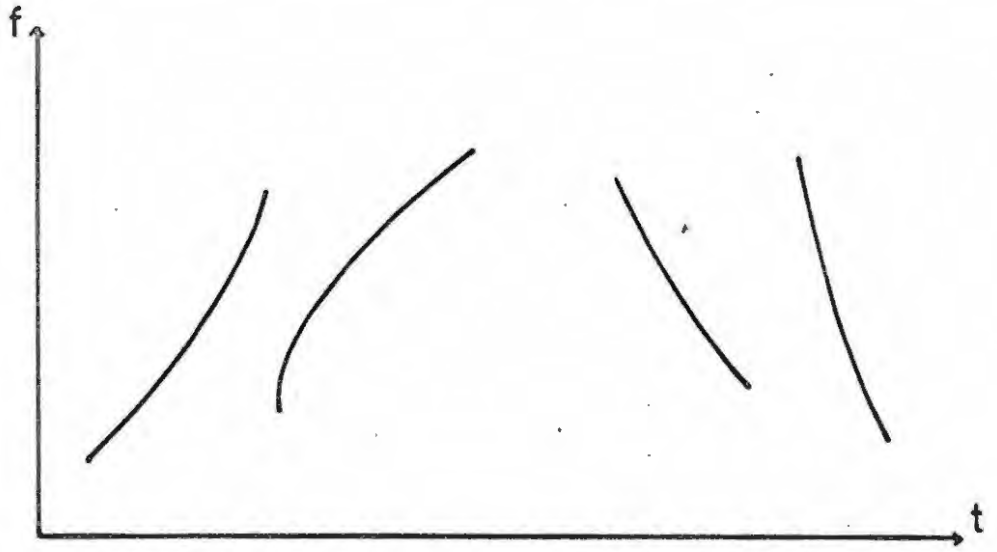

Risers. Falling tones.

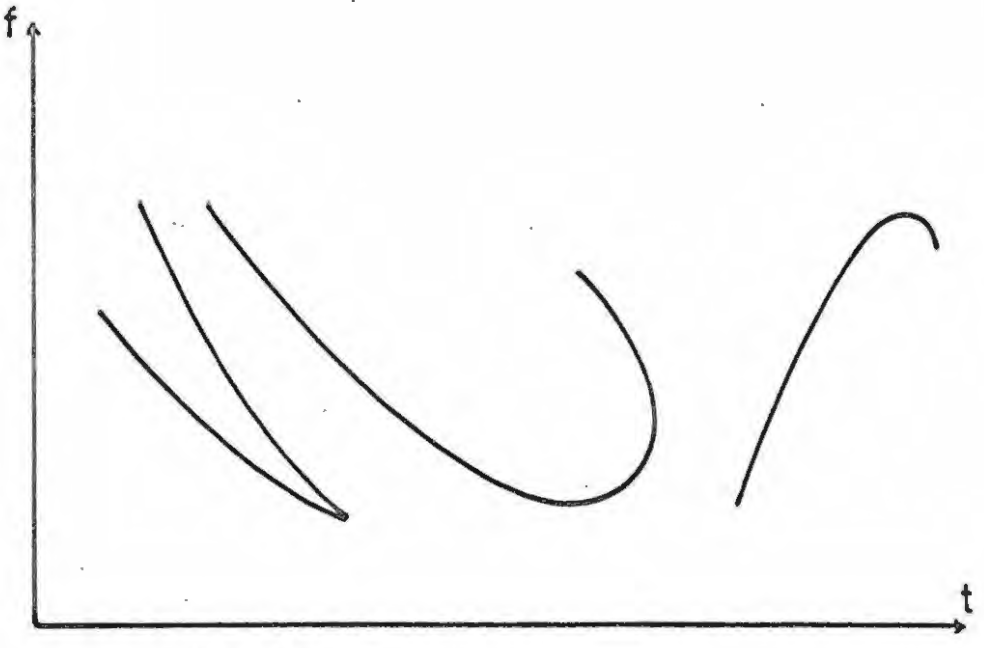

Hooks.

There are, in addition, several transmitters which operate in the V.L.F. region for scientific or military purposes. Besides reception of the more usual ground waves, observations of signals which have travelled in the "whistler mode" are possible at the transmitter's conjugate point. An example of this close to hand is provided by the C.N.R.S. project under GARNIER, in which the author has played a lowly part as a technical assistant. In this project whistlers, and transmissions from the 16.8 KHz FUB transmitter at Sainte-Assise are recorded on tape in Grahamstown, and "gyro echoes" (signals which have followed exospheric paths) have been identified.

Chapter 2.

Magneto-ionic theory; the propagation of radio waves through an ionized medium.

2.1 Introduction

The propagation of a radio wave through an ionized medium differs from the propagation through free space, because the electric and magnetic fields in the wave affect the motion of the ions and electrons, resulting in a continuous interchange of energy between the wave and the particles, and consequent changes in the speed and polarization of the wave. The problem is further complicated in the ionosphere by the presence of the terrestrial magnetic field, and by the mutual interactions of the particles in the plasma, which dissipate energy from the wave. It is found that, in the most general case, four "characteristic" waves can propagate in such a medium, two "upgoing" and two "downgoing". Nor may these always propagate independently - continual coupling and reflection processes are found everywhere as a result of the gradients of plasma density encountered.

Magneto-ionic theory, first put forward by APPLETON[6] and HARTREE[7] in the late 1920's, deals

/with...

with radio propagation through a homogeneous neutral plasma in the presence of a uniform magnetic field. Strictly speaking, this is insufficient to explain propagation in the terrestrial ionosphere, where the plasma density and magnetic field are both functions of space and time, but it is possible to apply the theory to fair accuracy by treating the ionosphere as a medium varying so slowly that it may be regarded as homogeneous at each level. A satisfactory treatment of the subject entails a so-called "full wave theory" which is more complex.

In the rest of this chapter we shall summarize the aspects of magneto-ionic theory which are needed for the development of ray-tracing.

2.2. Maxwell's Equations, Constitutive relations, Symbols and Units.

We shall employ rationalized m.k.s. units throughout. An electromagnetic field in a plasma may be described in terms of the vectors $\overline{E},\overline{B},\overline{D},\overline{H},\overline{J},\overline{P}$, subject to Maxwell's Equations

$$\text{Curl } \overline{E} = -\frac{\partial \overline{B}}{\partial T} \qquad 2.1$$

$$\text{Curl } \overline{H} = \frac{\partial \overline{D}}{\partial T} + \overline{J} \qquad 2.2$$

and the relations

$$\overline{B} = \mu \overline{H} \qquad 2.3$$

$$\overline{D} = \epsilon_o \overline{E} + \overline{P} \qquad 2.4$$

It is convenient for our purposes to extend the definition of $\bar{P}$ so that $\frac{\partial \bar{P}}{\partial t}$ includes the effect of the conduction current $\bar{J}$, and to work in terms of a variable defined by

$$\bar{\mathcal{H}} = \sqrt{\frac{\mu_o}{\epsilon_o}}\,\bar{H} \qquad 2.5$$

which is seen to have the same units as $\bar{E}$. Since the magnetic permeability of the ionosphere is taken to be unity, so that $\mu = \mu_o$, it is now possible to rewrite Maxwell's Equations:

$$\text{Curl } \bar{E} = -\frac{1}{c}\frac{\partial \bar{\mathcal{H}}}{\partial t} \qquad 2.6$$

$$\text{Curl } \bar{\mathcal{H}} = \frac{1}{c}\frac{\partial}{\partial t}\left\{\bar{E} + \frac{\bar{P}}{\epsilon_o}\right\} \qquad 2.7$$

where $c = \frac{1}{\sqrt{\mu_o \epsilon_o}}$ = velocity of electromagnetic radiation in free space.

The polarization $\bar{P}$ arises almost entirely from the motion of the free particles under the influence of the electric field in the wave - the effect due to the magnetic field in the wave is of second order through the $\bar{v} \times \bar{B}$ term - so it is possible to relate $\bar{P}$ to $\bar{E}$ by what is known as the "constitutive relation" of the plasma:

$$\frac{\bar{P}}{\epsilon_o} = \underset{\sim}{\mathcal{M}}\,\bar{E} \qquad 2.8$$

where $\underset{\sim}{\mathcal{M}}$ is a 3 x 3 matrix known as the susceptibility matrix, which has non-zero off-diagonal terms in an anisotropic medium. The exact form of $\mathcal{M}$ depends on

/what....

what co-ordinate system we adopt, and on what ions and electrons are present. In a plasma where only the electrons are deemed important, with a Cartesian frame in which the static magnetic field $\bar{B}$ has direction cosines L,M,N it can be shown (cf. BUDDEN[8]) that

$$\underset{\sim}{Y} = -\frac{X}{U(U^2-Y^2)}\begin{Bmatrix} U^2-L^2Y^2 & -jNYU-LMY^2 & jMYU-LNY^2 \\ jNYU-LMY^2 & U^2-M^2Y^2 & -jLYU-MNY^2 \\ -jMYU-LNY^2 & jLYU-MNY^2 & U^2-N^2Y^2 \end{Bmatrix} \qquad 2.9$$

where

$$X = \frac{f_n^2}{f^2}\ ,\quad Y = \frac{f_H}{f}\ ,\quad U = 1-jZ,\quad Z = \frac{\nu}{f}\ ,\quad j = \sqrt{-1}$$

and f_n = plasma frequency $= \sqrt{\dfrac{Ne^2}{4\Pi^2\epsilon_o m}}$

f_H = electron gyrofrequency $= eB/m$

f = wave frequency

ν = collision frequency

N = electron density, m = mass of electron,

e = electronic charge.

Maxwell's Equations now become

$$\text{Curl}\ \bar{E} = -\frac{1}{c}\frac{\partial \bar{\mathcal{H}}}{\partial t} \qquad 2.10$$

$$\text{Curl}\ \bar{\mathcal{H}} = \frac{1}{c}\{\underset{\sim}{I} + \underset{\sim}{M}\}\frac{\partial \bar{E}}{\partial t} \qquad 2.11$$

where $\underset{\sim}{I}$ is the identity matrix. Taking the curl of Equation 2.10 and substituting from 2.11 we get:

$$\nabla^2\bar{E} - \text{grad div}\ \bar{E} + \frac{1}{c^2}\{\underset{\sim}{I} + \underset{\sim}{M}\}\frac{\partial^2 \bar{E}}{\partial t^2} = \bar{0} \qquad 2.12$$

and similarly:

$$\nabla^2\bar{\mathcal{H}} - \text{grad div}\bar{\mathcal{H}} + \frac{1}{c^2}\{\underset{\sim}{I} + \underset{\sim}{M}\}\frac{\partial^2\bar{\mathcal{H}}}{\partial t^2} = \bar{0} \qquad 2.13$$

2.3. The Refractive Index, Refractive Index Surface, and the Ray.

Equations 2.12 and 2.13 are seen to be in the form of scalar wave equations, with solutions of the form

$$\bar{\Lambda} = \bar{\Lambda}_o\, e^{j(\omega t - \bar{\gamma}\cdot\bar{r})} \qquad 2.14$$

where $\bar{\Lambda} = \bar{E}$ or $\bar{\mathcal{H}}$ and where $\bar{\gamma}$ is a (generally complex) vector in the direction of the wave normal (i.e. normal to the surfaces of constant phase). We may write $\bar{\gamma} = kn\hat{\gamma}$ where $\hat{\gamma}$ is a unit vector in the direction of $\bar{\gamma}$, $k = \frac{\omega}{c}$, and $n = \mu - j\chi$ is the complex refractive index; when it is shown in elementary texts on wave motion that $\mu = \frac{c}{v_p}$ is the phase refractive index of the medium, v_p being the phase velocity. It is convenient for our purposes to define

$$\bar{\rho} = \mu\hat{\gamma} \qquad 2.15$$

as a "refractive index vector", the direction of which gives the direction of the wave normal, while the magnitude gives the phase refractive index.

Equations 2.12 and 2.13 may now be regarded as eigenvector equations for $\bar{E}$ and $\bar{\mathcal{H}}$. From the determinantal condition for non-trivial solutions it is possible to arrive at a quadratic equation in n^2;

/which...

which in the most general case of a multi-component plasma can be written (see STIX[9]).

$$An^4 + Bn^2 + C = 0 \qquad 2.16$$

where $A = S \sin^2\Psi + P \cos^2\Psi$

$$B = -\{RL \sin^2\Psi + PS(1 + \cos^2\Psi)\}$$

$$C = PRL \qquad 2.17$$

and $$R = 1 - \sum_j \frac{X_j}{U_j + \epsilon_j Y_j}$$

$$L = 1 - \sum_j \frac{X_j}{U_j - \epsilon_j Y_j}$$

$$P = 1 - \sum_j \frac{X_j}{U_j}$$

$$S = \tfrac{1}{2}\{R + L\} = 1 - \sum_j \frac{X_j U_j}{U_j^2 - Y_j^2}$$

$$D = \tfrac{1}{2}\{R + L\} = \sum_j \frac{\epsilon_j X_j Y_j}{U_j^2 - Y_j^2} \qquad 2.18$$

where Ψ = angle between wave normal and magnetic field. X_j Y_j and U_j have similar meanings for the jth species of ion as did X,Y and U for electrons in the previous section. $\epsilon_j = +1$ for positive ions, and -1 for negative ions.

If equation 2.16 is solved for n^2 for the case of electrons only, and the answer suitably manipulated, we arrive at the well-known Appleton-Hartree formula

$$n^2 = 1 - \frac{X}{U - \frac{Y^2 \sin^2\Psi}{2(U-X)} \pm \sqrt{\frac{Y^4 \sin^4\Psi}{4(U-X)^2} + Y^2 \cos^2\Psi}} \qquad 2.19$$

/n is...

n is in general a complex quantity, from the real part (μ) of which we can deduce the phase velocity, and from the imaginary part (χ) the attenuation.

Since the refractive index at a point in space depends only on the properties of the medium at that point, and on Ψ, a convenient pictorial representation of the behaviour of μ on Ψ may be obtained by drawing a set of surfaces in a system of polar co-ordinates (r,Ψ,Φ) with polar axis along $\overline{B}$, so that the surface is the locus of the vector $\overline{\rho}$ as defined in equation 2.15 (The locus being essentially a function of Ψ). Since for a given X and Y there are in general two values of n^2, there will be two such surfaces at each point in space. In Figure 4 we depict one such surface, showing the refractive index vector $\overline{\rho}$ in relation to the surface and to the co-ordinate axes.

In this Figure will also be seen a direction marked "ray". The directions of propagation of energy in a wave ("ray direction") and of the wave-normal are in general different, because the refractive index depends on the direction of the wave-normal. A "real" wave can be considered as synthesized of many plane waves propagating in all

/directions.

Figure 4. The refractive index surface and the ray.

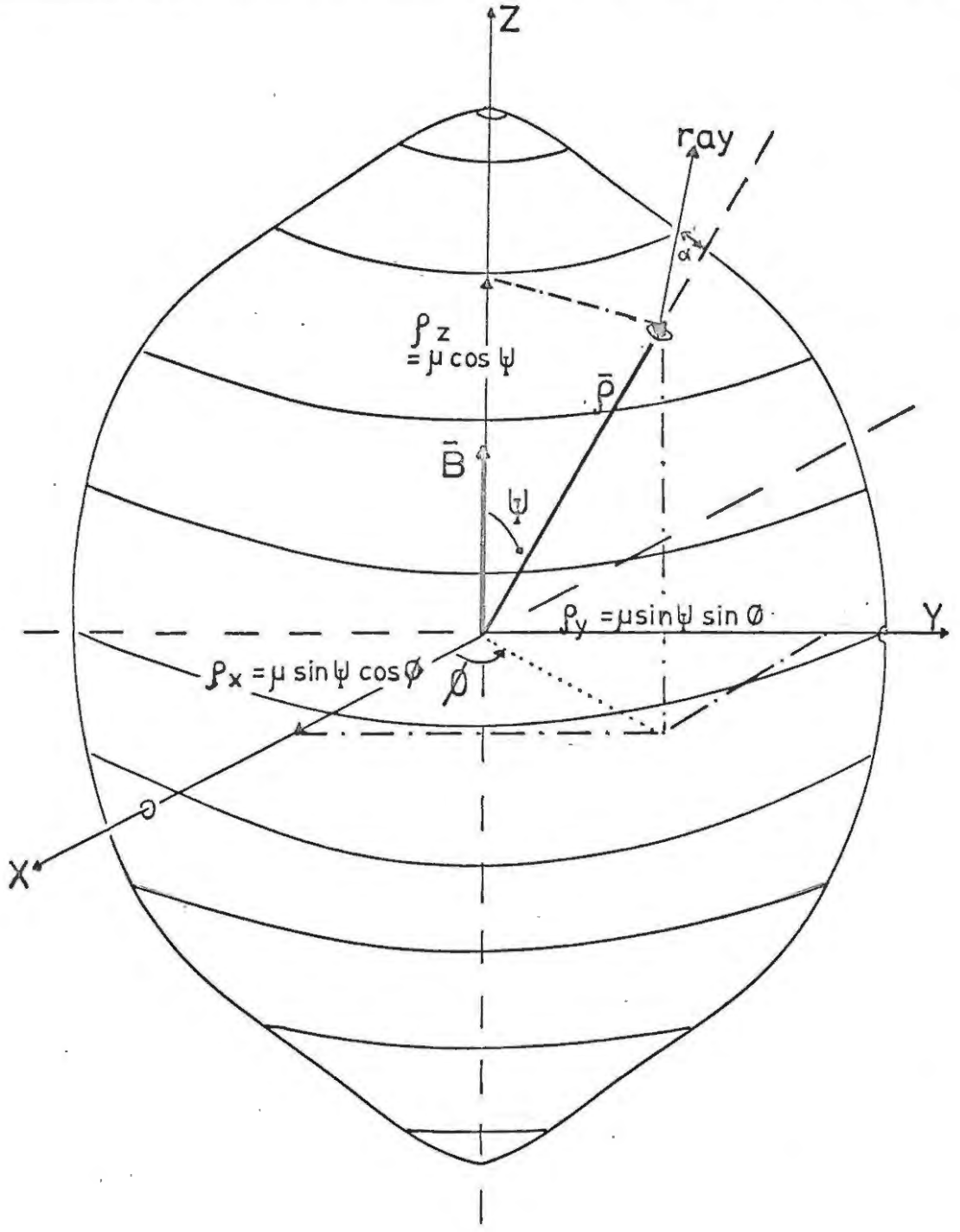

directions. Along most directions destructive interference of the component waves occurs, but along the path of energy transfer - the "ray path" - the interference must be constructive. Now a given frequency component plane wave behaves as $A\, e^{jk\{ct-\bar{\rho}\cdot\bar{r}\}}$, which in our refractive index space r,Ψ, Φ may be written

$$A\, e^{jk(ct-\mu(\Psi)\{(x\cos\Phi+y\sin\Phi)\sin\Psi+z\cos\Psi\}}$$

The complete wave is then given by a Fourier integral

$$\iiint A(k,\Psi,\Phi)\, e^{jk(ct-\mu\{(x\cos\Phi+y\sin\Phi)\sin\Psi+z\cos\Psi\}} dk\,d\Psi\,d\Phi \qquad 2.20$$

where we have written $A = A(k,\Psi,\Phi)$ to emphasize that A is a function peaked at the frequency and in the direction in which we are interested. The condition for constructive interference is that the rate of change of the exponent must be zero with respect to Φ and Ψ. Partial differentiation and equating to zero gives

$$y\cos\Phi_o = x\sin\Phi_o \qquad 2.21$$

$$\{z\cos\Psi_o+(x\cos\Phi_o+y\sin\Phi_o)\sin\Psi_o\}\left(\frac{\partial\mu}{\partial\Psi}\right)_o$$

$$+\mu_o\left((x\cos\Phi_o+y\sin\Phi_o)\cos\Psi_o-z\sin\Psi_o\right) = 0 \qquad 2.22$$

Equation 2.21 shows that $\tan\Phi_o = \frac{y}{x}$, so that the wave packet remains in the plane $\Phi = \Phi_o$ with ray, wave normal and $\bar{B}$ coplanar. Choosing $\Phi_o = 0$ and letting the ray make an angle α with the wave normal,

/and, ...

Figure 5. The ray is normal to the refractive index surface.

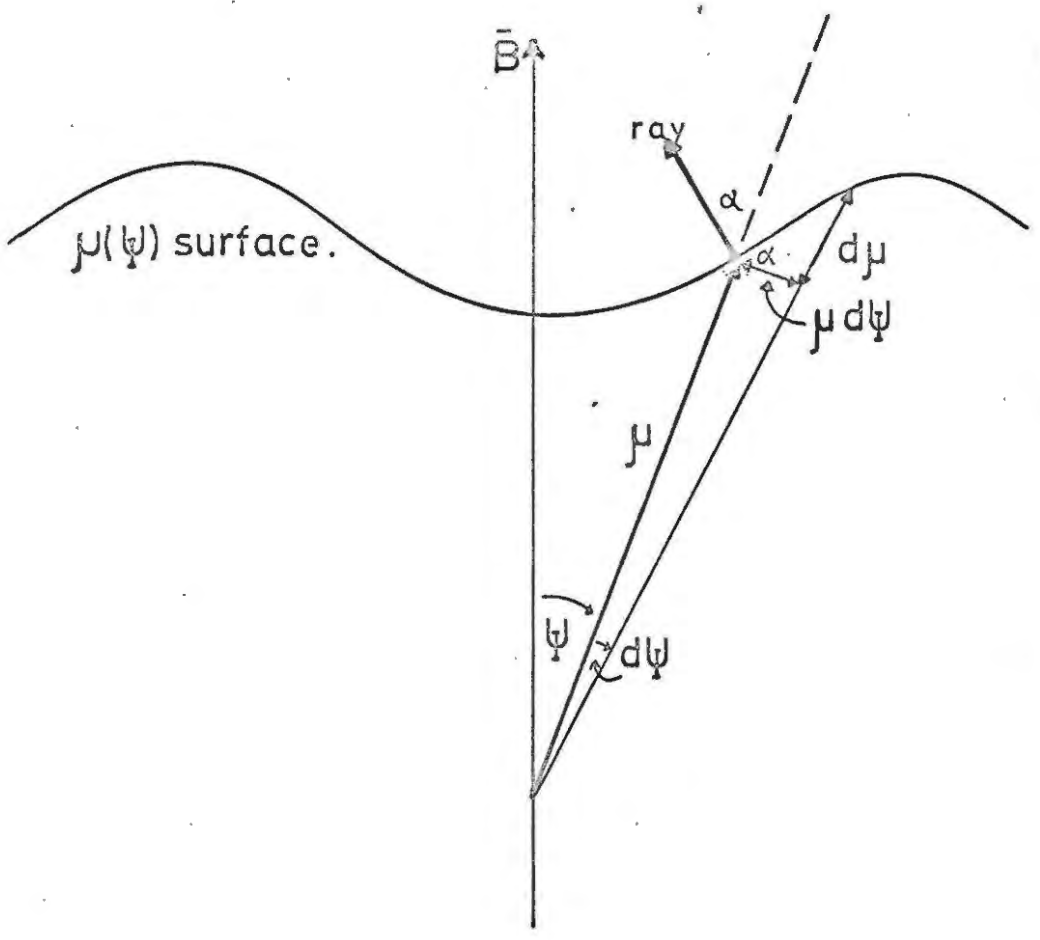

and $\Psi_o - \alpha$ with the z or $\bar{B}$ axis it is possible to manipulate equation 2.22 to yield

$$\tan \alpha = \left\{ \frac{1}{\mu} \cdot \frac{\partial \mu}{\partial \Psi} \right\}_{\Psi = \Psi_o} \qquad 2.23$$

Comparison with Figure 5 shows that the ray is thus normal to the refractive index surface. This important fact will be made use of in the derivation of equations governing the path of a ray.

2.4 Oblique Propagation - the Booker Quartic

When working within a homogeneous medium we have seen that propagation of electromagnetic waves may be efficiently described in terms of a refractive index n which depends on the X_j, Y_j and U_j and on the angle Ψ. In such a medium it is often convenient to take one of the co-ordinate axes aligned with $\bar{B}$ or $\bar{\rho}$ and to align one co-ordinate plane to contain them both (since we have seen that they are always coplanar). This reduction to a two dimensional problem may not always be possible when we extend our treatment to inhomogeneous media and to propagation across boundaries; and it is useful to develop formulae in terms of arbitrary orientations of $\bar{\rho}$ and $\bar{Y}$ with the co-ordinate axes. We may however still confine $\bar{\rho}$ to one plane, say the xz plane without loss of generality.

/Now...

Now suppose we let

$$S = n \sin \chi \qquad 2.24$$

$$q = n \cos \chi \qquad 2.25$$

where χ is the angle between ρ and the z axis. Clearly if we can determine q and S we can determine n and χ. From Figure 6 we see that for our choice of axes $\rho_x = S$ and $\rho_z = q$, so that the solutions of Maxwell's equations of the form

$$\bar{A} = \bar{A}_o \, e^{-jk\bar{\rho}.\bar{r}} \qquad 2.26$$

may be written in the form

$$\bar{A} = \bar{A}_o \, e^{-jk(Sx+qz)} \qquad 2.27$$

where $\bar{A}$ refers to either $\bar{E}\, e^{j\omega t}$ or to $\bar{\mathcal{H}}\, e^{j\omega t}$ With this notation we may let $\frac{\partial}{\partial x} = -jkS$ and $\frac{\partial}{\partial z} = -jkq$, when on writing out Maxwell's equations component by component, and obtaining expressions for Ex Ey $\mathcal{H}_x$ and $\mathcal{H}_y$ in terms of one another it is easily shown that

$$q \begin{Bmatrix} Ex \\ -Ey \\ \mathcal{H}x \\ \mathcal{H}y \end{Bmatrix} = \underset{\sim}{T} \begin{Bmatrix} Ex \\ -Ey \\ \mathcal{H}x \\ \mathcal{H}y \end{Bmatrix} \qquad 2.28$$

where $\underset{\sim}{T}$ is a 4x4 matrix given by

$$\underset{\sim}{T} = \begin{Bmatrix} \frac{-SM_{zx}}{1+M_{zz}} & \frac{SM_{zy}}{1+M_{zz}} & 0 & \frac{C^2+M_{zz}}{1+M_{zz}} \\ 0 & 0 & 1 & 0 \\ \frac{M_{yz}M_{zx}}{1+M_{zz}} - M_{yz} & C^2+M_{yy} - \frac{M_{yz}M_{zy}}{1+M_{zz}} & 0 & \frac{SM_{yz}}{1+M_{zz}} \\ 1+M_{xx} - \frac{M_{xz}M_{zx}}{1+M_{zz}} & \frac{M_{xz}M_{zy}}{1+M_{zz}} - M_{xy} & 0 & \frac{-SM_{xz}}{1+M_{zz}} \end{Bmatrix} \qquad 2.29$$

Figure 6. The variables S and q

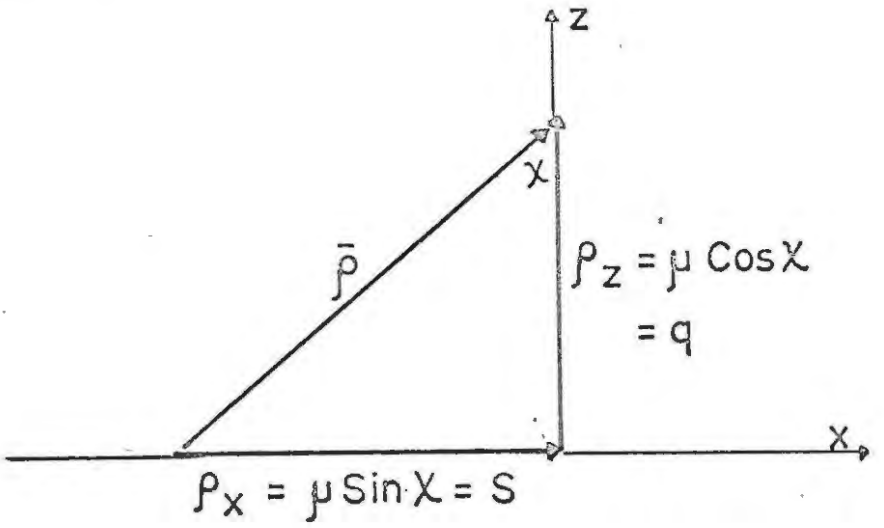

Figure 7 Transition to a continuous medium - Propagation across a sharp boundary between two homogeneous layers.

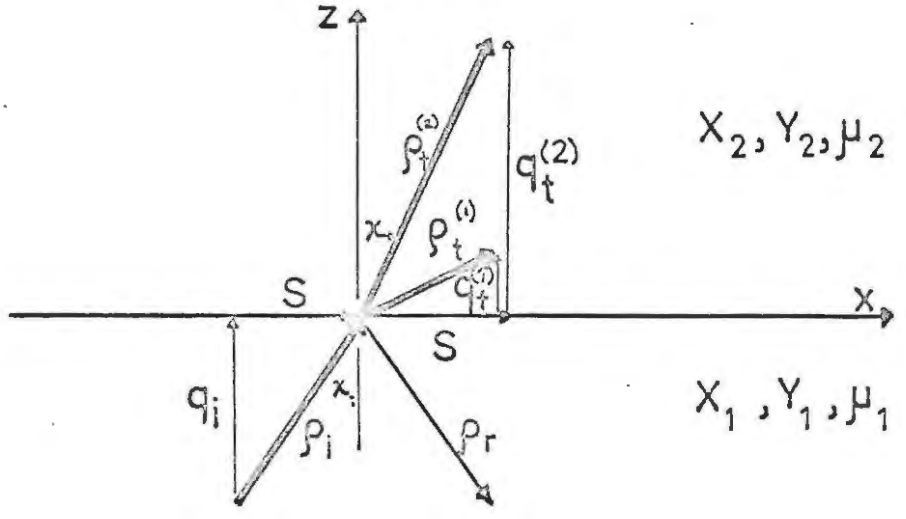

and the Mij are the elements of the susceptibility matrix for the given co-ordinate system.

Clearly for a non trivial solution of the eigen-vector problem implied in equation 2.28 we must have

$$\det \left| \underline{\underline{T}} - \underline{\underline{I}} q \right| = 0 \qquad 2.30$$

which gives a quartic equation in q with four roots, each corresponding to one of the four characteristic waves (two upgoing and two downgoing) which can propagate in the medium. This quartic equation is the "Booker Quartic", first derived by BOOKER[10], and since then extensively applied to propagation in the ionosphere. Writing this equation

$$\alpha q^4 + \beta q^3 + \gamma q^2 + \delta q + \epsilon = 0 \qquad 2.31$$

we can show for the coefficients in an electrons-only plasma:

$$\begin{aligned}
\alpha &= U(U^2-v^2) + X(N^2Y^2-U^2) \\
\beta &= 2LNSXY^2 \\
\gamma &= -2U(U-X)(C^2U-X) + 2Y^2(C^2U-X) + XY^2(1-C^2N^2+L^2S^2) \\
\delta &= -2LNSXY^2C^2 \\
\epsilon &= (U-X)(C^2U-X)^2 - C^2Y^2(C^2U-X) - L^2S^2C^2Y^2X
\end{aligned} \qquad 2.32$$

The advantages to be gained by the above formulation of the theory for homogeneous media are two-fold; firstly we obtain generality in terms of choice of co-ordinate axes, and secondly, if we take the x-y plane to be the one in which boundaries between

/media....

media lie, then the quantities Ex, Ey, $\mathcal{K}x$ and $\mathcal{K}y$ will be continuous across these boundaries. When dealing with boundary problems, as we shall have to do when extending our treatment to inhomogeneous media, it is necessary to distinguish between normal and oblique incidence, but within a homogeneous region there is no such distinction.

2.5 The transition to an inhomogeneous medium - W.K.B.J. Solutions.

The ionosphere - the inhomogeneous medium we work with - may be thought of as a fairly slowly varying horizontally stratified medium for most applications. It is thus convenient to take the z axis vertically, so that the plasma density, collision frequency, and to a first approximation the magnetic field and the refractive index are functions of z only.

The transition to a continuously varying medium can be thought of as the limiting process for transition across many boundaries between thin slabs of homogeneous plasma, in each of which four characteristic waves can propagate. With reference to Figure 7 we see that a wave incident on a sharp boundary gives rise to two transmitted upgoing waves and to one reflected wave. These processes are caused essentially by the change in refractive index across

/the....

the boundary. When the change is not abrupt, but gradual, it is found that reflection processes are continuous; at each level reflection, and coupling between the characteristic waves can occur. It is not, therefore, strictly correct to talk about a progressive wave, for which the refractive index n must be constant, but nevertheless progressive energy propagation can and does occur. As was stated previously, study of this really requires a "full wave" theory, but approximate results can be gleaned from an extension of the progressive wave theory.

The total field of a wave must satisfy Maxwell's Equations, which we have seen can be manipulated to yield

$$\nabla^2\overline{E} - \text{grad div } \overline{E} + k^2n^2\overline{E} = \overline{0} \qquad 2.33$$

Taking first the case of a wave at normal incidence, so that E = E(z) only, this reduces to

$$\frac{d^2E_y}{dz^2} + k^2n^2E_y = 0 \qquad 2.34$$

with similar expressions for the other components of $\overline{E}$ and $\overline{\mathcal{H}}$ This appears to be a simple wave equation with the solution

$$\overline{E} = \overline{E}_o\, e^{-jknz} \qquad 2.35$$

but since n = n(z) this does not apply, and there is

/in...

in fact no solution of equation 2.34 which represents a progressive wave, which must have n = constant. Nevertheless it is possible to derive approximate solutions to equation 2.34 of the form

$$E = A_{(z)}\ e^{j\Phi(z)} \qquad 2.36$$

where $A_{(z)}$ is a very slowly varying amplitude function. These are known as W.K.B.J. solutions,* and for a wave at normal incidence take the form:

$$E_y = E_0 n^{-\frac{1}{2}}\ e^{+jk\int ndz} \qquad 2.37$$

$$H_x = H_0 n^{\frac{1}{2}}\ e^{+jk\int ndz} \qquad 2.38$$

provided that the condition

$$\frac{1}{k^2}\left|\ \frac{3}{4}\left(\frac{1}{n^2}\frac{dn}{dz}\right)^2 - \frac{1}{2n^3}\frac{d^2n}{dz^2}\ \right| << 1 \qquad 2.39$$

is fulfilled, which is a quantitative definition of the term "slowly varying".

At oblique incidence, taking the plane of incidence to be the xz plane the problem is a little more complex, as n = n (x,z). In this case it is convenient to introduce the parameters S and q of the previous section. At each level Snell's laws must hold, so that

$$S = n \sin\theta = \text{constant} \qquad 2.40$$

and we are dealing with waves varying with x and z so that $\frac{\partial}{\partial x} = -jkSx$. In this case equation 2.33 /becomes..

* The initials standing for Wentzel, Kramers, Brillouin and Jeffreys.

becomes, for horizontal polarization

$$\frac{d^2E_y}{dz^2} - k^2S^2E_y + k^2n^2E_y = 0 \qquad 2.41$$

or

$$\frac{d^2E_y}{dz^2} + k^2q^2E_y = 0 \qquad 2.42$$

which is seen to be of the same form as equation 2.34 with q fulfilling the same purpose for oblique incidence as did n for vertical incidence. The W.K.B.J. solution is then

$$E_y = Aq^{-\frac{1}{2}} e^{\mp jk\int q\,dz} \qquad 2.43$$

$$\mathcal{H}_x = Aq^{\frac{1}{2}} e^{\mp jk\int q\,dz} \qquad 2.44$$

provided that the condition

$$\frac{1}{k^2}\left|\frac{3}{4}\left(\frac{1}{q^2}\frac{dq}{dz}\right)^2 - \frac{1}{2}\frac{1}{q^3}\frac{d^2q}{dz^2}\right| << 1 \qquad 2.45$$

is fulfilled.

(Within the factor A in equations 2.43,44 is implied a factor $e^{j(\omega t - kSx)}$).

The above condition holds only for the horizontally polarised case ($E_x = 0$) For the other polarization ($E_y = 0$) it can be shown that the solutions reduce to

$$\mathcal{H}_y = Anq^{-\frac{1}{2}} e^{\mp jk\int q\,dz} \qquad 2.46$$

$$E_x = An^{-1}q^{\frac{1}{2}} e^{\mp jk\int q\,dz} \qquad 2.47$$

with the condition

$$\frac{1}{k^2}\left|\frac{3}{4}\left(\frac{1}{q^2}\frac{dq}{dz}\right)^2 - \frac{1}{2q^3}\frac{d^2q}{dz^2} + \frac{1}{q^2}\left\{\frac{1}{n}\frac{d^2n}{dz^2} - 2\left(\frac{1}{n}\frac{dn}{dz}\right)^2\right\}\right| << 1 \qquad 2.48$$

These conditions are seen to break down when $k_{\perp} 0$ (the v.l.f. limit) or when q and $n \rightarrow 0$; i.e. at levels where the reflection processes become increasingly important,.

Chapter 3.

The Haselgrove Equations governing the path of a ray.

3.1 Introduction.

In the last chapter we summarised some parts of magneto-ionic theory, and discussed under what conditions it could be extended to cover approximate propagation in an inhomogeneous medium. In particular we saw that the concept of a refractive index surface could be of great use, because the direction of energy propagation is given by the normal to the surface at the point of intersection of the wave normal. One way of tracing a ray would thus be to plot many refractive index surfaces and observe the behaviour of the normals to the surfaces. This is, in fact, the basis of a graphical method of ray tracing due to POEVERLEIN.[11]

Following BUDDEN,[12] we shall now develop the differential equations for a ray path in a general co-ordinate system, and then extend the treatment to give the equations to be used in our study.

3.2 Equations of the refractive index surfaces.

Consider the three-dimensional refractive index space mapped by co-ordinates ρ_u, ρ_v, ρ_w in an orthogonal system, and consider a wave front at u,v,w where

/the....

the u,v,w axes are parallel to the ρ_u, ρ_v, ρ_w axes. Recalling from chapter 2.3 how the refractive index surface is defined, we see that we may write the equation of this surface

$$G(u,v,w,\rho_u,\rho_v,\rho_w) = \frac{\sqrt{\rho_u^2+\rho_v^2+\rho_w^2}}{\mu(u,v,w,\rho_u,\rho_v,\rho_w)} = 1 \qquad 3.1$$

The ray direction and ray velocity $\bar{V}_r$ are normal to the refractive index surface, and are thus proportional to Grad G. Since u, v, w are the co-ordinates of the point where the wave-front intersects the ray, the components of $\bar{V}_r$ are $\dot{u},\dot{v},\dot{w}$ where the dot denotes $\frac{d}{dt}$.

The constant of proportionality between $\bar{V}_r$ and Grad G is c, as is easily seen by considering a wave with wave normal and ray parallel to the field. Thus

$$\bar{V}_r = C \text{ Grad } G \qquad 3.2$$

Defining a new variable s by

$$s = ct \qquad 3.3$$

we get

$$\frac{du}{ds} = \frac{1}{h_u}\frac{\partial G}{\partial \rho_u}$$

$$\frac{dv}{ds} = \frac{1}{h_v}\frac{\partial G}{\partial \rho_v} \qquad 3.3$$

$$\frac{dw}{ds} = \frac{1}{h_w}\frac{\partial G}{\partial \rho_w}$$

where h_u, h_v, h_w are the scale factors of the co-ordinate system.

/3.3....

3.3 The canonical equations for a ray.

In a homogeneous medium we know that one solution of Maxwell's equations may be written

$$\bar{E} = \bar{E}_o \, e^{-jk\bar{\rho}\bar{r}} \qquad 3.4$$

and that in undergoing transition to a slowly varying medium we may write a solution

$$\bar{E} = \bar{E}_o \, e^{-jk\int \rho d\bar{r}} \qquad 3.5$$

provided that the medium is slowly varying; so that the W.K.B.J. conditions must hold. Clearly then

$$\oint \bar{\rho} \cdot d\bar{r} = 0 \qquad 3.6$$

which, by Stoke's Theorem implies that

$$\text{Curl}\, \rho = \bar{0} \qquad 3.7$$

From the equation for the refractive index surface (3.1) we see that

$$\frac{dG}{du} = \frac{dG}{dv} = \frac{dG}{dw} = 0 \qquad 3.8$$

i.e.
$$\frac{\partial G}{\partial l} + \sum_k \frac{\partial G}{\partial \rho_k} \cdot \frac{\partial \rho_k}{\partial l} = 0 \qquad 3.9$$

for $l = u,v,w$ and $k = u,v,w$.

From equations 3.9 and 3.7 we may derive expressions for $\frac{\partial \rho u}{\partial s}$, $\frac{\partial \rho v}{\partial s}$, $\frac{\partial \rho w}{\partial s}$ which, together with equations 3.3, are known as the canonical equations for the ray.

3.4 The Canonical Equations in the Geophysical System

In the geophysical system of co-ordinates (r,Θ,Φ) we measure Θ up from the geomagnetic equator, and Φ

/west....

west of Greenwich. In this system $(h_r, h_\Theta, h\Phi) = (1, r, r\cos\Theta)$

Equations 3.3 yield

$$\frac{dr}{ds} = \frac{\partial G}{\partial \rho_r} = \frac{1}{\mu^2}\left\{\rho_r - \frac{\mu\partial\mu}{\partial\rho_r}\right\} \qquad 3.10$$

$$\frac{d\Theta}{ds} = \frac{1}{r}\frac{\partial G}{\partial \rho_\Theta} = \frac{1}{r\,\mu^2}\left\{\rho_\Theta - \frac{\mu\partial\mu}{\partial\rho_\Theta}\right\} \qquad 3.11$$

$$\frac{d\Phi}{ds} = \frac{1}{r\cos\Theta}\frac{\partial G}{\partial \rho_\Phi} = \frac{1}{r\mu^2\cos\Theta}\left\{\rho_\Phi - \mu\frac{\partial\mu}{\partial\rho_\Phi}\right\} \qquad 3.12$$

The relation Curl $\bar{\rho} = \bar{0}$ gives

$$\frac{\partial\rho_\Theta}{\partial\Phi} = \cos\Theta\frac{\partial\rho_\Phi}{\partial\Theta} - \rho_\Phi\sin\Theta \qquad 3.13$$

$$\frac{\partial\rho_r}{\partial\Phi} = r\cos\Theta\frac{\partial\rho_\Phi}{\partial r} + \rho_\Phi\cos\Theta \qquad 3.14$$

$$\frac{\partial\rho_r}{\partial\Theta} = r\frac{\partial\rho_\Theta}{\partial r} + \rho_\Theta \qquad 3.15$$

These, together with the three equations 3.9 give, after suitable manipulation:

$$\frac{d\rho_r}{ds} = \frac{1}{\mu}\frac{\partial\mu}{\partial r} + \rho_\Theta\frac{d\Theta}{ds} - \rho_\Phi\cos\Theta\frac{d\Phi}{ds} \qquad 3.16$$

$$\frac{d\rho_\Theta}{ds} = \frac{1}{r}\left\{\frac{1}{\mu}\frac{\partial\mu}{\partial\Theta} - \rho_\Theta\frac{dr}{ds} - r\rho_\Phi\sin\Theta\frac{d\Phi}{ds}\right\} \qquad 3.17$$

$$\frac{d\rho_\Phi}{ds} = \frac{1}{r\cos\Theta}\left\{\frac{1}{\mu}\frac{\partial\mu}{\partial\Phi} - \rho_\Phi\cos\Theta\frac{dr}{ds} + r\rho_\Phi\sin\Theta\frac{d\Theta}{ds}\right\} \qquad 3.18$$

The derivation of these equations is given in Appendix A.

The six equations 3.10, 3.11, 3.12, 3.16, 3.17, 3.18 when solved give the path of the ray in a geophysical system. The original derivation was

/performed...

performed by HASELGROVE[13] who presented the results in generalized co-ordinates, using as a starting point Fermat's Principle of stationary time, which states that the ray between two points follows a path such that the time of travel of a wave front is a maximum or minimum; or stated mathematically

$$\delta \int \frac{ds}{V_r} = 0 \qquad 3.19$$

It may be shown that the approach outlined above is equivalent to this more sophisticated one. (See BUDDEN[14].)

3.5 Degrees of freedom of the system.

Although we have arrived at six simultaneous differential equations in six unknowns, only five of these are needed to specify the direction of ρ. The sixth equation and the definition that $|\bar{\rho}| = \mu$ give one more degree of freedom than is necessary. However, this may be used to advantage in restraining the stability of the set of equations, as was pointed out by YABROFF[15].

3.6 The differential equations for a two-dimensional frame

In chapter 2.3 we saw that in a homogeneous medium the magnetic field, wave normal and ray

/direction...

Figure 8. Geometry of ray-tracing.

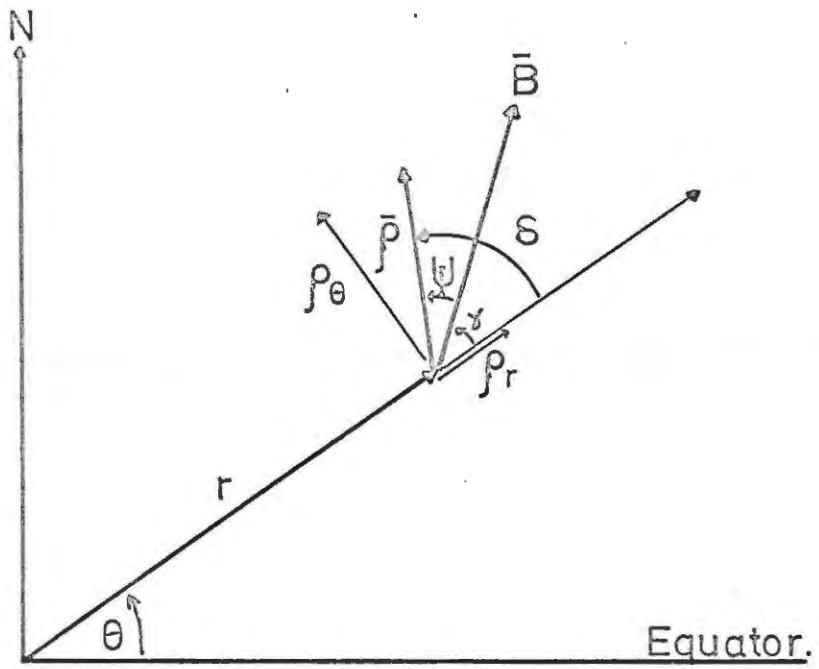

direction were all co-planer. Hence if we use a magnetic dipole model for the earth's field, as we shall do, the deviation out of the magnetic meridian will be small even in an inhomogeneous medium, and we may simplify the study by restricting ourselves to the two dimensional frame (r, Θ) in which the canonical equations reduce to

$$\begin{aligned}
\frac{dr}{ds} &= \frac{1}{\mu^2}\left(\rho_r - \mu \frac{\partial \mu}{\partial \rho_r}\right) \\
\frac{d\Theta}{ds} &= \frac{1}{r\mu^2}\left(\rho_\Theta - \mu \frac{\partial \mu}{\partial \rho_\Theta}\right) \\
\frac{d\rho_r}{ds} &= \frac{1}{\mu}\frac{\partial \mu}{\partial r} + \rho_\Theta \frac{d\Theta}{ds} \\
\frac{d\rho_\Theta}{ds} &= \frac{1}{r}\left(\frac{1}{\mu}\frac{\partial \mu}{\partial \Theta} - \rho_\Theta \frac{dr}{ds}\right)
\end{aligned} \qquad 3.20$$

In figure 8 we depict the two dimensional geometry of the system of co-ordinates in which we shall perform numerical calculations.

3.7 The time of travel of the wave.

It is usually advantageous to compute, in addition to the path of the ray, the time of travel, which must of course be found from the ray velocity and hence from the group refractive index μ_g. This is related to the phase refractive index μ by

$$\mu_g = \frac{d}{df}\left\{\mu f\right\} = \mu + f \frac{d\mu}{df} \qquad 3.21$$

/The...

The time of travel is then found from

$$\frac{dT}{ds} = \frac{1}{C}\frac{\mu_g}{\mu} = \frac{1}{C}\left\{1 + \frac{f}{\mu}\frac{d\mu}{df}\right\} \qquad 3.22$$

PART 2.

MATHEMATICAL METHODS AND MODELS.

Chapter 4.

The numerical solution of the Heslegrove equations

4.1. Introduction

In the last chapter we have seen how the path of a ray through space mapped by polar co-ordinates may be found as the solution to a set of first order differential equations, providing the W.K.B.J. conditions for a slowly varying medium apply. The equations are non-linear, and contain derivatives of the refractive index with respect to each of the parameters $\rho_r, \rho_\theta, \rho_\varphi$, r, Θ, Φ. It is the purpose of this chapter to indicate the derivation of expressions for these derivatives, and to indicate how the equations were solved on a digital computer.

4.2. μ and its derivatives.

The refractive index μ is most easily obtained in this case from the quadratic equation

$$A\mu^4 + B\mu^2 + C=0 \qquad 4.1$$

(Where we have used μ, not n as in our cases the refractive index is always real) as indicated in chapter 2.3 where the coefficients A,B,C are as given in that chapter. $\cos\Psi$ and $\sin\Psi$ may be found from

$$\cos\Psi = \frac{\bar{\rho}.\bar{Y}}{\rho Y} = \frac{\rho_r Y_r + \rho_\theta Y_\theta}{\rho Y} \qquad 4.2$$

$$\sin\Psi = \frac{(\bar{\rho}\times\bar{Y})_\Phi}{\rho Y} = \frac{\rho_r Y_\theta - \rho_\theta Y_r}{\rho Y} \qquad 4.3$$

/Since...

Since the solution of equation 4.1 generally yields two modes, the correct one must be chosen. It turns out that if we write the solution

$$\mu^2 = \frac{-B \pm \sqrt{B - 4AC}}{2A}$$

then the adoption of the negative radical gives the correct mode. (See, for example, SHAWAN[18]).

The derivatives of μ with respect to each component of $\bar{\rho}$ are found from

$$\frac{\partial \mu}{\partial \rho_k} = \frac{\partial \mu}{\partial \Psi} \frac{\partial \Psi}{\partial \rho_k} = \frac{\partial \mu}{\partial \Psi} \left\{ \frac{\rho_k Y \cos\Psi - \mu Y_k}{Y \mu^2 \sin\Psi} \right\} \qquad 4.4$$

for $k = r, \Theta, \Phi$

The derivative $\frac{\partial \mu}{\partial \Psi}$ is calculated from

$$\frac{\partial A}{\partial \Psi}\mu^4 + 4A\mu^3 \frac{\partial \mu}{\partial \Psi} + \frac{\partial B}{\partial \Psi}\mu^2 + 2B\mu \frac{\partial \mu}{\partial \Psi} + \frac{\partial C}{\partial \Psi} = 0$$

$$\frac{\partial \mu}{\partial \Psi} = \frac{-\frac{\partial A}{\partial \Psi}\mu^4 + \frac{\partial B}{\partial \Psi}\mu^2 + \frac{\partial C}{\partial \Psi}}{4A\mu^3 + 2B\mu} \qquad 4.5$$

The derivatives of μ with respect to each component of $\bar{r}$ are found from

$$\frac{\partial \mu}{\partial l} = \sum_j \frac{\partial \mu}{\partial x_j} \cdot \frac{\partial x_j}{\partial l} + \sum_j \frac{\partial \mu}{\partial Y_j} \cdot \frac{\partial Y_j}{\partial l} + \frac{\partial \mu}{\partial \Psi} \cdot \frac{\partial \Psi}{\partial l} \qquad 4.6$$

for $l = r, \Theta, \Phi$

where

$$\frac{\partial \mu}{\partial X_j} = -\frac{\frac{\partial A}{\partial X_j}\mu^4 + \frac{\partial B}{\partial X_j}\mu^2 + \frac{\partial C}{\partial X_j}}{4A\mu^3 + 2B\mu} \qquad 4.7$$

$$\frac{\partial \mu}{\partial Y_j} = -\frac{\frac{\partial A}{\partial Y_j}\mu^4 + \frac{\partial B}{\partial Y_j}\mu^2 + \frac{\partial C}{\partial Y_j}}{4A\mu^3 + 2B\mu} \qquad 4.8$$

The derivatives of X_j and Y_j are obtained from the models of exosphere used.

The derivative of μ with respect to f is found from

$$\frac{\partial \mu}{\partial f} = -\frac{\frac{\partial A}{\partial f}\mu^4 + \frac{\partial B}{\partial f}\mu^2 + \frac{\partial C}{\partial f}}{4A\mu^3 + 2B\mu}$$

The expressions for the derivatives of A B and C with respect to Ψ, X_j, Y_j and f are given in full in Appendix B.

4.3 The method of digital computation.

Equations 3.20 and 3.21 form a set of five simultaneous first order equations to be solved for a suitable set of initial values for r, Θ, ρ_r, ρ_Θ, T, by a suitable step-by-step process. To evaluate initial values for ρ_r and ρ_θ it is easiest to supply an initial value of Ψ, say Ψ_o. μ_o may then be calculated, and the ρ_{k_o} obtained from the equations

$$\rho_{r_o} = \mu_o \cos\{\gamma_o + \Psi_o\} \qquad 4.10$$

$$\rho_{\Theta_o} = \mu_o \sin\{\gamma_o + \Psi_o\} \qquad 4.11$$

as can be easily seen from figure 8. γ_o is the initial angle between $\bar{V}$ and the radial $\bar{r}$, found from

$$\mathrm{Tan}\gamma_o = -\frac{1}{2}\mathrm{Cot}\,\Theta_o \qquad 4.12$$

/Integration....

Integration may then proceed step by step, until the ray reaches some predetermined altitude, or is lost when the index of refraction becomes purely imaginary.

As we have seen in chapter 3.5 we have more equations than degrees of freedom. The rounding errors involved in calculating μ and in integrating the $\frac{d\rho_k}{ds}$ will result in $|\bar{\rho}| \neq \mu$ after a few steps of integration, unless we constrain the ρ_k by using the correction

$$\rho'_k = \rho_k \frac{\mu}{|\bar{\rho}|} \qquad 4.13$$

at each point, as was first done by YABROFF[15].

This correction is valid, as $|\bar{\rho}|$ is not used to calculate μ.

The GILL[16] modification to the Runge-Kutha process was used to integrate the equations. This method is of a high degree of accuracy, carrying correction factors between steps to minimize rounding errors, and for this reason was preferred to the usual predictor-corrector methods used for solution.

Accuracy of integration depends to a great extent on the size of step length $\{\Delta s\}$ used, and on the gradients of refractive index. As an initial guide to the step length to be used we examine the Appleton-

/-Hartree...

-Hartree formula for the case of no collisions, when $\bar{\rho}$ lies along $\bar{B}$, which is the condition hoped for in whistler propagation.

The formula becomes, for the whistler mode

$$n^2 = 1 - \frac{X}{1-Y} \qquad 4.14$$

and at very low frequencies where X and Y I this reduces to

$$n^2 \simeq \frac{X}{Y} = \frac{f_n^2}{f f_H} \qquad 4.15$$

so that at a given point in space we have

$$n \propto \frac{1}{\sqrt{f}} \qquad 4.16$$

Now $n = c/v = ct/vt = \delta s/\delta S$, where δS is the path length for an increment δs in s. This shows that for approximately equal path lengths per step we must take

$$\delta s_0 \propto \frac{1}{\sqrt{f}} \qquad 4.17$$

The constant of proportionality was found by trial and error, but is not very critical. A suitable value was found to be 2000 Km KHz$^{\frac{1}{2}}$.

This approximation holds only for very small angles Ψ. If the angle Ψ increases we must decrease the step length to retain accuracy; this is particularly true if $\Psi \rightarrow \pm 90^{\circ}$, when μ starts to diverge; this decrease can be done automatically.

/Programs....

Programs to carry out the above integration procedures were written by the author to run on the Rhodes University I.C.L. 1301 digital computer. The scientific autocode MAC (similar to FORTRAN) as used on this machine is slow and clumsy on account of the often wasteful use made of the limited core-store "fast" memory, and the author found it a stimulating exercise to modify the existing compiler to enable efficiently coded "machine language" sections to be compatible with the existing autocode facilities; and to introduce several new autocode facilities with the help of Mr. W.A. Lawrie. These new facilities are now an integral part of the computing both at Rhodes and at Cape Town Universities, and a brief summary of the modifications appears in Appendix C for the record.

It is estimated that the efficiency of the long and involved ray-tracing program was increased by orders of magnitude over simpler autocode versions; the disadvantage being that the writing and testing time was much longer. The author is now also fully aware of the fascination of software assembly - a fascination which can easily detract from the physical problem of ray-tracing!

A flow chart of the program used is presented in Appendix D.

/Another...

Another point which gave trouble in numerical calculations concerned rounding errors in the solution of quadratic equations. It is well known that the simple formula

$$x = \frac{-B \pm \sqrt{B^2-4AC}}{2A}$$

is inefficient when the roots are not of the same order of magnitude, and that a better solution is to use the sign for the radical giving the "bigger" root and then to use the relation $x_1 x_2 = C$ to give the smaller root. The author found that, for real roots, the accuracy of these answers could, in several cases, be increased by iteration on the formula

$$x_1 = -B-x_2$$
$$x_2 = C/x_1$$

with a threefold iteration seemingly the optimum.

It is difficult to check on the accuracy of such lengthy programs. One test is to trace a ray into the opposite hemisphere and then to take the "final conditions" for this ray as the "initial conditions" for a ray traced in the opposite direction, which latter should retrace the original path. This test was performed for several rays, when it was found that the rays arrived back well within 5% of the original starting point, as can be seen from Table I.

TABLE 1

Comparison between initial conditions of some rays and the final conditions of rays traced backwards.

frequency KHz	No. of ions	Initial Conditions r_o(Km)	θ_o °	ψ_o °	Final Conditions r_f(Km)	θ_f °	ψ_f °	Final Retraced Conditions r_o'(Km)	θ_f' °	ψ_f' °
5	3	6670	30	-139	13739	- .3	283.7	6670	30.2	-139.7
50	3	6670	30	-139	6620	-30.3	267.6	6670	29.4	-140.7
100	3	6670	30	-139	7132	-15.6	257.4	6670	31.5	-139.3
1	1	7370	30	180	15584	13.9	277.3	7370	30.0	179.0
5	1	7370	30	180	6657	-43.3	184.9	7370	30.7	177.8
10	1	7370	30	180	6667	-41.5	197.3	7370	31.2	174.9
20	1	7370	30	180	6664	-38.3	244.2	7370	29.8	169.6
50	1	7370	30	180	6664	-31.0	261.5	7370	31.0	176.7
100	1	7370	30	180	7322	-16.6	253.6	7370	30.1	179.4
20	1	6870	40	-149	12093	-22.1	259.3	6870	40.5	-151.1

Chapter 5.

The models of ionosphere and exosphere used.

5.1. The dipole approximation to the Earth's magnetic field

At low and mid latitudes the Earth's magnetic field may conveniently be represented by that of a dipole. For completeness we summarise the salient formulae in our system of geomagnetic polar co-ordinates

Remembering that the earth's dipole is oriented with the North pole in the South we have

$$\overline{B} = \frac{\mu_o m}{4\pi r^3}\left\{-2\sin\Theta, \cos\Theta, 0\right\} = B_o\left[\frac{a}{r}\right]^3\left\{-2\sin\Theta, \cos\Theta, 0\right\} \qquad 5.1$$

where a = radius of the earth, B_o = magnitude of B at the geomagnetic equator. The magnitude of the field is

$$B = B_o \frac{a^3}{r^3}\sqrt{4 - 3\cos^2\Theta} \qquad 5.2$$

and the equation of a field line is

$$r = \Lambda \cos^2\Theta = a\frac{\cos^2\Theta}{\cos^2\lambda} \qquad 5.3$$

where λ = latitude at which the line intersects the earth. Rather than B, we use $Y = {}^{f_H}/_{f}$. If f_{H_o} is the electron gyro frequency at the geomagnetic equator, then we have

$$Y_e = \frac{f_{H_o}}{f}\cdot\frac{a^3}{r^3}\sqrt{4-3\cos^2\Theta} \qquad 5.4$$

where the numerical value of f_{H_o} = 870 KHz. The

/values....

values of Y_i for the ith species of positive ions may then be found from

$$Y_i = \frac{m_e}{m_i} \cdot Y_e \qquad 5.5$$

where m_e = mass of electron, m_i = mass of ion.

The derivatives of Y needed in equations 4.6 are

$$\frac{\partial Y}{\partial_r} = \frac{-3Y}{r} \qquad 5.6$$

$$\frac{\partial Y}{\partial \Theta} = \frac{3Y \ \mathrm{Sin}\,\Theta \ \mathrm{Cos}\,\Theta}{4-3 \ \mathrm{Cos}^2 \Theta} \qquad 5.7$$

If γ is the angle between Y and the radius vector we have

$$\mathrm{Tan}\gamma = \frac{Y_\Theta}{Y_r} = -\tfrac{1}{2} \cot \Theta \qquad 5.8$$

If Ψ is the angle between the wave normal and the magnetic field, then the derivatives of Ψ are found from

$$\frac{\partial \Psi}{\partial l} = \frac{\partial \Psi}{\partial \gamma} \cdot \frac{\partial \gamma}{\partial l} \quad \text{for } l = r, \Theta, \Phi \qquad 5.9$$

where

$$\frac{\partial \gamma}{\partial_r} = 0 \qquad 5.10$$

$$\frac{\partial \gamma}{\partial \Theta} = \frac{1}{2 \ \mathrm{Sin}^2 \Theta + \frac{1}{2} \cos^2 \Theta} \qquad 5.11$$

$$\frac{\partial \gamma}{\partial \Phi} = 0 \qquad 5.12$$

$$\frac{\partial \Psi}{\partial \gamma} = \frac{\partial}{\partial \gamma}\left\{ \mathrm{Arcos} \frac{\bar{\rho} \cdot \bar{Y}}{\rho Y} \right\} = \frac{\rho_r Y_\Theta - \rho_\Theta Y_r}{\rho Y \ \mathrm{Sin}\,\Psi} \qquad 5.13$$

where as $\Psi \to 0$, $\frac{\partial \Psi}{\partial \gamma} \to 1$ as may be seen from l'Hospitals

/rule...

Figure 9. Geometry of Dipole field, showing wave normal vector $\bar{p}$.

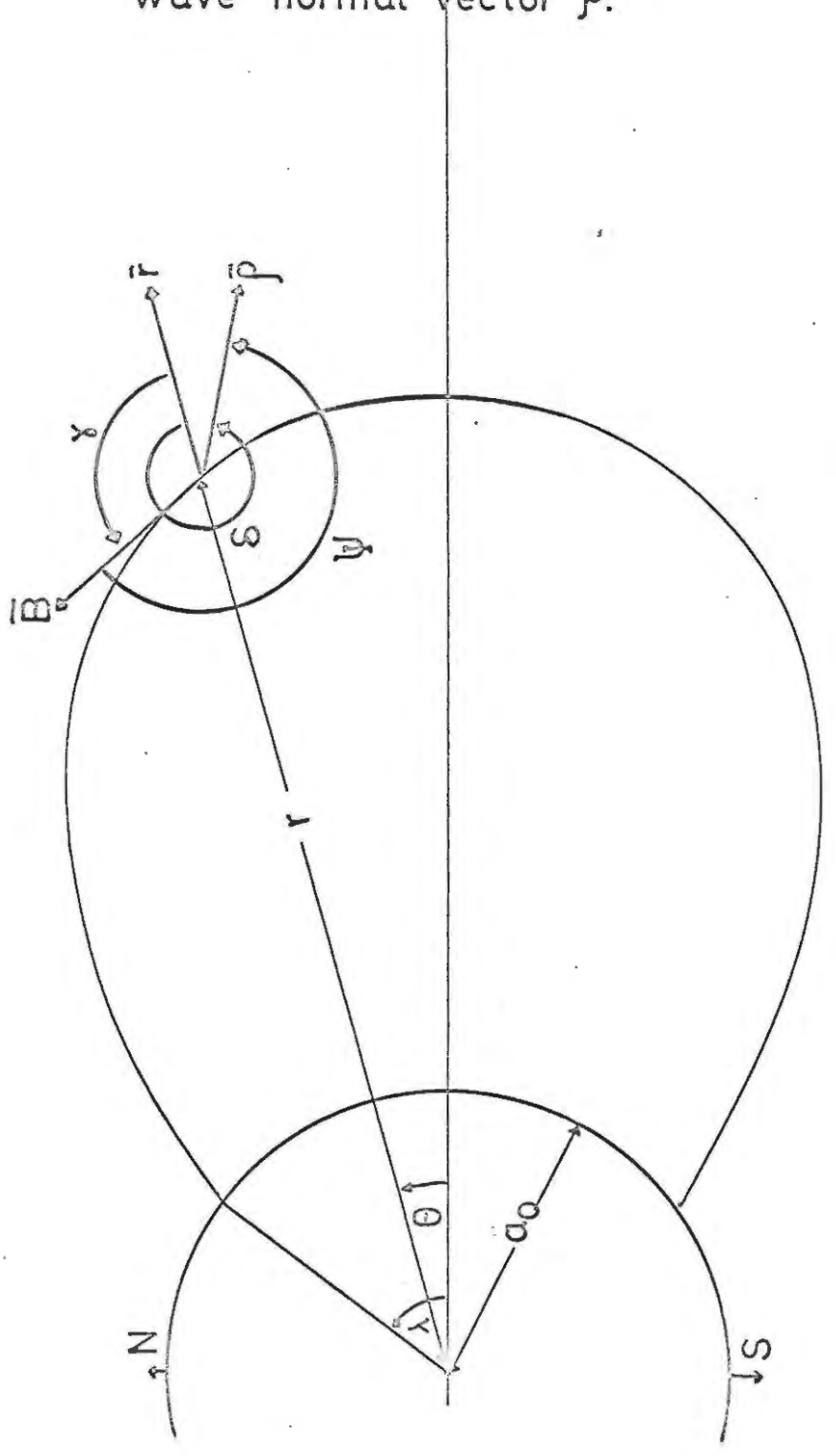

rule.

The magnetic field and the symbols used above are depicted in figure 9.

5.2. The Diffusive Equilibrium model of plasma densities.

The earliest ray-tracing studies by MAEDA and KIMURA[17] and by YABROFF[15] used simple exponential variation of electron densities and neglected the presence of ions. More sophisticated studies such as those of KIMURA[1] and of SHAWAN[18] have used density models based partly or entirely on the ANGERAMI and THOMAS[19] model, first put forward in 1962 in a classic paper, taking into account the effect of the electric field that arises from charge separation, the centrifugal force due to the rotation of the earth, and the effect of the gravitational field; at the same time assuming that the charged particles move only along the field lines. The ion composition of the exosphere at great heights is predominantly $H^+|e^-$, but at lower heights it is strongly dependent on the composition at a base level at a height of about 500 Km, where the main charge exchange processes occur.

The model yields the mathematical result that

$$n_i = \frac{\eta_i \, e^{-Z/H_i}}{\eta \, C^{\frac{1}{2}}} \, n_{eo} \qquad 5.14$$

$$n_e = \Sigma n_i = C^{\frac{1}{2}} n_{eo} \qquad 5.15$$

/where....

where n_i = concentration of ith ion, n_e = electron concentration, n_{eo} = electron concentration at base level, $r = a_o$

$$Q = \sum_i \frac{\eta_i}{\eta} e^{-Z/H_i} \qquad 5.16$$

and $\eta_i = \frac{\text{ion density of ith species}}{\text{ion density of } O^+}$ at base level

$$\eta = \Sigma\eta_i = \frac{\text{electron density}}{\text{ion density of } O^+}$$

$$Z = \text{geopotential height} = \frac{a_o}{r}(r-a_o) \qquad 5.17$$

$$H_i = \text{scale height of ith species} = \frac{kT_i}{m_i g}$$

The above formulae apply to the simple case of an isothermal exosphere, and we have neglected the small effect due to the earth's rotation, as do most authors.

The subscripts i refer to H^+ He^+ and O^+, and two compositions at the base level were considered:

a. Angerami and Thomas composition

Based on electron density measurements at the time, ANGERAMI and THOMAS[19] arrived at the following parameters to fit their model to experiment

a_o = 6870 Km (Base level at 500 Km)
T = 1000 K
Neo = 3.5×10^4 el cc

Ion composition at base level: ·157% H^+, 1·96% He^+, 97·883% O^+

/Values....

60

Values of η_i : $\eta_i = \cdot 0016$, $\eta_2 = \cdot 02$, $\eta_3 = 1$,

$\eta = 1 \cdot 0216$

Most of the ray tracing studies done in this work were done using this model. In the course of the work a subsequent paper by SHAWAN and GURNETT[20] was discovered giving parameters for the diffusive equilibrium model based on the results of Injun III measurements.

b. SHAWAN and GURNETT composition.

For a model based on these results the author adopted the parameters:

$$a_o = 6870 \text{ Km}$$
$$T = 800^{\circ}K$$
$$Neo = 7 \times 10^4 \text{ e/cc}$$

Ion composition at base level 2·25% H_+, 11·4% He^+, 86·35% O^+

Values of η_i : $\eta_1 = \cdot 026$ $\eta_2 = \cdot 132$ $\eta_3 = 1.0$

$\eta = 1 \cdot 158$

In figures 10 and 11 can be seen plots of the electron and ion densities for these two models.

For ray tracing below the F Region bulge a modification was built into the program using the simple formula as given by KIMURA[1]

$$Ne^1 = \left\{1 - e^{-\frac{(r-6460)^2}{140}}\right\} Ne \qquad 5.18$$

where Ne is as given by the diffusive equilibrium model.

/Since...

Since N_i and hence X_i depend only on r, the only derivative in equation 4.6 which we need consider is $\frac{\partial X_i}{\partial r}$ Since we may write $X_i = A_i N_i$, $\frac{\partial X_i}{\partial r} = A_i \frac{\partial N_i}{\partial r}$ which yields

$$\frac{\partial X_i}{\partial r} = -\frac{\sigma_o}{r^2}^2 X_i \left\{ \frac{1}{H_i} + \frac{1}{2Q} \cdot \frac{\partial Q}{\partial Z} \right\} \qquad 5.19$$

where $\frac{\partial Q}{\partial Z} = -\sum_i \frac{\eta_i}{\eta H_i} e^{-Z/H_i}$ 5.20

For electrons we get similarly

$$\frac{\partial X_e}{\partial r} = \frac{a^2}{r^2} \cdot \frac{X}{2Q} \cdot \frac{\partial Q}{\partial Z} \qquad 5.21$$

It must be appreciated that these simple diffusive-equilibrium models will not explain all the known features of plasma density; especially the diurnal, secular and temperature dependent variations. Nevertheless, ray-tracing in such a model should exhibit the major features of propagation.

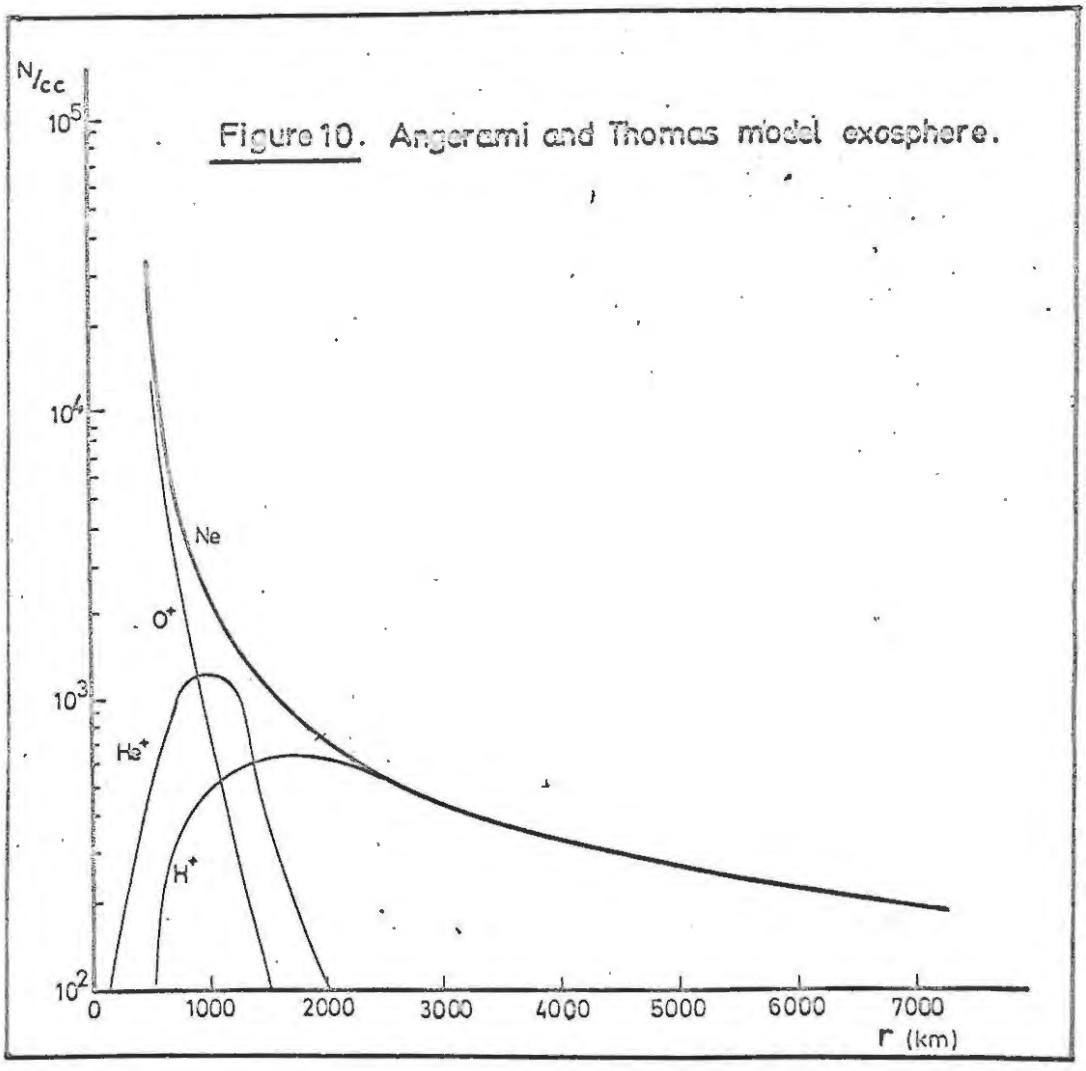

Figure 10. Angerami and Thomas model exosphere.

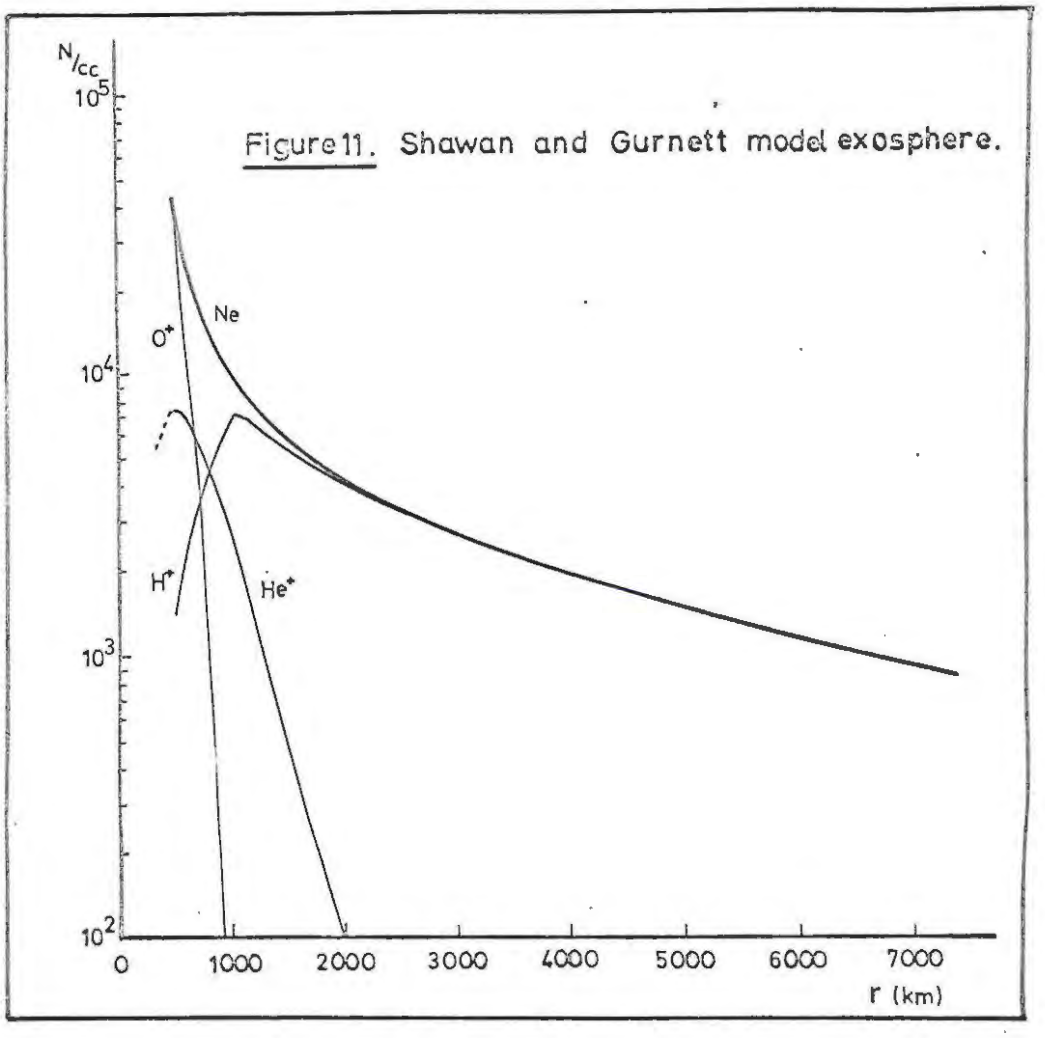

Figure 11. Shawan and Gurnett model exosphere.

PART 3.

RESULTS OF COMPUTATIONS

Chapter 6.

Ray-tracing in an exosphere where the effects of heavy ions are disregarded.

Although the present work is largely concerned with the effects of heavy positive ions on the propagation of V.L.F. signals, it is of interest for comparison purposes to summarize the results of earlier workers, who neglected these effects.

6.1 The results of MAEDA and KIMURA.

The first ray-tracing studies through the exosphere were performed by MAEDA and KIMURA[17] in 1956. They used a crude form of integration process, and assumed that the quasi-longitudinal approximation to the Appleton-Hartree formula (Equation 4.14) would apply along the path; i.e. that the wave normal would lie almost along the field-line direction throughout. The electron distribution in the exosphere was taken to be

$$N = 1.8 \times 10^{5} \, e^{-6.57\times10^{-4}(r-6670)} \qquad 6.1$$

where N is in e/cc and r is in Km. Integration was commenced in each case at an initial height of 300 Km.

With these assumptions and initial values, they were able to give quantitative consistency with the observed dispersion values of the day. They also found that the ray paths for rays commencing at low

/latitudes....

latitudes were asymmetric about the magnetic equator, but that this asymmetry was reduced at higher latitudes. Although they did not then examine the spatial coherence or latitude focussing as a function of frequency (something which should, of course, be done in a prediction of whistler paths) they concluded that the asymmetry of low-latitude whistler paths accounted for the observed absence of "long" whistlers at these latitudes; while the symmetry at higher latitudes was borne out by the observed "long" whistlers at higher latitudes (a long whistler is one which has been reflected back into the original hemisphere from the opposite hemisphere).

These authors further pointed out the importance of investigating the propagation through the lower and topside ionosphere, since much dispersion and refraction takes place in this region. They also expressed doubts about the correctness of assuming the accuracy of the dipolar approximation to the earth's field.

6.2 The results of YABROFF

The next important study of whistler ray paths disregarding the effects of heavy ions was undertaken by YABROFF[15] in 1961. He employed a predictor-corrector solution to the HASELGROVE[13]

/equations,...

equations, and used the Appleton-Hartree formula for the refractive index, neglecting all collisions. The same electron density distribution as in 6.1 was taken, and integration was again started at an altitude of 300 Km.

YABROFF observed discrepancies between his and the MAEDA/KIMURA results, but put this down to the differences in the numerical methods used. He investigated latitude focussing as a function of frequency, and found that there was evidence of this in regions where the Eckersley dispersion approximation held (Equation 1.1), but that above the "nose" frequency the rays came down closer to the equator. Again, however, the ray paths were asymmetric at low latitudes.

The total time delay for a given frequency was found to be constant over a wide range of initial latitudes, which was surprising, considering the corresponding wide range of path lengths. YABROFF concluded that at higher latitudes the group velocity was greater than at lower latitudes.

He also investigated the behaviour of the wave normal direction. Most of his results are presented for initial values of $\delta = 0^{o}$; some investigated the effect of varying δ_{o} by 10^{o}. The behaviour of the

/wave...

wave normal direction was found to be largely independent of δ_o; for initial latitudes above 35° it swung from outside to inside the field lines, and for initial latitudes below 35° it swung further away from the field lines. Further, the final latitude reached was found to be much the same over the 20° range of variation of δ_o, even though the rays reached different maximum altitudes.

A few computations were performed for rays starting with wave normal aligned with the field. These were found to follow the lines of force more closely. Further, some computations were performed in an exosphere where the electron density was slightly enhanced in field aligned columns. This was found to give ray paths accurately along the field lines, lending support to SMITH'S[21] hypothesis that such enhancement is necessary to provide spatial coherence for whistler production.

6.3 Ray Tracing in the Diffusive Equilibrium Model when the effects of heavy ions are ignored.

As stated previously, the first ray-tracing study to include the effect of heavy ions was performed by KIMURA[1], whose main objective was to interpret the "Subprotonospheric Whistler" (S.P. Whistler).

/KIMURA.....

KIMURA was also the first to employ a diffusive equilibrium model of plasma distribution, but confined his studies to the region below about 1000 Km. However, he does present one "exospheric" path for the case where ions are ignored. This path, for a ray of 1KH$_z$ starting from 300 Km at a latitude of 30°, was found to be almost exactly duplicated by our program; lending further confidence in the accuracy thereof.

As the ANGERAMI and THOMAS[19] model of plasma density yields somewhat lower electron densities at great heights than the MAEDA-YABROFF model, it may be of interest to present some ray paths traced by our program for cases where the effects of ions were ignored. These are depicted in Figures 12 to 18; and further information from these studies is depicted in Figures 19 to 24. The effects of ions were ignored by limiting the summations in the expressions for the Astrom-Hines coefficients, equations 2.18 However, the full plasma density distribution must be evaluated for the diffusive equilibrium model to yield the correct results for the electron density.

In Figures 12 to 18 we have depicted the earth's magnetic field by means of dashed lines; and have denoted the direction of the wave normal at a given point by small arrows. These two conventions are

/adhered....

adhered to in all future ray paths.

Some rays are shown from an initial altitude of 300 Km, directed initially radially outward, while others are from an initial altitude of 1000 Km, directed initially in the $-\overline{B}$ direction. The direction of the wave-normal was found to change most rapidly in the lower exosphere, where the gradients of refractive index are more severe, and the rays starting along the field lines were started at a greater altitude in an attempt to minimize this effect. This matter will be taken up again in chapter 8.

It will be observed that the rays do not follow the magnetic field lines closely, (although they do so to a greater extent when initially along the field), and in general manifest much the same behaviour as YABROFF observed, even though the electron density is rather different. However we cannot claim to support his observation that the time of travel at a given frequency is largely independent of latitude. (See Figures 19,20,21)

For frequencies well below the "nose" frequency (which is about 30% of the electron gyrofrequency at the top of the path) some slight degree of latitude focussing can be observed in Figure 22, possibly sufficient to provide observable "whistlers" of these frequency components. This focussing is seen to

/depreciate....

depreciate at higher latitudes, but that can be related to the drop in nose frequency.

At these low frequencies for which latitude focussing is evident, the Eckersley dispersion $D = t\sqrt{f}$ is approximately constant, although comparison with Table 2, which gives typical observed whistler dispersion values, shows that our results both for dispersion and hence also for time of travel are somewhat too low.

Table 2.

Latitude	Observed Dispersions	Calculated Dispersions.
30°	30 - 50	~11
40°	45 - 90	~18
50°	45 - 80	~27

A low dispersion and travel time is indicative of small group refractive index over the path, due possibly to a low electron density. The SHAWAN and GURNETT[20] model gives slightly higher electron density, and some rays were traced accordingly. As can be seen from Figure 21, this gave slightly better results, although still low.

In Figures 23 and 24 we have plotted the acute angle between magnetic field line and wave-normal as a function of latitude for a frequency of 5 KH_z.

/It....

It will be seen that the behaviour is much the same for different latitudes and different initial wave-normal directions; but is somewhat different from that observed by YABROFF. An initial swing towards the inside of the field lines is followed in all cases by a swing towards the outside, until the opposite hemisphere is reached, when the wave normal frequency swings in the topside ionosphere, once more to lie along the local field line. This last swing is shown dotted as it was difficult to observe the exact extent of the phenomenon from the tabulations used in this section, which paid more attention to the higher altitudes.

Table 3.

Approximate nose frequencies for whistlers observed at differing latitudes.

Latitude	Approximate nose frequency.
20°	175 KH_z
30°	110 KH_z
40°	55 KH_z
50°	18 KH_z

Figure 12. Ray paths from 20°. Ions neglected.

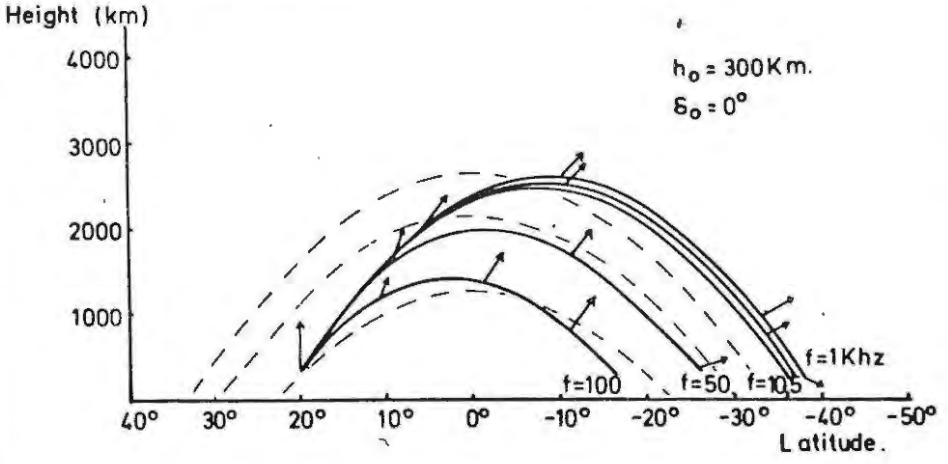

Figure 13. Ray paths from 20° along field initially. Ions neglected.

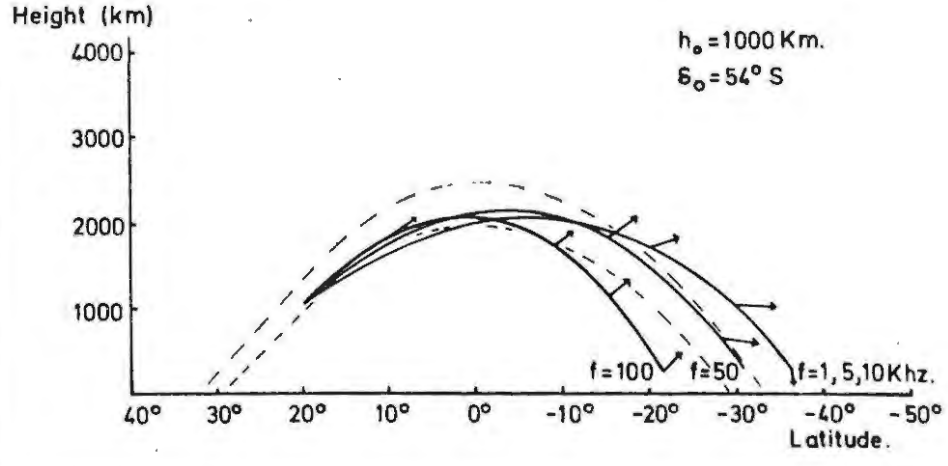

Figure 14. Ray paths from 30°. Ions neglected.

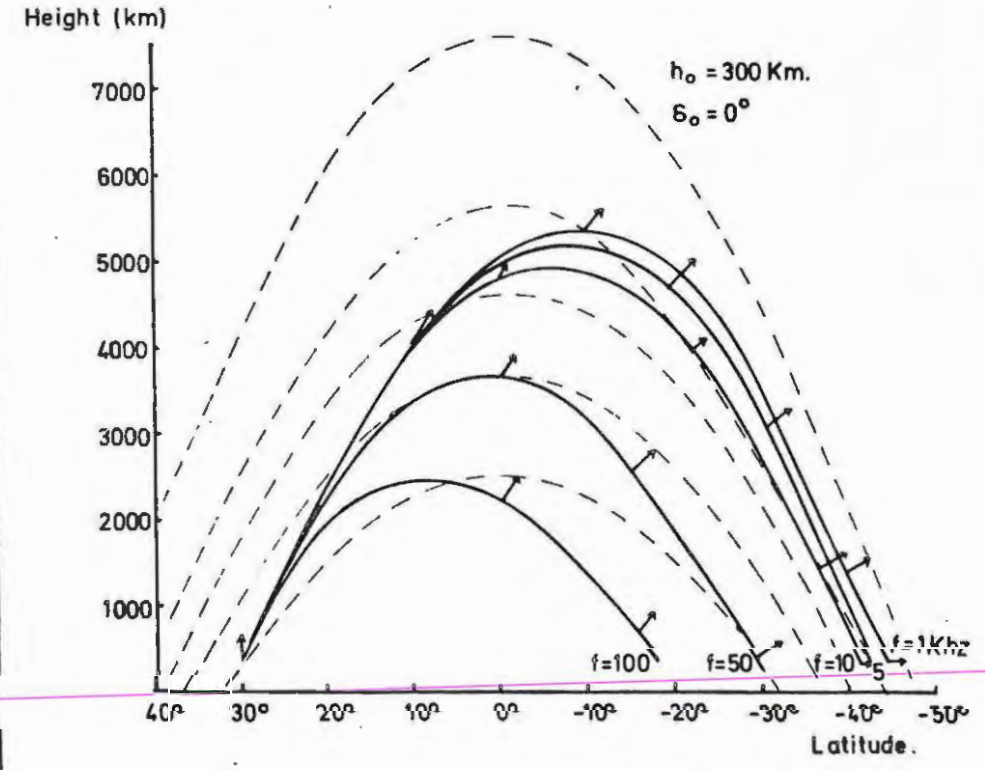

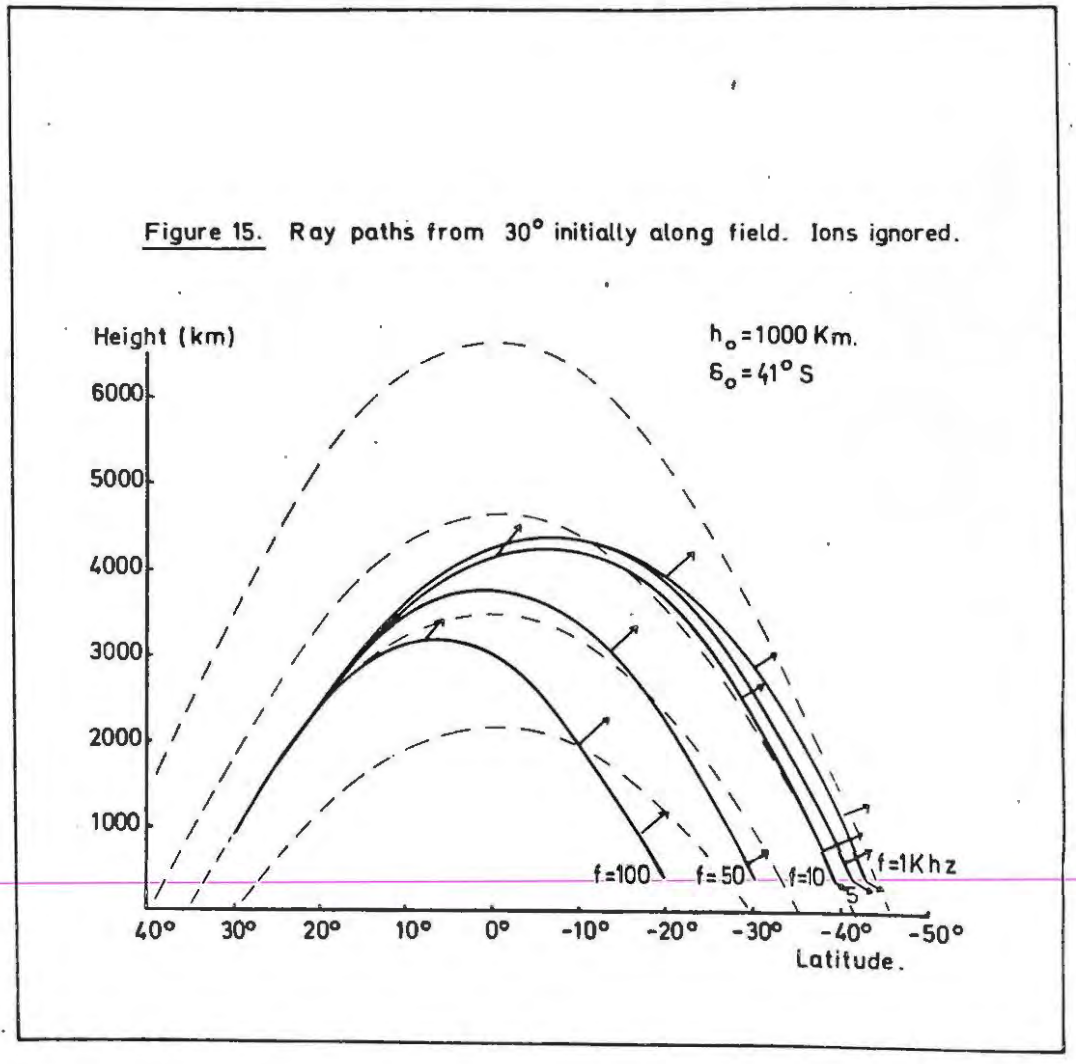

Figure 15. Ray paths from 30° initially along field. Ions ignored.

Figure 16. Ray paths from 40°. Ions neglected.

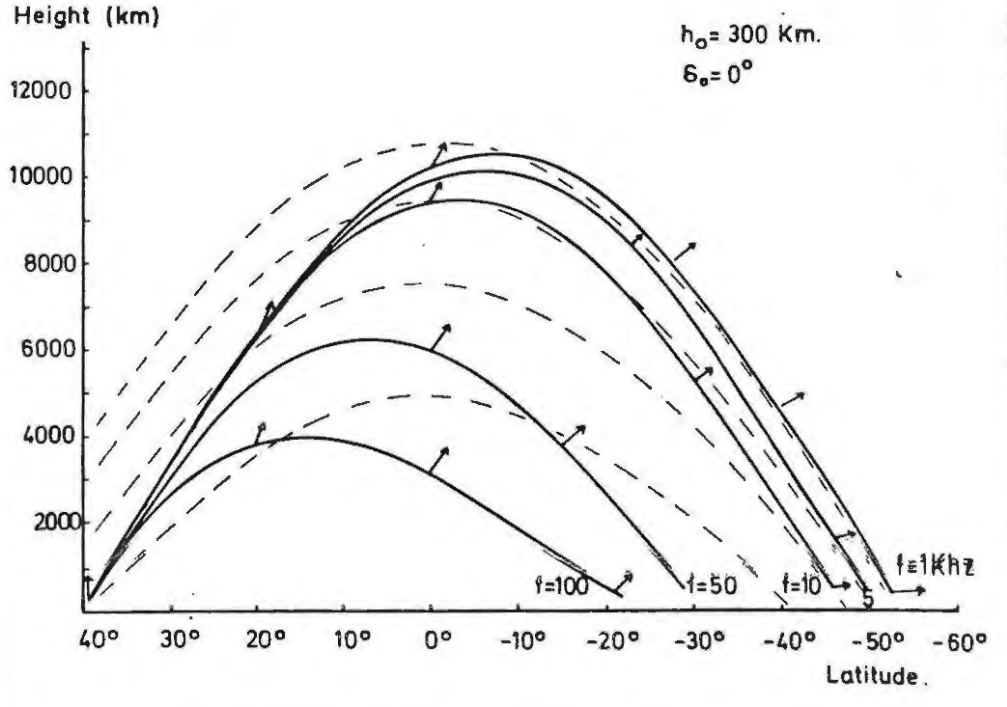

Figure 17. Ray paths from 40° along field initially. Ions neglected.

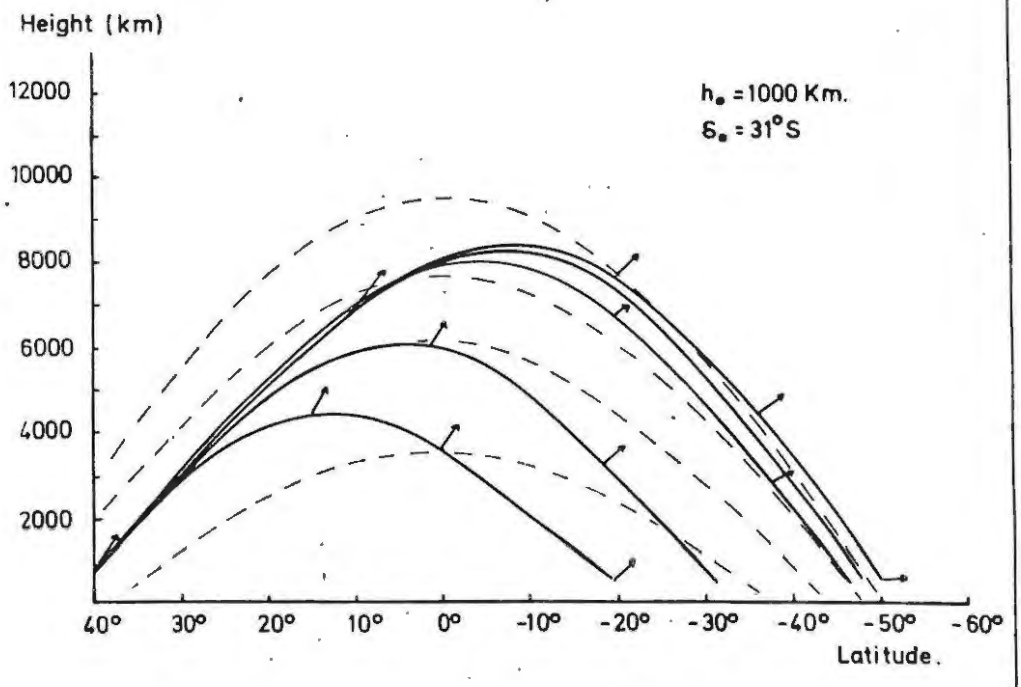

Figure 18. Ray paths from 50° along field initially. Ions neglected.

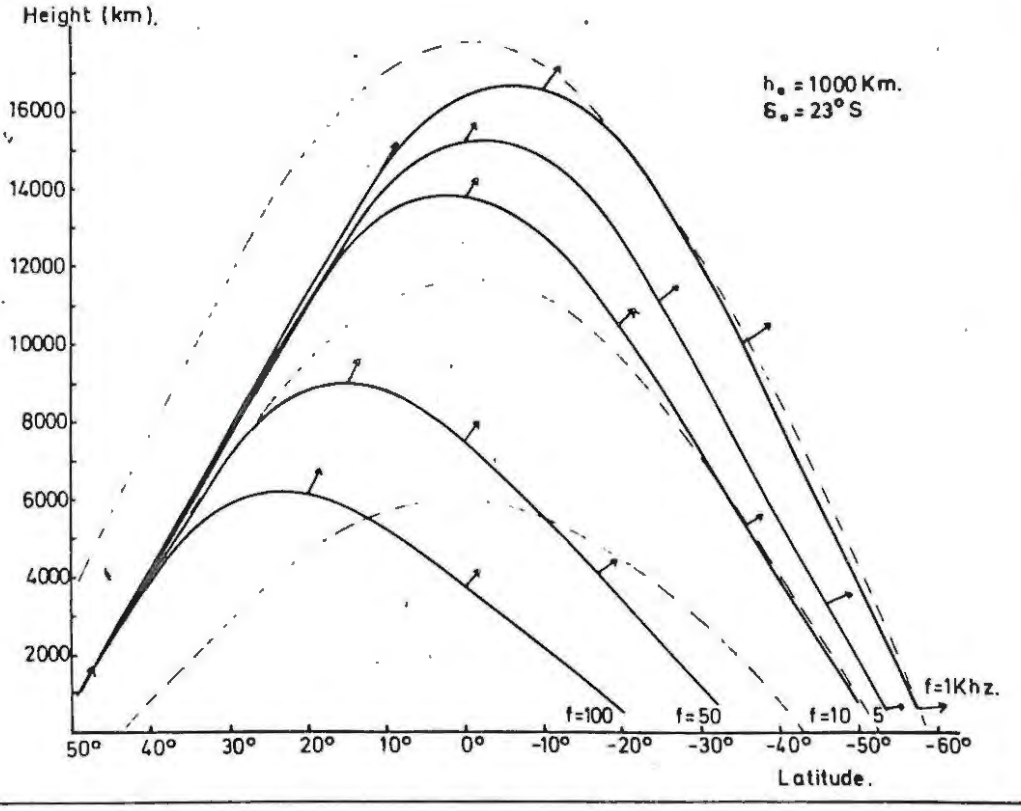

Figure 19. Dispersion and travel times for rays initially vertical, neglecting ions.

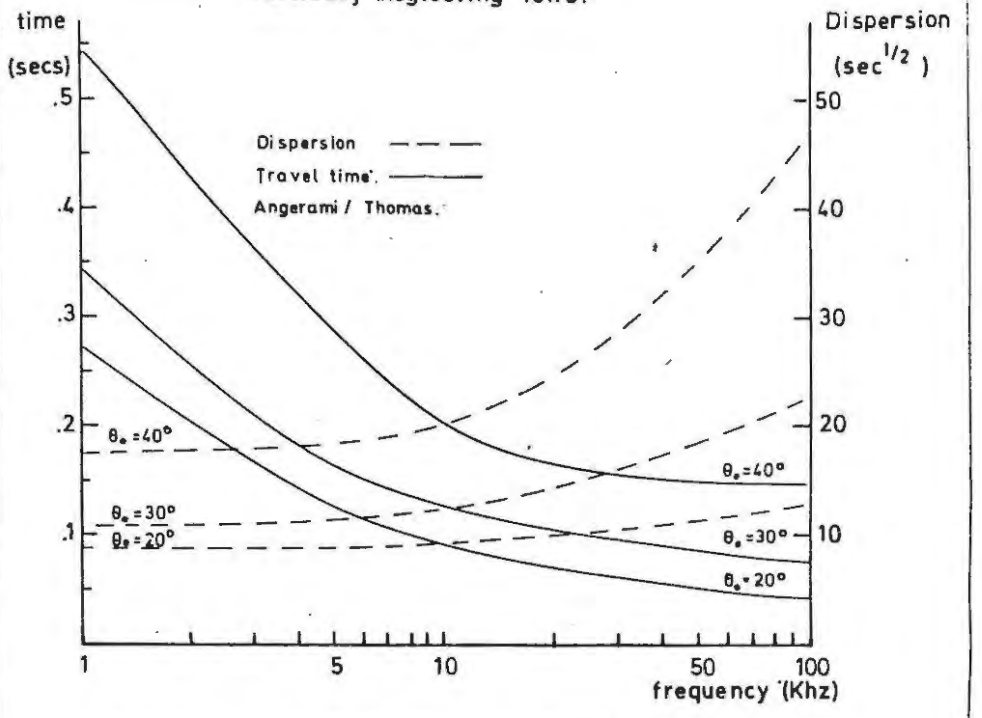

Figure 20. Dispersion and travel times for rays initially along the field, neglecting ions.

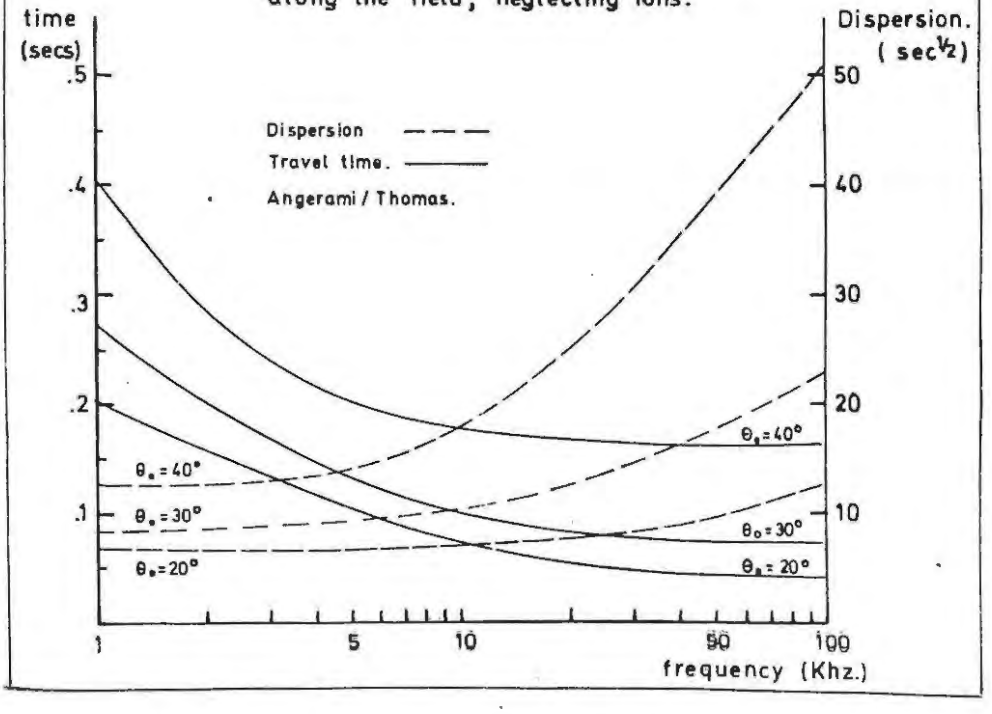

Figure 21. Dispersion and travel times for rays initially vertical, neglecting ions.

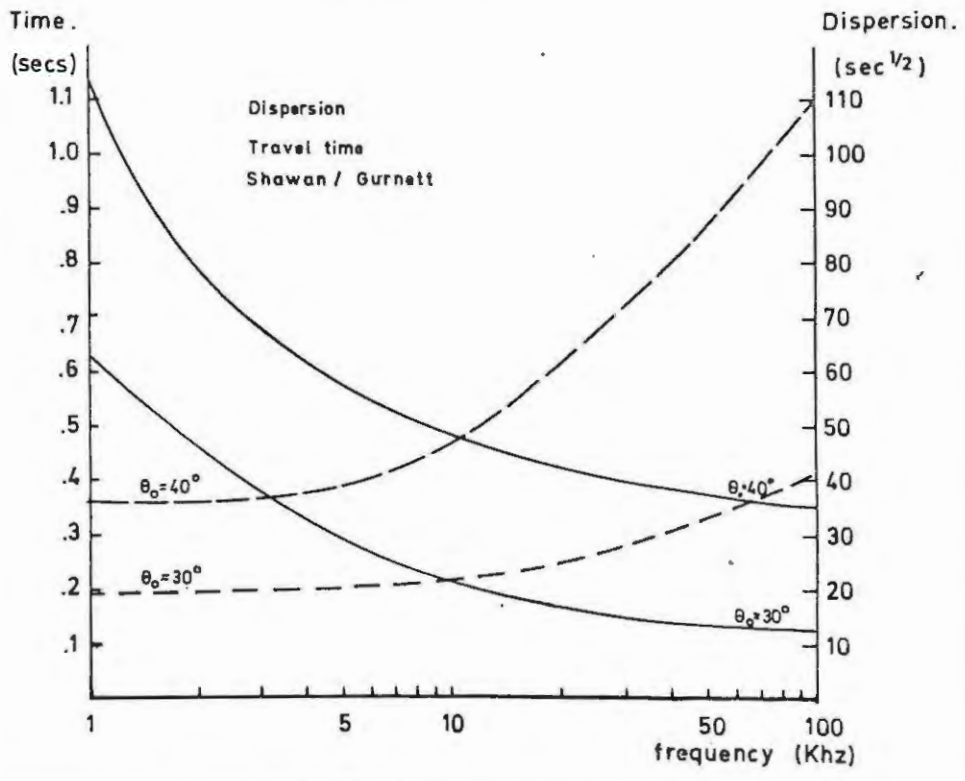

Figure 22. Final latitude against frequency, ions neglected.

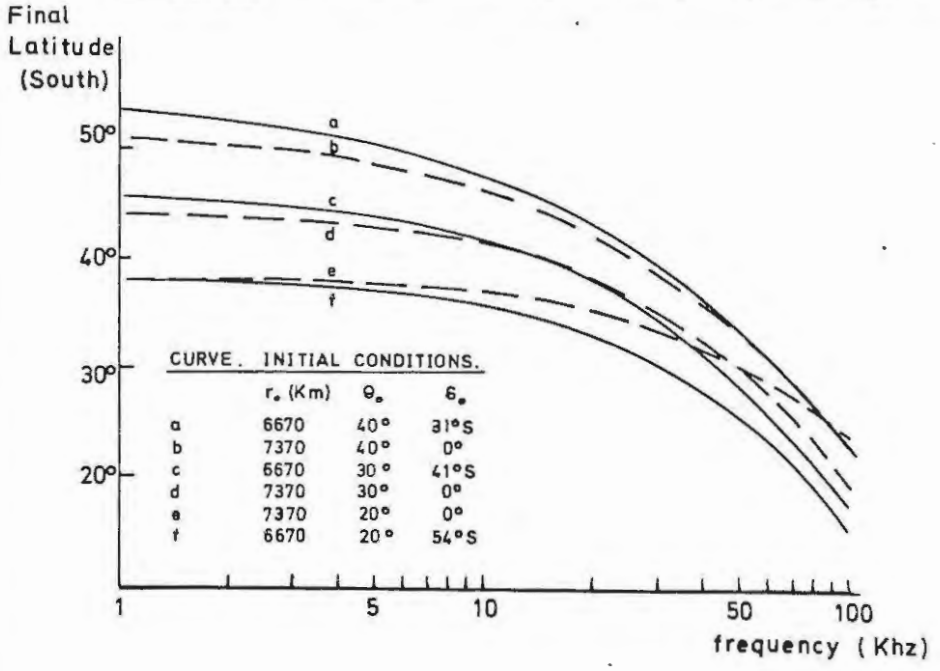

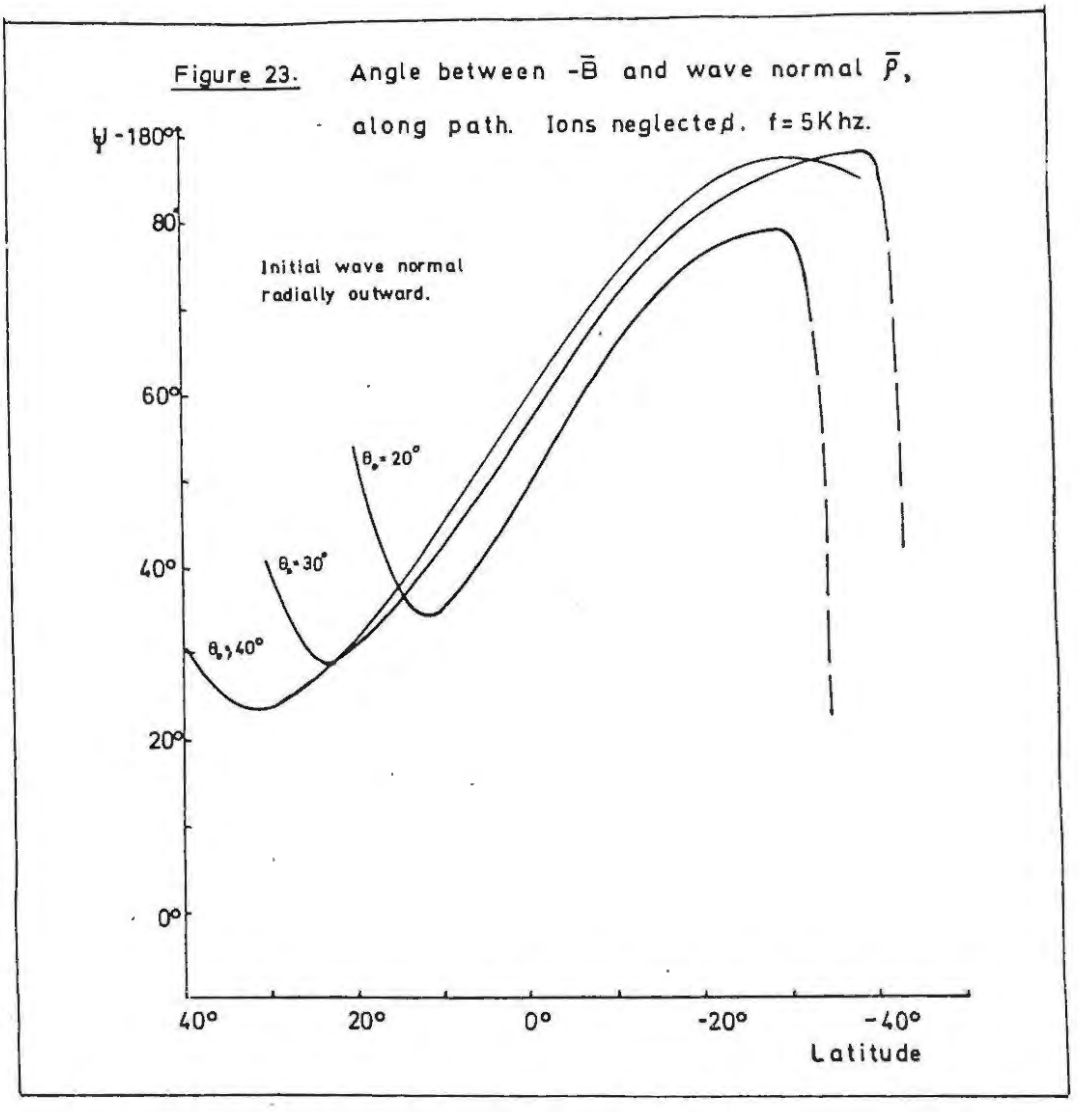

Figure 23. Angle between $-\bar{B}$ and wave normal $\bar{P}$, along path. Ions neglected. f=5Khz.

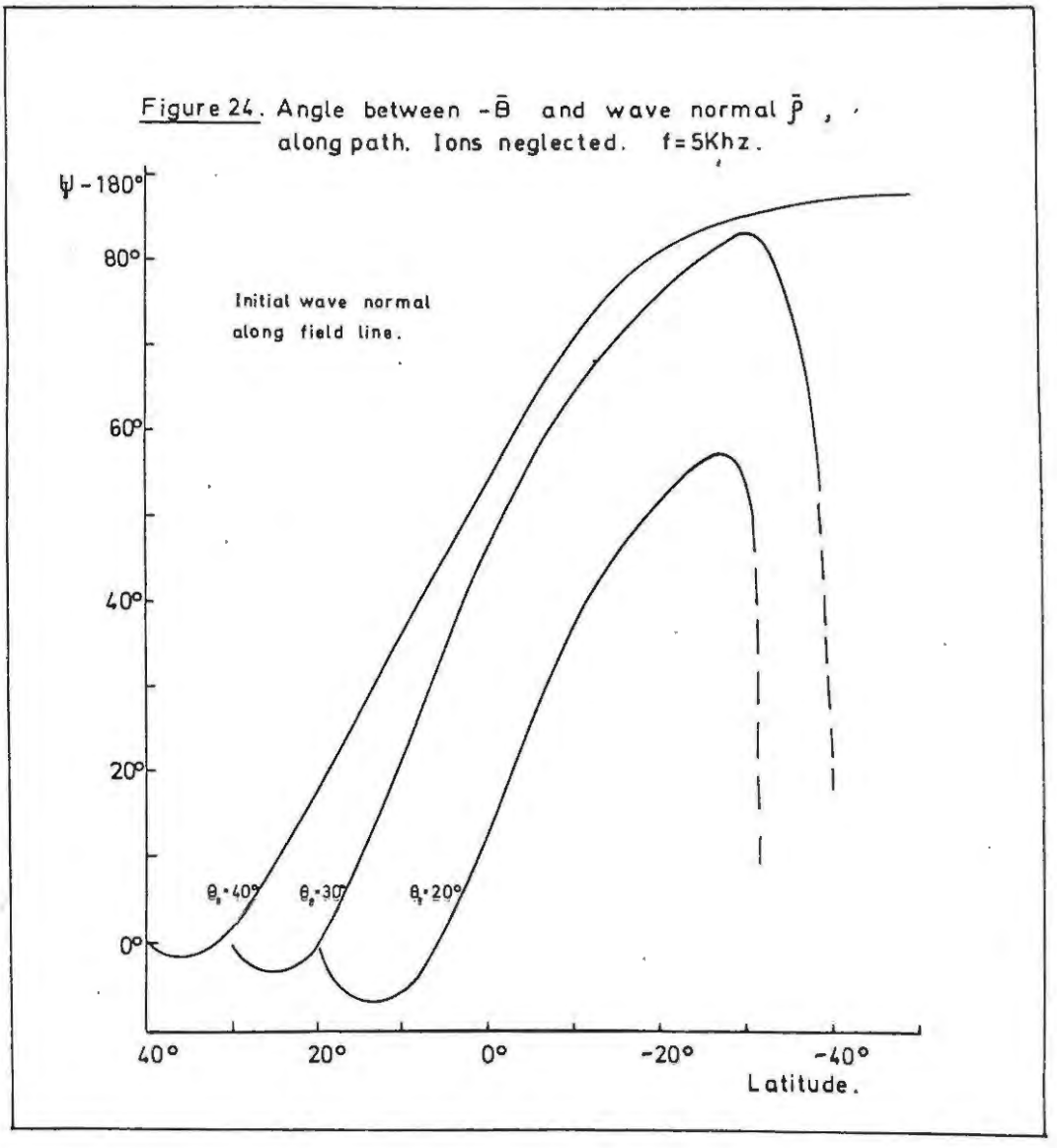

Figure 24. Angle between $-\bar{\theta}$ and wave normal $\bar{p}$, along path. Ions neglected. f = 5Khz.

Chapter 7.

Ray tracing in an exosphere where the effects of heavy ions are considered.

7.1 Introduction.

The first investigators into radio wave propagation through the ionosphere and exosphere completely disregarded the effects of heavy ions in their computations. At first sight this appears justifiable. For the lightest species of positive ion (H^+), the gyrofrequency is about $\frac{1}{2000}$ of the electron gyro frequency, while the plasma frequency is about $\frac{1}{40}$ of the electron plasma frequency. The terms X_{H^+} and Y_{H^+} involved in our magneto-ionic theory are thus negligible in comparison with X_e and Y_e except at the extremely low frequencies which are of the same order as the ion gyro- and plasma frequencies. These frequencies are of the order of .5 - 5 KH_z in the topside ionosphere, and are even lower in the exosphere.

The first study of the effects of heavy ions at these frequencies was undertaken by HINES(22) in 1957.

In the next section we shall outline his treatment, and then in later sections present the results of our computations when ion effects were considered.

/7.2. ....

7.2 The effects of heavy ions on the propagation at very low frequencies.

If we consider the Astrom-Hines formula for the refractive index, equation 2.16

$$An^4 + Bn^2 + C = 0 \qquad 7.1$$

we see that if A = 0 we have one infinite root for n^2. This occurs when

$$\mathrm{Tan}^2 \Psi_{co} = -\frac{P}{S} \qquad 7.2$$

as can be easily seen from the definition of A. For the case where no ions are considered this becomes

$$\mathrm{Tan}^2 \Psi_{co} = -\frac{(1-X)(1-Y^2)}{1-X-Y^2} \qquad 7.3$$

which has a real solution for Ψ_{co} at low frequencies where X and Y are generally much greater than unity. This value of Ψ is then the angle of greatest departure of wave normal from magnetic field direction for which the refractive index can remain finite. Normally this "cut off" angle is in fact close to 90^o.

For high frequencies the presence of positive ions has little effect, but at low frequencies they may cause S to change sign, resulting in an imaginary value for Ψ_{co}, simply implying that propagation is possible for any alignment of wave normal with magnetic field.

/From...

From the refractive index surface point of view, we have open surfaces when we ignore ions, and closed surfaces at low frequencies when we consider ions. This can be seen in Figure 25, where we have plotted (in one quadrant only) refractive index surfaces for fixed typical values of f_n = 200 KH_z and f_H = 600 Kh_z and for wave frequencies below 5 KH_z.

This figure also illustrates a more important difference in the propagation characteristics. Bearing in mind that the normal to the surface gives the direction of the ray, we see that for the no-ion case the ray and magnetic field direction are similar for all allowed Ψ, whereas in the ion case the ray direction may easily become perpendicular to the field direction, resulting in possible reflection effects for values of $\Psi \approx 90^{\circ}$. It should also be noted that when transverse conditions hold, the lower frequencies propagate more rapidly than the higher frequencies, unlike the case for longitudinal propagation.

The frequency at which the effects of heavy ions become important in this way has been investigated by SMITH and BRICE[23]. It can be shown that for frequencies below the "lower hybrid resonance" frequency f_{LHR}, one should take heavy ion effects into account. This frequency is defined by

$$\frac{1}{f_{LHR}^2} = \frac{M_{eff}}{M_e}\left(\frac{1}{f_n^2} + \frac{1}{f_H^2}\right) \qquad 7.4$$

/where...

Figure 25. Refractive index surfaces for frequencies < 5Khz

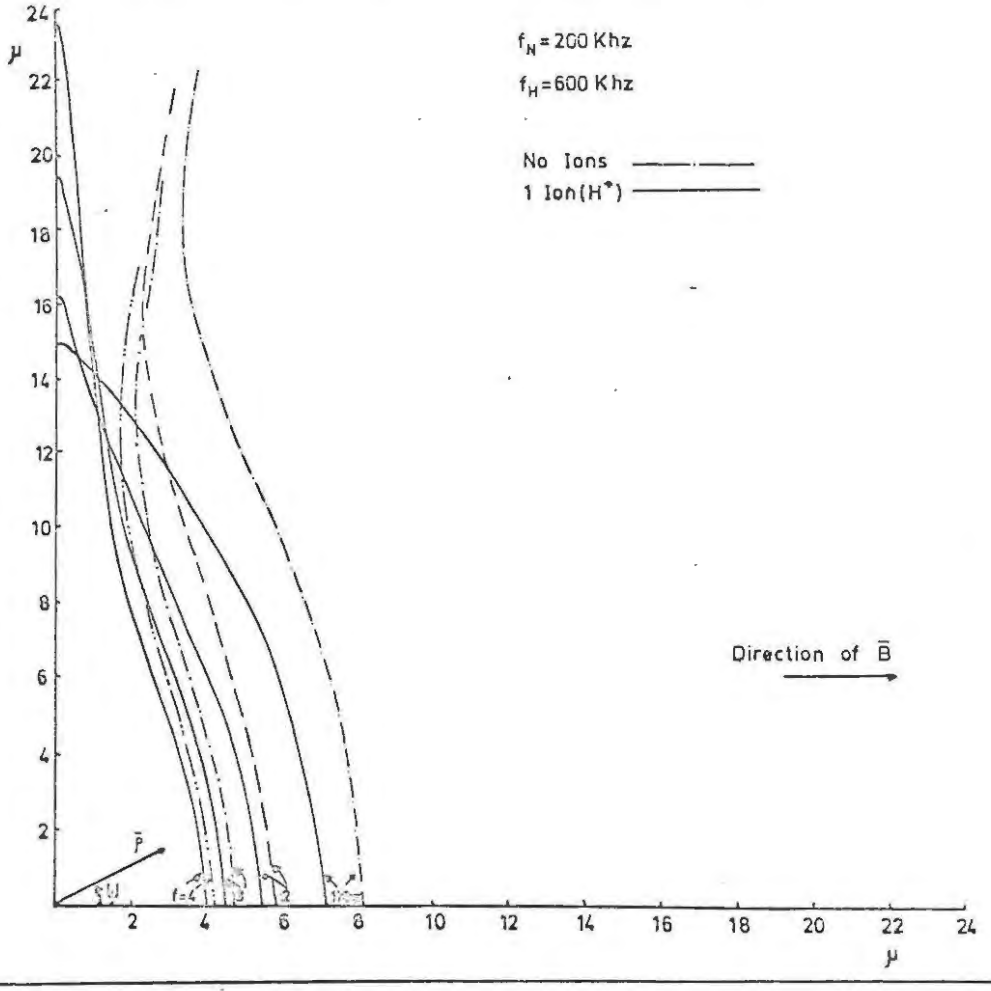

where M_e = mass of electron

M_{eff} = weighted mean mass of the ions, given by

$$M_{eff} = \sum_j \frac{\eta_j}{\eta M_j} \qquad 7.5$$

7.3 The effects of collisions.

KIMURA(1) showed that the effect of a non-zero collision frequency ν could safely be ignored in calculating ray paths, even at altitudes below 2000 Km, since the imaginary part introduced to the refractive index by collisions was only of the order of 1% of the real part. The author decided that it would thus be even more justifiable to ignore collisions in the present study, which was confined mainly to the exosphere where the collision frequencies would be even smaller than those contemplated by KIMURA.

If the effects of collisions are ignored, all the U_j terms in equations 2.18 reduce to unity, and the whistler-mode phase refractive index is completely real for all values of Ψ below the cut-off Ψ_{co}.

In the present study we have not undertaken investigation of the attenuation of the waves through damping. Were this to be done, the effects of collisions could most certainly not be disregarded; KIMURA has further shown that for frequencies below f_{LHR} in the ionosphere the attenuation due to

/collisional...

collisional damping may become appreciable.

7.4 Characteristics of Ray Paths when the effects of ions are included.

Several hundred ray paths have been computed in the present study for various initial conditions; and while it is obviously impossible to present and comment on all of these, a representative set of results has been presented in Figures 26 to 46 and tables 4 and 5.

It will be noticed that many results are presented for the "I Ion" case where H^+ was the only positive ion considered. Examination of Table 4 shows that the effect of including He^+ and O^+ into the calculations is extremely small - the differences could in most cases be accounted for as rounding errors - except at very low frequencies below about 1 KH_z. This is to be expected; not only is the amount of He^+ and O^+ negligible in the exopshere above an altitude of 2000 Km in comparison with the amount of H^+; but even when there is sufficient He^+ and O^+ to be observable, the X_i and Y_i terms for these ions are orders of magnitude smaller than the corresponding terms for electrons. Consequently most paths have been evaluated for the I ion case, since this also resulted in much shorter computation times.

/The...

The results obtained were in agreement with the discussion in section 7.2 of this chapter. For frequencies above about 10 KH_z the paths, travel times and dispersions showed fair agreement with the no-ion cases presented in chapter 6.

However at much lower frequencies reflection is seen to take place when the wave-normal becomes transverse to the field direction. This is shown on several ray paths; in fact, although only one reflection is shown in these cases, the process keeps occurring and the rays are predicted to reflect back and forth at successively higher altitudes. It is unlikely that this sort of effect could ever be observed experimentally, as the wave would be damped out quickly in or near the regions of transverse propagation, for there the index of refraction can become rather large.

In Figures 26 to 33 we present these ray paths, most of which were computed in the ANGERAMI and THOMAS[19] model exosphere. Figure 30 shows rays plotted in the SHAWAN and GURNETT exosphere, but nothing new of interest is apparent. The ray for 10 KH_z is reflected, but this can be put down as a consequence of the higher electron densities encountered.

In Figure 34 we have plotted the variation of f_{LHR} along the path of the 1 KH_z rays when ion effects are

/ignored....

ignored. We have seen that for frequencies of that order some amount of latitude focussing is experienced when ions are ignored, and it is reasonable to expect that the variation of f_{LHR} along the path when ions are included would be much the same if reflection did not occur. The predictions of section 7.2 are borne out; namely that propagation transverse to the field can (and does) take place for frequencies below f_{LHR}. For the rays traced from a latitude of 30^{o}, for example, the minimum value of f_{LHR} along the path was almost 3 KH_z, and reflection was observed only for frequencies below 4 KH_z.

In Figure 35 we have plotted the final latitude against frequency for the 1 ion case. For frequencies above the minimum f_{LHR} the behaviour is again much the same as in the no-ion case, and evidence of latitude focussing is not well supplied. For frequencies below the minimum f_{LHR}, which is where latitude focussing was apparent to some extent in the no-ion case, the rays do not even reach the ionosphere in the opposite hemisphere. Viewed in conjunction, these results certainly do not support the formation of observed whistlers; and this can be taken as further evidence that some other guiding mechanism such as field-aligned enhancement must apply

/to....

to explain the observed effects.

It will be seen that on curve e in Figure 35 a final latitude of 27° is plotted for a frequency of 1 KH_z, which we should expect to have been reflected. This is thought to be a result of the finite processes involved in numerical integration causing overstepping of the point where reflection should have taken place; this difficulty is to be discussed more fully in the next section.

In Figures 36 and 37 are presented the dispersion and time of travel curves. It is seen that, except at very low latitudes, the frequencies for which the dispersion was constant in the no-ion case are those which are now reflected.

In Figure 38 we have plotted the maximum altitude (attained on the first crossing of the equator) as a function of frequency for rays from 30°. This is seen to remain substantially constant for frequencies below about 10 KH_z, i.e. even above the minimum f_{LHR}. This indicates that up to this point along the path spatial coherence is observed in whistler paths, even without field aligned ducts, and that in fact the defocussing occurs further down the path where propagation is more nearly or exactly transverse.

The acute angle between wave-normal and field direction has much the same behaviour above f_{LHR} as

/it....

it had in the no-ion case, becoming almost 90° before being bent back rapidly as the ray re-enters the ionosphere. Below f_{LHR} the behaviour is much the same, except that the value of 90° is attained. (See Figure 42).

The reflection phenomenon is perhaps the most interesting aspect of these results, and we have plotted the ray paths for frequencies below 5 KH_z from an initial latitude of 30° in Figures 40 and 41. Lower frequencies are seen to penetrate less into the opposite hemisphere before being reflected. In addition, a resonance effect can be observed, for frequencies less than 600 H_z, which are reflected back after only a few hundred Km of travel. (See also Figure 43). Closer investigation revealed that this was occurring for wave frequencies with values of the proton gyrofrequency, i.e. where $Y_H^+ = I$; in the topside ionosphere at the latitude concerned the electron gyrofrequency is of the order of 1200 KH_z, so that the proton gyrofrequency is of the order of 600 H_z, which is the frequency at which the effect was observed. Now it is well known that the upper cut-off frequency for waves propagating in the whistler mode is of the order of the electron gyrofrequency at the top of the path; (for $Y < 1$ the

/whistler-.....

whistler-mode phase refractive index for purely longitudinal propagation becomes imaginary). The results of this study indicate that a lower cut-off frequency might be governed by the proton gyrofrequency at the start of the path.

The effect of trying different initial values of δ_o, the angle between wave normal and field line, was investigated to a limited extent, and Figures 44 and 45 are representative of the results obtained. YABROFF[15] reported that in the no-ion case the final latitude was the same for quite a wider range of δ_o, this is found to be the case here for frequencies above the minimum f_{LHR} along the path. However, for f = 1 KH_Z the ray path is seen to be strongly dependent on the initial wave normal direction, and "subprotonospheric" whistlers of the type investigated by KIMURA[1] are readily predicted.

This raises the interesting possibility of being able to "avoid" the reflection process by a suitable choice of initial wave-normal angle. In fact the dependence on the initial wave-normal angle should, in the author's opinion, receive more attention than has hitherto been the case. It has not been possible in this instance to implement this recommendation as would have been liked, owing to a lack of time; perhaps the matter can receive attention at a later

/Date. ..

date. Some further considerations of this aspect of ray tracing will be presented in the next chapter.

7.5 Comparison with the results of KIMURA and of SHAWAN

KIMURA[1] was concerned in his ray tracing study mainly with explaining the sub-protonospheric whistler, and presents only one ray path traced through the exosphere; for a wave frequency of 1 KH_Z, initial altitude 300 Km, initial latitude 30°, initial wave normal direction radially outward. SHAWAN[18] was concerned mainly with trying to find explanations of multi-component, hook and riser whistlers. However he also traces a ray for the initial conditions outlined above. The author, in turn, traced the same ray; the object of the exercise being, in both of the latter cases, to check on the accuracy of the programs used.

These three rays are presented together for comparison in Figure 46. It will be seen that the rays of KIMURA and of the author are very similar, being reflected at a latitude of about 24°S; whereas SHAWAN'S ray penetrated into the ionosphere in the opposite hemisphere, much as in the no-ion case.

These discrepancies are regarded by the author as fairly serious, and may point to a fundamental

/weakness...

weakness in the whole concept of numerical ray-tracing. It is, of course, tempting to conclude that SHAMAN has a mistake in his program. It is reasonable to conclude that this is unlikely.

We have made several attempts to duplicate SHAMAN'S path with our program (without overwhelming success). By varying the initial conditions slightly and by varying the size of step length used in the integration process. Our program was used in this case with basic step length $\delta s = 2000$. Reducing this length seemingly had little effect. Nor did increasing it to 18,000 except that the effects of rounding errors were apparent. However, as can be seen from Table 5, a point is reached where reflection is not detected, and the ray penetrates through to the opposite hemisphere for step lengths greater than 18400.

The results presented in Table 5 should not be taken too seriously; for these large step lengths rounding errors are bound to predominate; but they serve to emphasize the problem confronting us, which is essentially this: when the wave normal becomes transverse to the field, reflection is not excluded as a physical possibility. However if this transverse condition is approached in finite steps, it must be possible to step right over the critical situation, and so not observe reflection; as will occur easily

/if...

if too large a step length is employed.

It is hard to fault SHAWAN on these grounds, because he is aware of exactly this difficulty, and has most carefully reduced his step length whenever Ψ tends to 90°. However it is possible that he used large step lengths in the initial stages of his computation, for the region below about 2000 Km, where the direction of the wave normal may fluctuate extensively; since the behaviour of his wave normal is rather different from that found in the present case, remaining almost vertically upwards over the whole of the first 2000 Km of travel. Further, at a latitude somewhere between 0°and 10°his diagram would seem to indicate that a region of transverse propagation must have been passed through.

This does not settle the question of which ray, if either, would be observed in practice. SHAWAN presents arguments as to why his path should be correct and KIMURA'S incorrect. Most plausible is the retraceability test; however this was also successfully applied in the present study. SHAWAN also assumed that the behaviour of the wave normal must have been very nearly the same in both cases (KIMURA did not indicate the behaviour of his wave normal) and found that at KIMURA'S reflection latitude his value of Ψ was only 45°, thus ruling out transverse propagation.

/Further,....

Further, at this latitude he found ρ_r to be zero, and suggested that the sign of ρ_r did not change as it sent through zero- resulting in an abrupt change in Ψ and hence "reflection". This is certainly not borne out by the present study, so that SHAWAN'S arguments on those lines must be refuted.

Finally, SHAWAN claims that the explanations of V.L.F. noise phenomena which he then subsequently presents exhibit quantitative agreement with observed phenomena, and concludes that this vouchsafes for the correctness of his program. In the author's opinion this is a risky statement, whether applied to SHAWAN'S, the present or any other ray tracing study. We have shown that it is possible to step through the reflection condition. Should this occur, it is very possible that quantitative agreement with the "observed phenomena" could be achieved; if indeed the term "quantitative agreement" has much significance in the context of accuracy. We must try, in a study of this nature, to explain the latitude focussing, travel times and dispersions of observed whistlers, and also the paths of travel insofar as it is known that they start and end at conjugate points of a field line. The whole of the path cannot be observed in practice with modern experimental techniques, nor can the behaviour of the wave normal, so that these are

/secondary...

secondary effects.

We have seen that the latitude focussing predicted in this way is insufficient to account for the production of observed whistlers. Nor has our program predicted the correct values of dispersion and travel times, although this is not regarded as very serious, as we have not taken into account the effects of the lower ionosphere, nor investigated throughly the effects of other ion compositions; effects which must surely be taken into account by virtue of the complex behaviour of the ionosphere and exosphere.

As has been remarked previously, it has not been possible to date to investigate fully the effects on the reflection phenomenon of slightly varying the initial wave normal angle. It is conceivable that quantitative agreement with observed phenomena could be achieved in this way by trial and error. However this would not be profitable on a slow computer such as was at our disposal, and for that reason had to be shelved as a workable project. SHAWAN'S attention seems to have been attracted by multipath propagation of this type; but he claims that his autocode program could calculate 10 points/sec, which is somewhat faster than the 10 secs/point estimated for our program.

/Conclusion.

7.6. Conclusion.

It is the author's conclusion that ray-tracing of this nature can sensibly be taken only as a first approximation to explaining the behaviour of V.L.F. signals in the exosphere. The effects of rounding errors can be minimized by subtle numerical analysis and stable integration procedures; but there is a danger of stepping through reflections which it is felt has not been fully realised up until now.

Table 4.

Comparison of ray paths for the no-ion, 1 ion and 3 ion cases.

a. Rays starting from a latitude of 30° at an initial altitude of 300 Km, vertically upwards.

f KH_z	No ions	Top of path r	Top of path Θ	Reflection Latitude	Final Latitude	time secs.
.7	0	5318	-7	-	-41	.34
	1	5495	-11	-22	-	-
	3	5512	-10	-22	-	-
1	0	5311	-10	-	-43	.29
	1	5425	-11	-23	-	-
	3	5177	-10	-24	-	-
2	0	5283	-9	-	-43	.21
	1	5336	-9	-28	-	-
	3	5341	-9	-28	-	-
3	0	5243	-7	-	-43	.18
	1	5280	-8	-32	-	-
	3	5283	-8	-32	-	-
4	0	5211	-8	-	-41	.16
	1	5232	-7	-34	-	-
	3	5235	-7	-34	-	-
5	0	5180	-7	-	-41	.15
	1	5205	-7	-	-43	.16
	3	5210	-7	-38	-	-
10	0	5000	4	-	-39	.12
	1	5015	-5	-	-40	.12
	3	5020	-5	-	-40	.12
50	0	3720	3	-	-27	.08
	1	3725	3	-	-28	.08
	3	3725	3	-	-28	.08
100	0	2520	8	-	-16	.06
	1	2520	8	-	-16	.06
	3	2520	8	-	-16	.06

/b. ....

b. Rays starting from a latitude of 30° at an initial altitude of 1000 Km, along the field line.

f KH_z	No ions	Top of path r	Top of path Θ	Reflection Latitude	Final Latitude	time secs
.7	0	10687	-11	-	-43	.27
	1	10669	-12	-23	-	-
	3	10853	-11	-23	-	-
1	0	10690	-9	-	-41	-23
	1	10640	-10	-26	-	-
	3	10780	-10	-25	-	-
2	0	4318	-10	-	-41	.17
	1	10632	-12	-30	-	-
	3	4328	-12	-29	-	-
3	0	4310	-10	-	-41	.15
	1	4313	- 8	-33	-	-
	3	4314	- 8	-33	-	-
4	0	4310	- 8	-	-41	.12
	1	4284	- 9	-	-41	.14
	3	4314	- 9	-	-41	.16
5	0	4310	- 8	-	-39	.11
	1	4287	- 9	-	-40	.12
	3	4309	- 9	-	-41	.12
10	0	4270	- 6	-	-38	.08
	1	4262	- 6	-	-39	.09
	3	4272	- 6	-	-39	.09
50	0	4850	0	-	-28	.07
	1	4851	0	-	-28	.06
	3	4851	0	-	-28	.06
100	0	3195	8	-	-19	.06
	1	3195	8	-	-19	.06
	3	3195	8	-	-19	.06

Altitudes are given in Km; latitudes in degrees.

Table 5.

Effects of using different initial step lengths on the path of the 1 KH_z ray from an altitude of 300 Km at a latitude of 30o.

Step length δS	Maximum Altitude	Reflection Latitude	Final Latitude	time secs.	
				(a)	(b)
2000	5177	-24	-	.30	-
10000	4664	-22	-	.28	-
15000	4118	-24	-	.27	-
18000	3839	-22	-	.30	-
18300	3044	-27	-	.26	-
18380	2251	-32	-	.27	-
18390	2860	-37	-	.32	-
18395	2552	-40	-	.32	-
18397	5638	-43	-	.51	-
18398	6939	-48	-	.46	-
18399	2446	-	-59	-	.45
18400	2434	-	-55	-	.43
18410	2410	-	-46	-	.37
18420	2200	-	-42	-	.32
18430	2123	-	-38	-	.32
18500	1735	-	-16	-	.28
19000	1091	-	-11	-	.39

Time (a) is the time taken to reach the reflection point.

Time (b) is the time taken to reach an altitude of 500 Km.

Altitudes are given in Km; Latitudes in degrees.

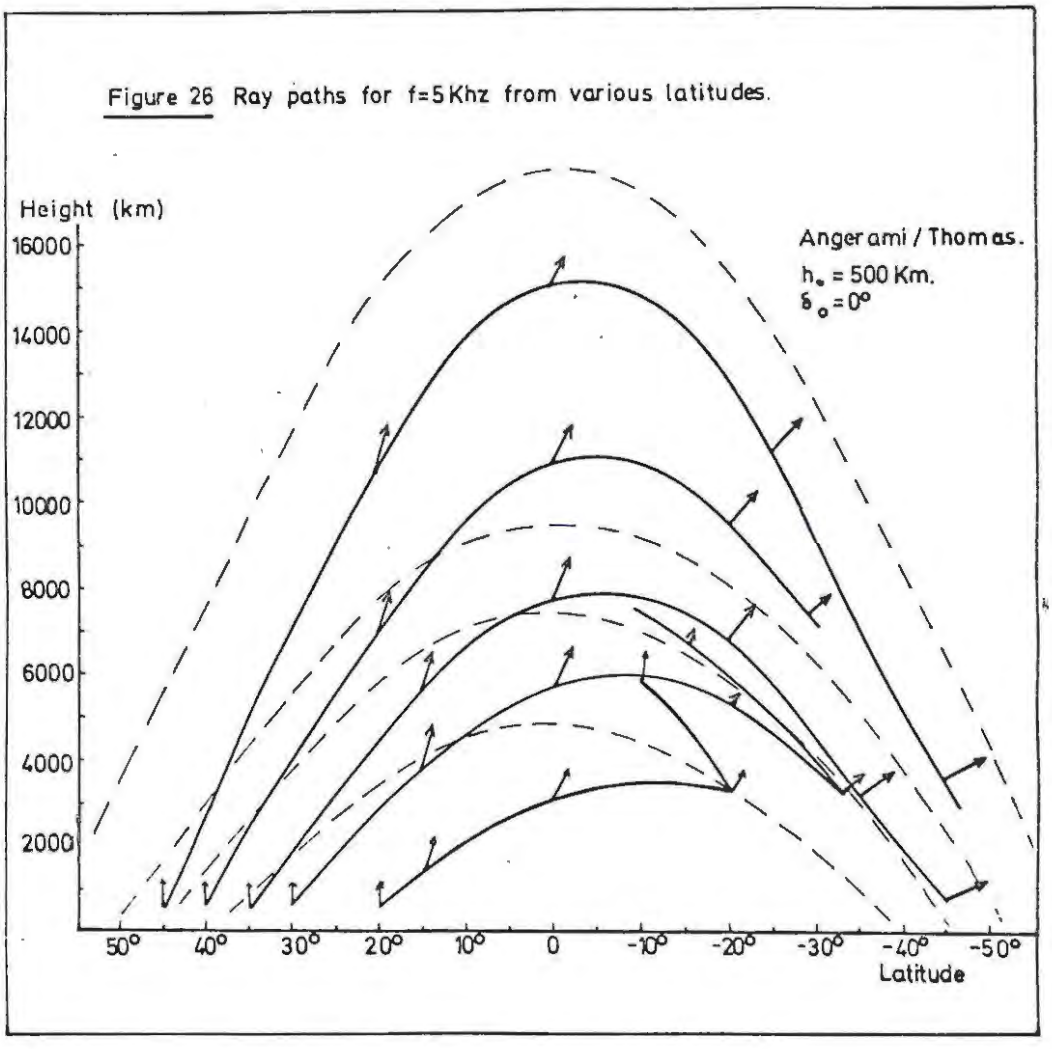

Figure 26 Ray paths for f=5 Khz from various latitudes.

Figure 27. Ray paths from 20°. 1 Ion (H^+) considered.

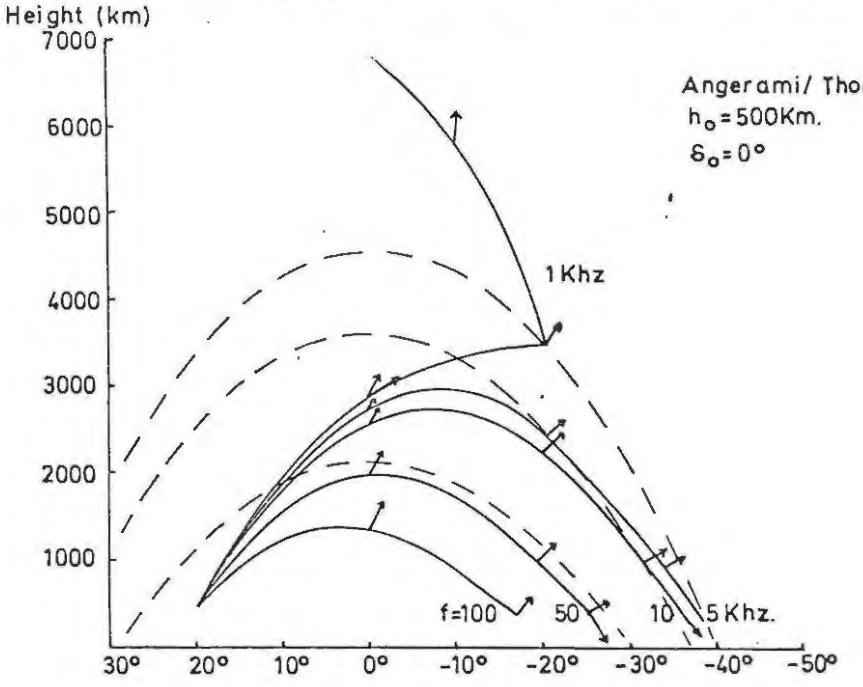

Figure 28 Ray paths from 20° along field initially. 1 Ion.

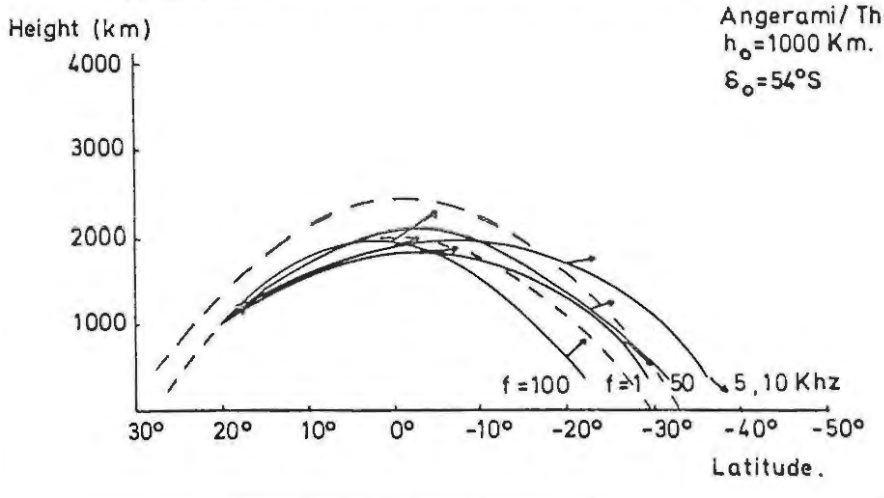

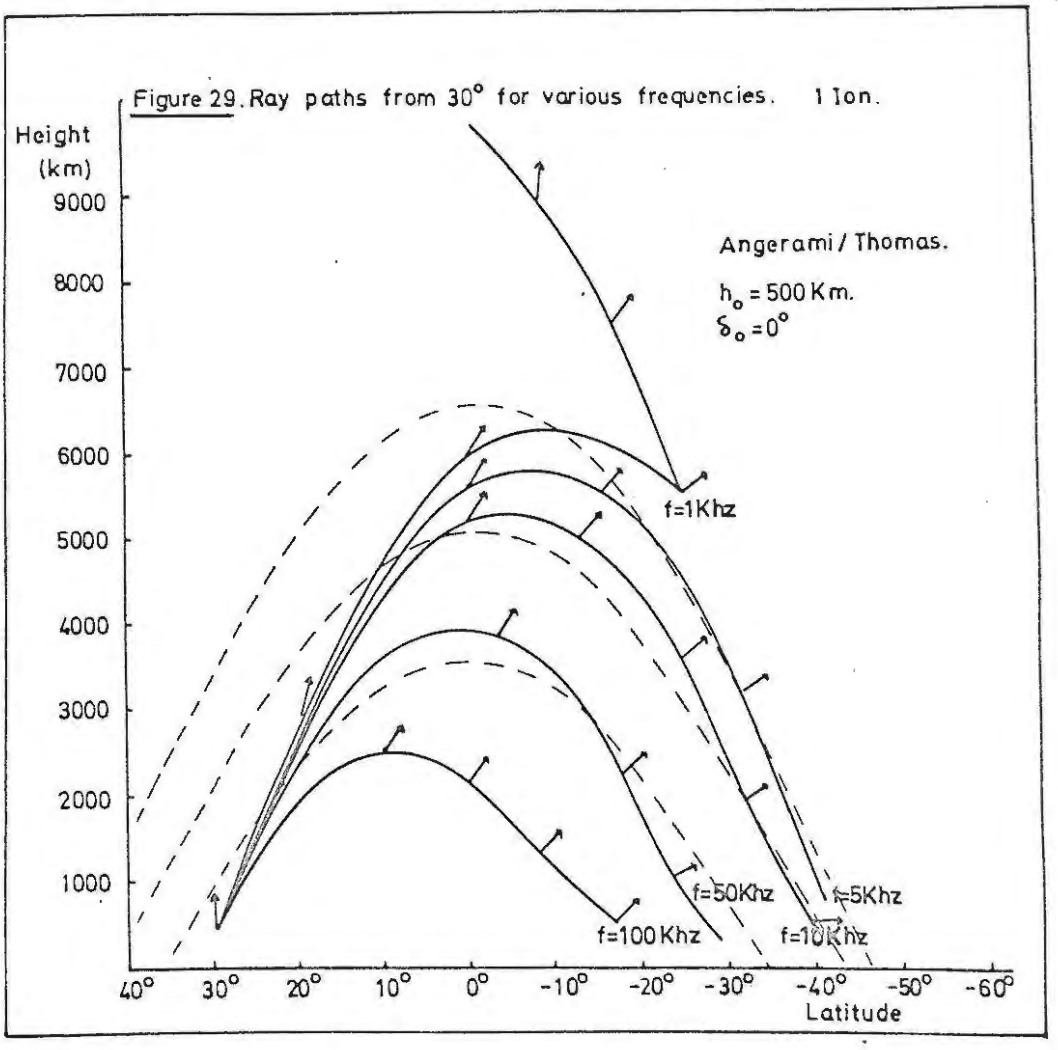
Figure 29. Ray paths from 30° for various frequencies. 1 Ion.
Height (km)
9000
8000
7000
6000
5000
4000
3000
2000
1000
Angerami / Thomas.
h_o = 500 Km.
δ_o = 0°
f=1Khz
f=5Khz
f=10Khz
f=50Khz
f=100Khz
40° 30° 20° 10° 0° -10° -20° -30° -40° -50° -60°
Latitude

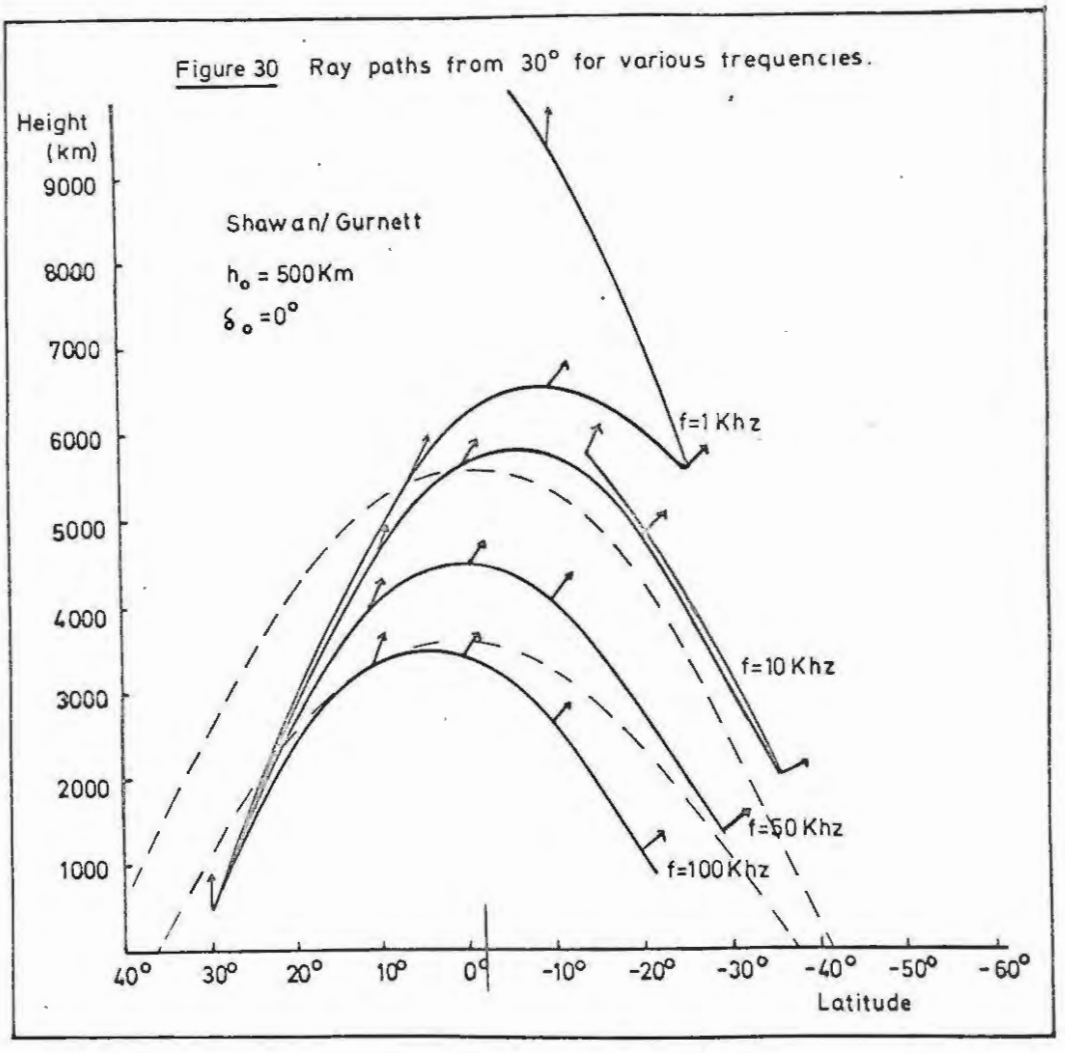

Figure 30 Ray paths from 30° for various frequencies.

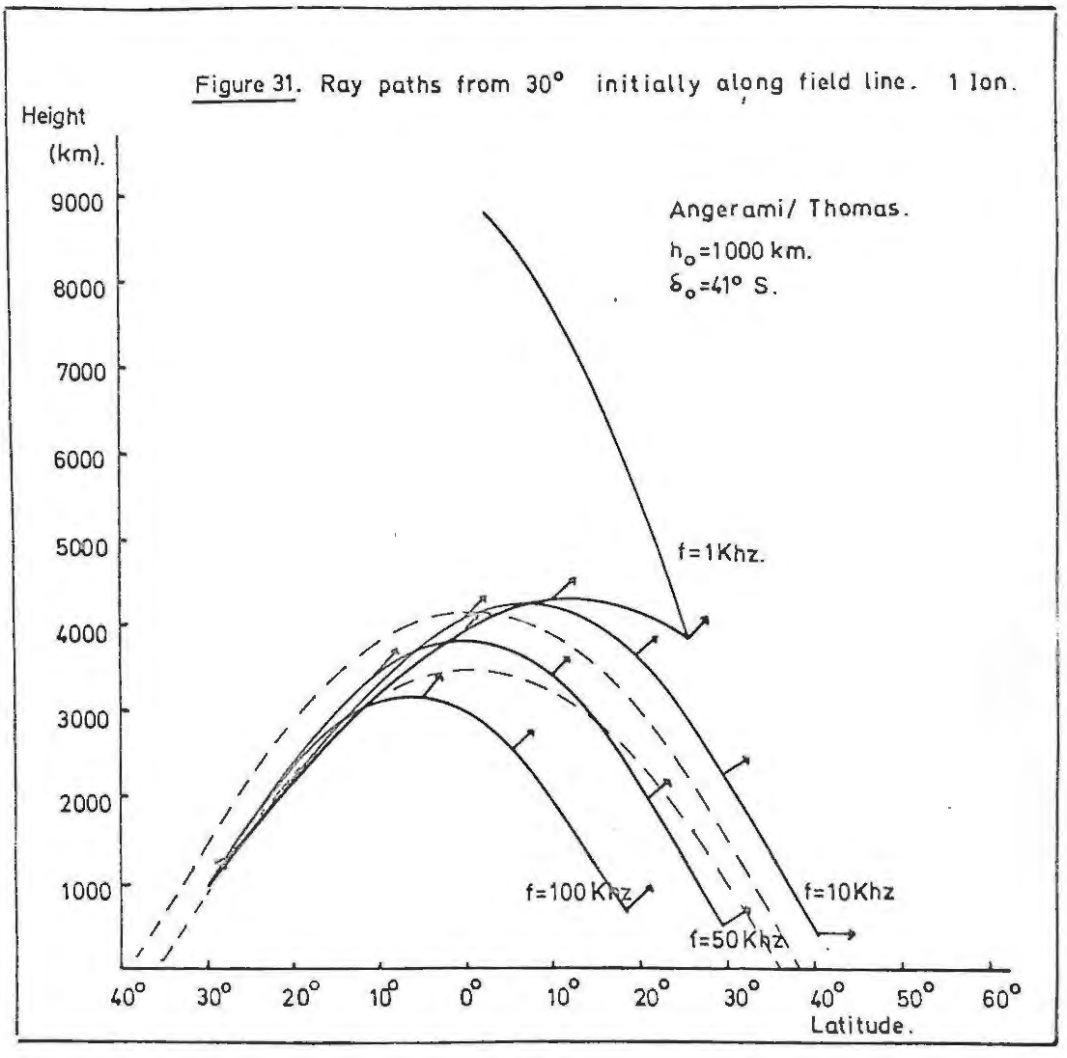

Figure 31. Ray paths from 30° initially along field line. 1 Ion.

Figure 32 Ray paths from 40° for various frequencies. 1 Ion.

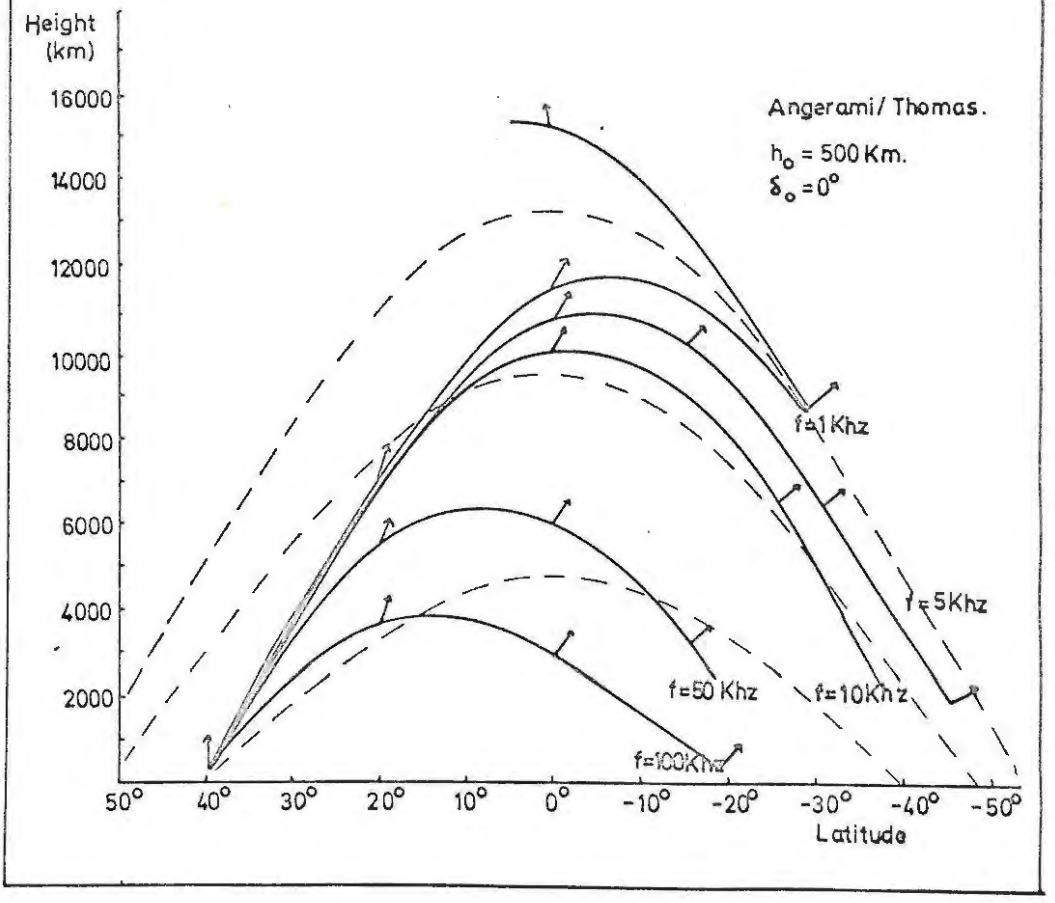

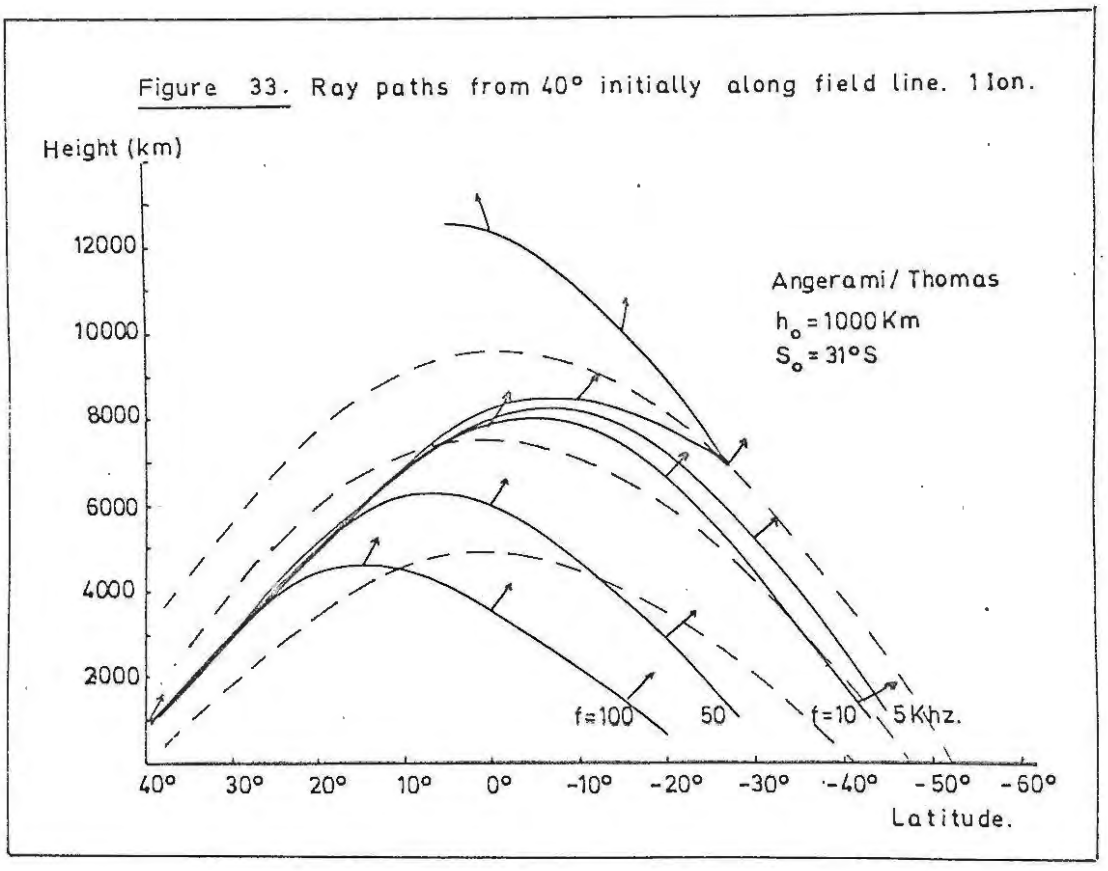

Figure 33. Ray paths from 40° initially along field line. 1 Ion.

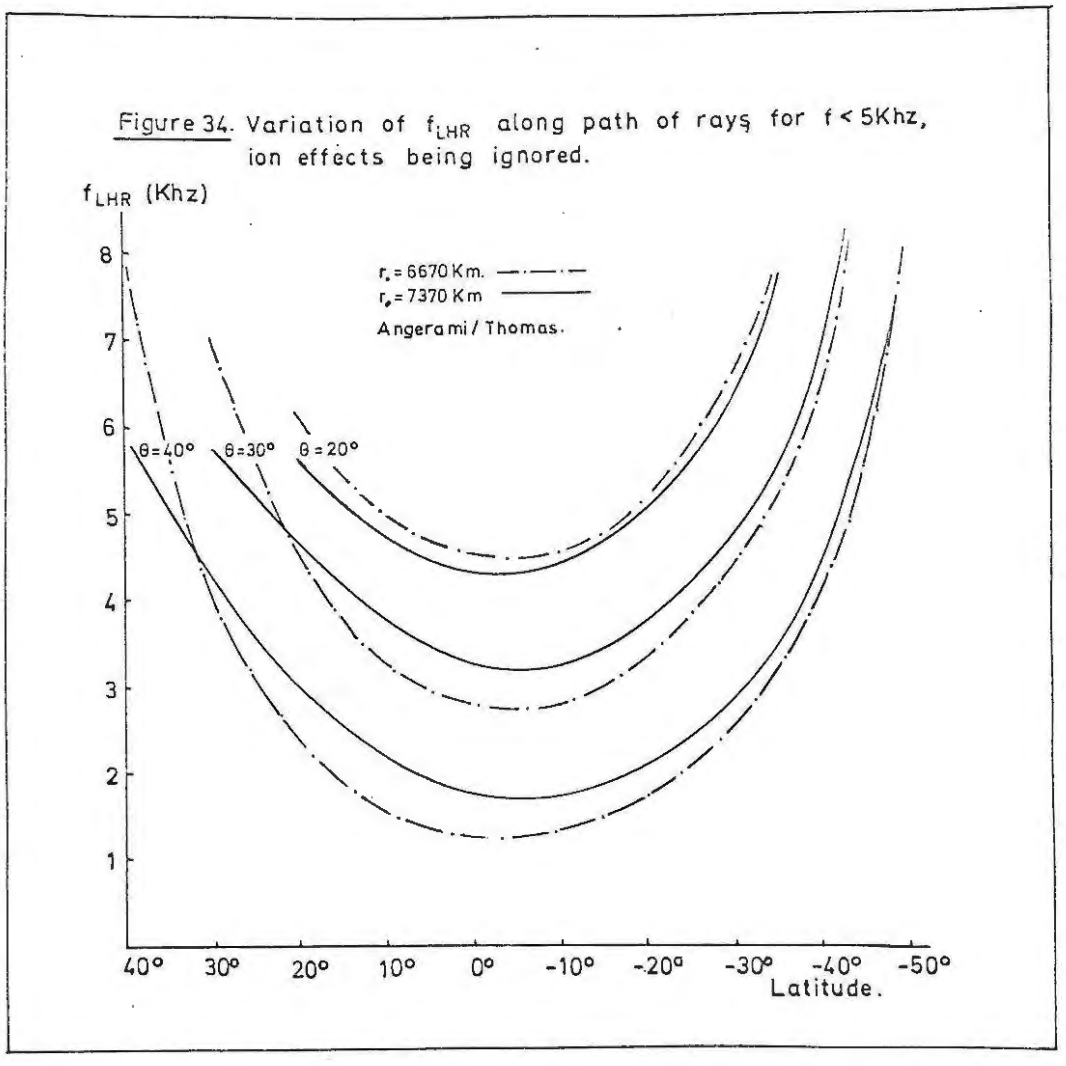

Figure 34. Variation of f_{LHR} along path of rays for f < 5Khz, ion effects being ignored.

Figure 35. Final latitude against frequency. 1 Ion.

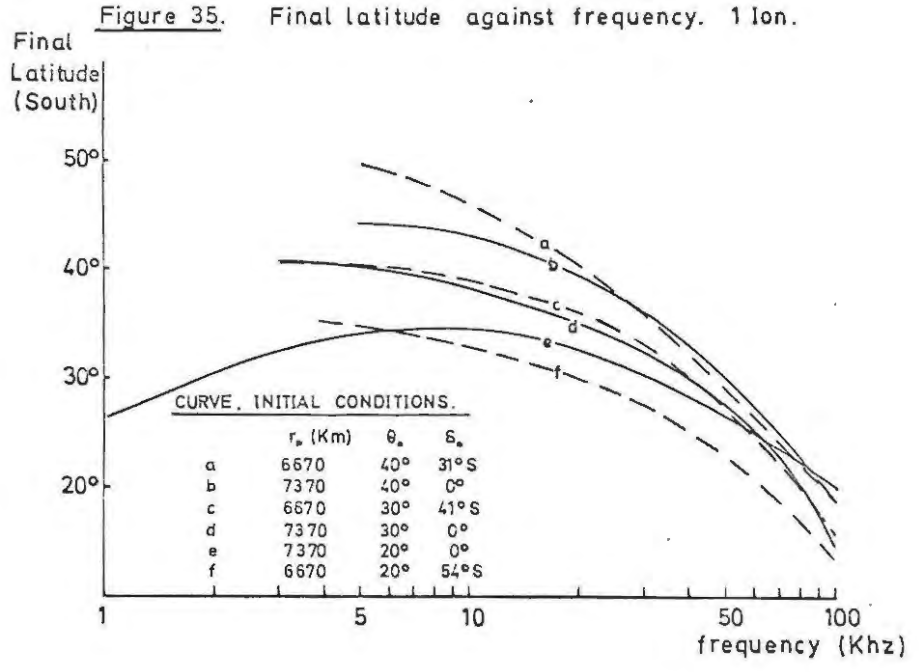

Figure 36 Dispersion and travel times for rays initially vertical, 1 Ion considered.

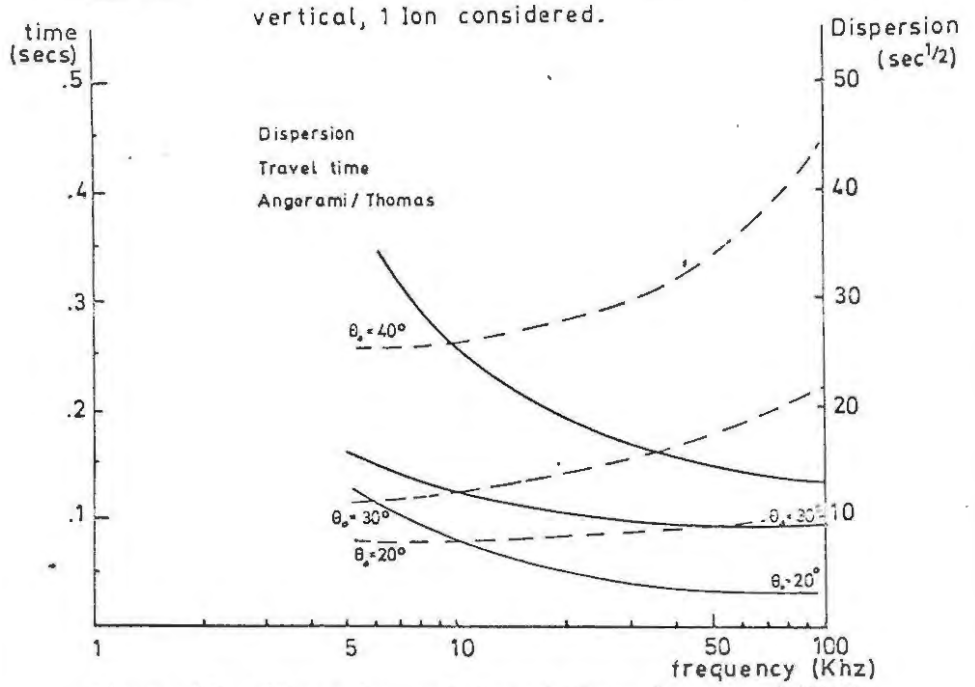

Figure 37 Dispersion and travel times for rays initially along the field, 1 Ion considered.

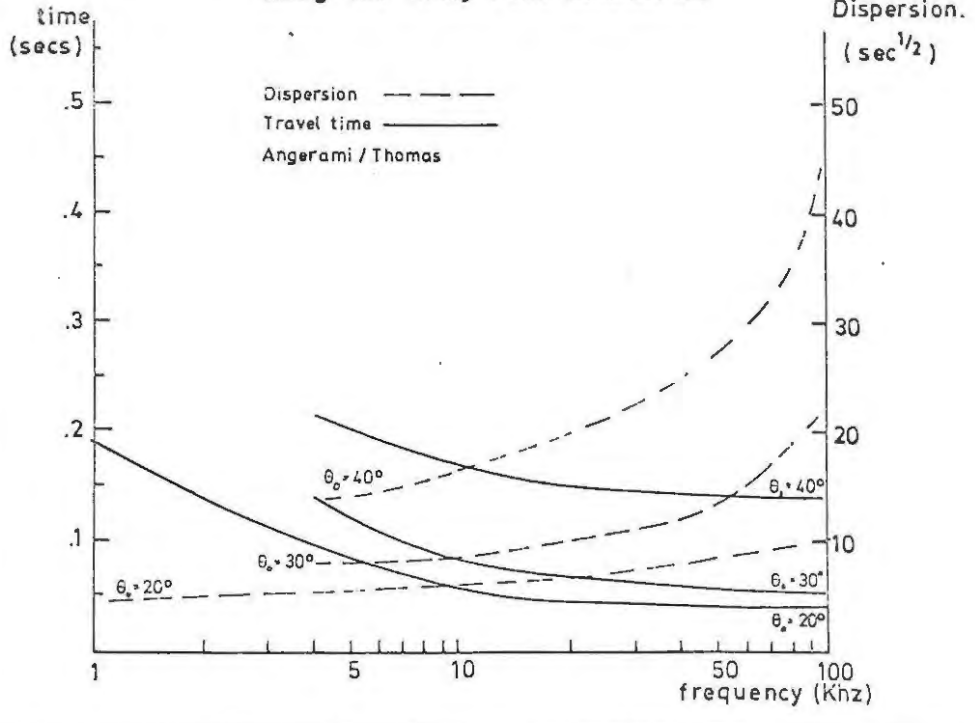

Figure 38. Maximum altitude as a function of frequency for rays from 30°

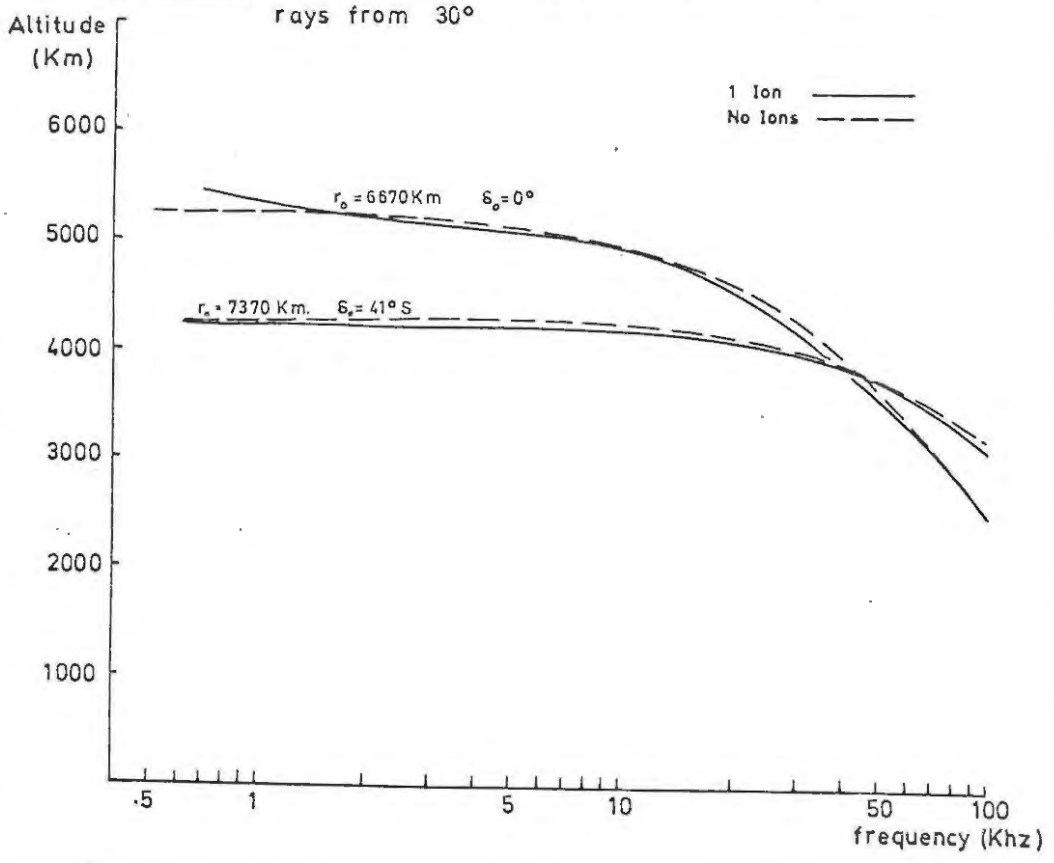

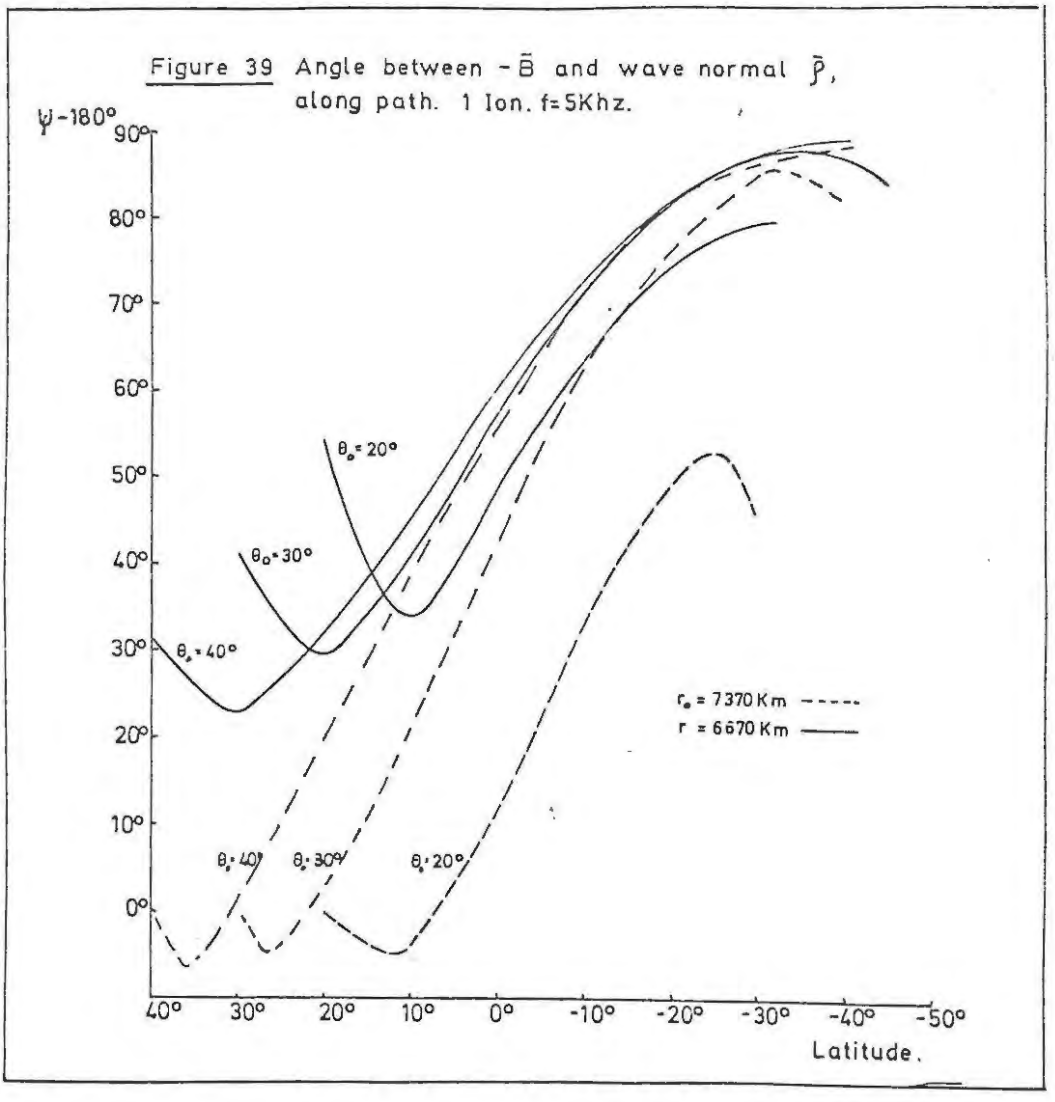
Figure 39 Angle between $-\bar{B}$ and wave normal $\bar{p}$, along path. 1 Ion. f=5Khz.
ψ-180°
90°
80°
70°
60°
50°
40°
30°
20°
10°
0°
θ₀=20°
θ₀=30°
θ₀=40°
r₀ = 7370 Km
r = 6670 Km
θ₀=40°
θ₀=30°
θ₀=20°
40°
30°
20°
10°
0°
-10°
-20°
-30°
-40°
-50°
Latitude.

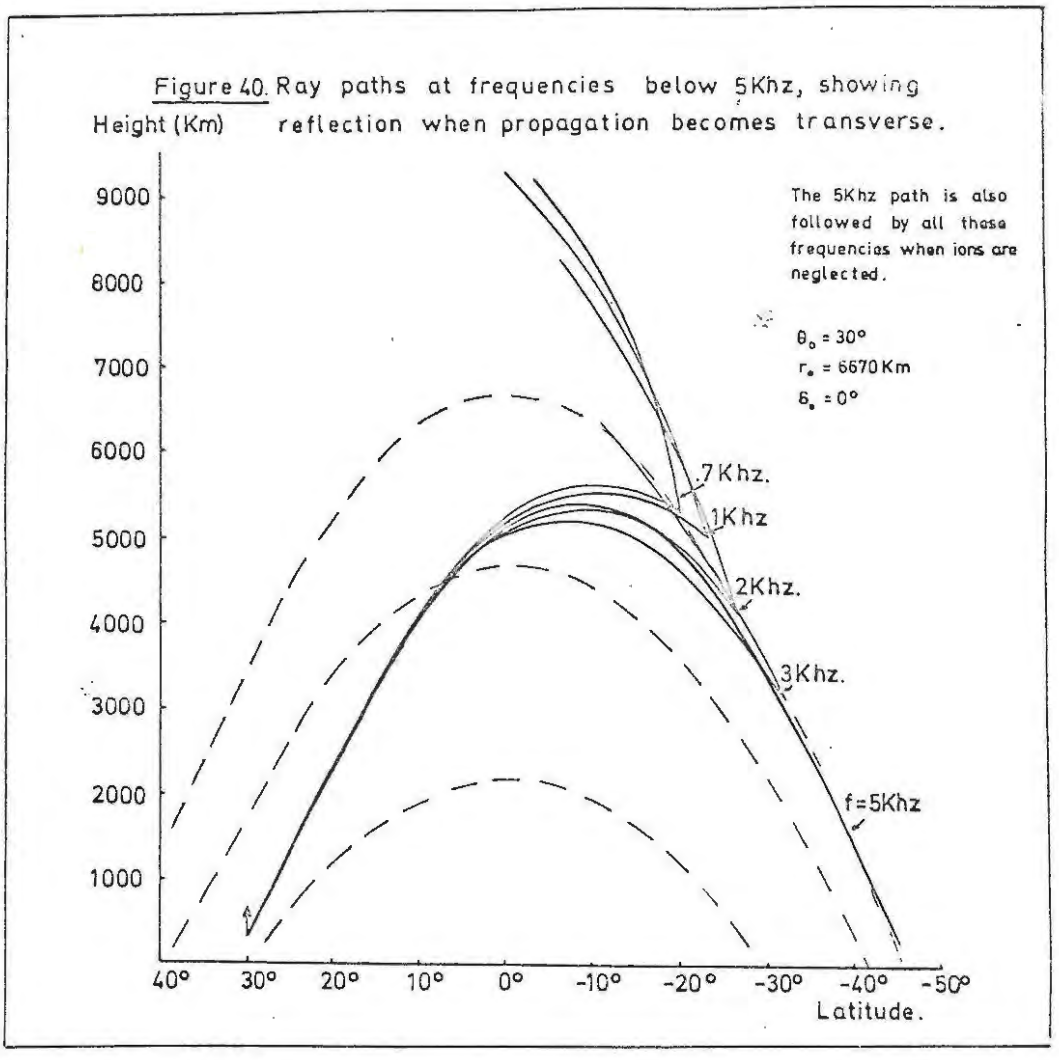

Figure 40. Ray paths at frequencies below 5Khz, showing reflection when propagation becomes transverse.

Figure 41 Ray paths below 5Khz, initially along field, showing reflection at transverse propagation.

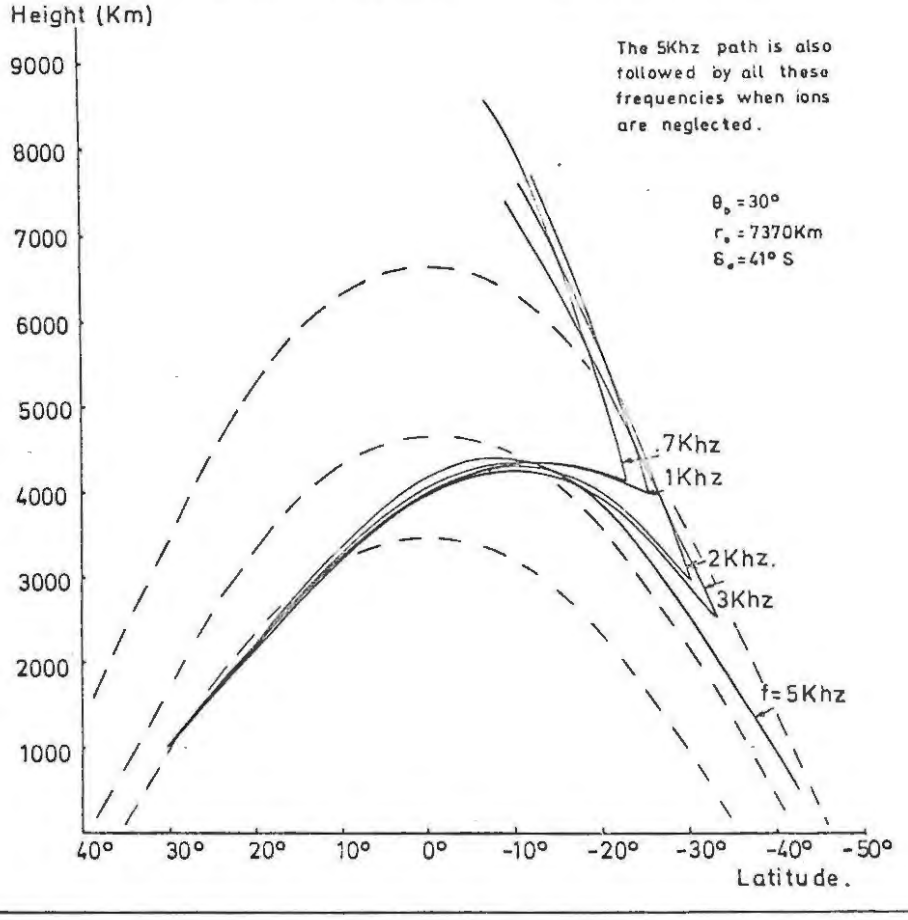

Figure 42. Angle between $-\bar{B}$ and wave normal $\bar{p}$ along path, for frequencies which are reflected. 3 Ions considered.

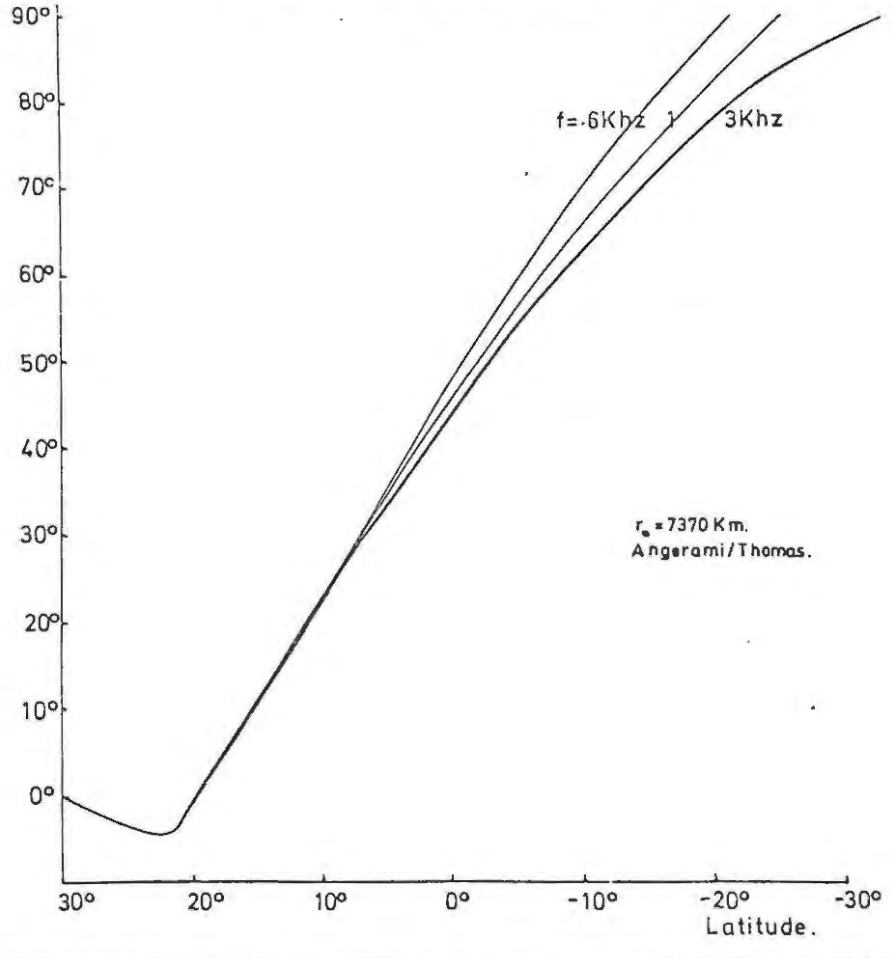

Figure 43. Latitude of reflection as a function of frequency.
Angerami / Thomas 3 Ion model.

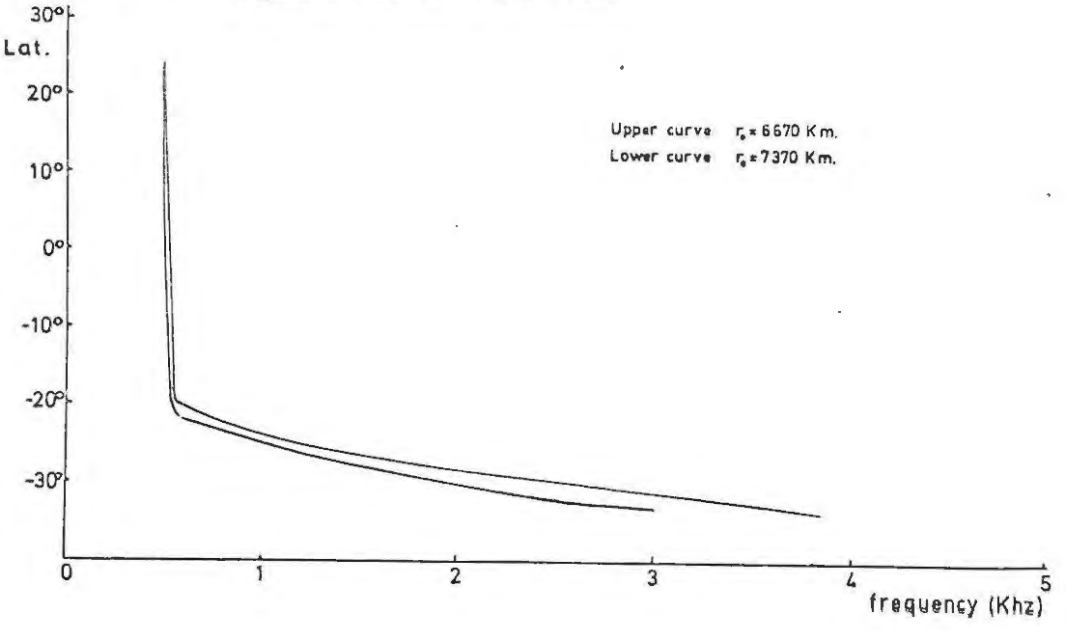

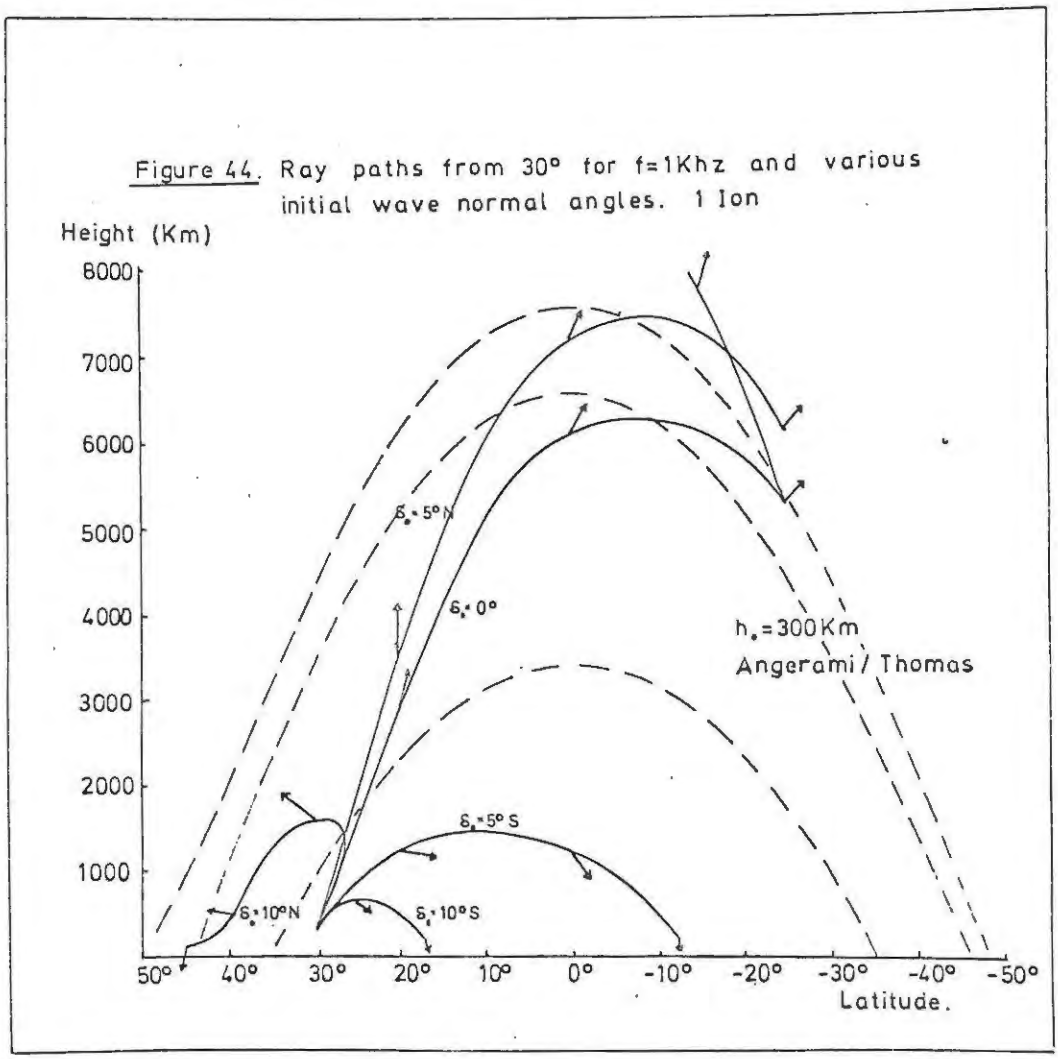

Figure 44. Ray paths from 30° for f=1Khz and various initial wave normal angles. 1 Ion

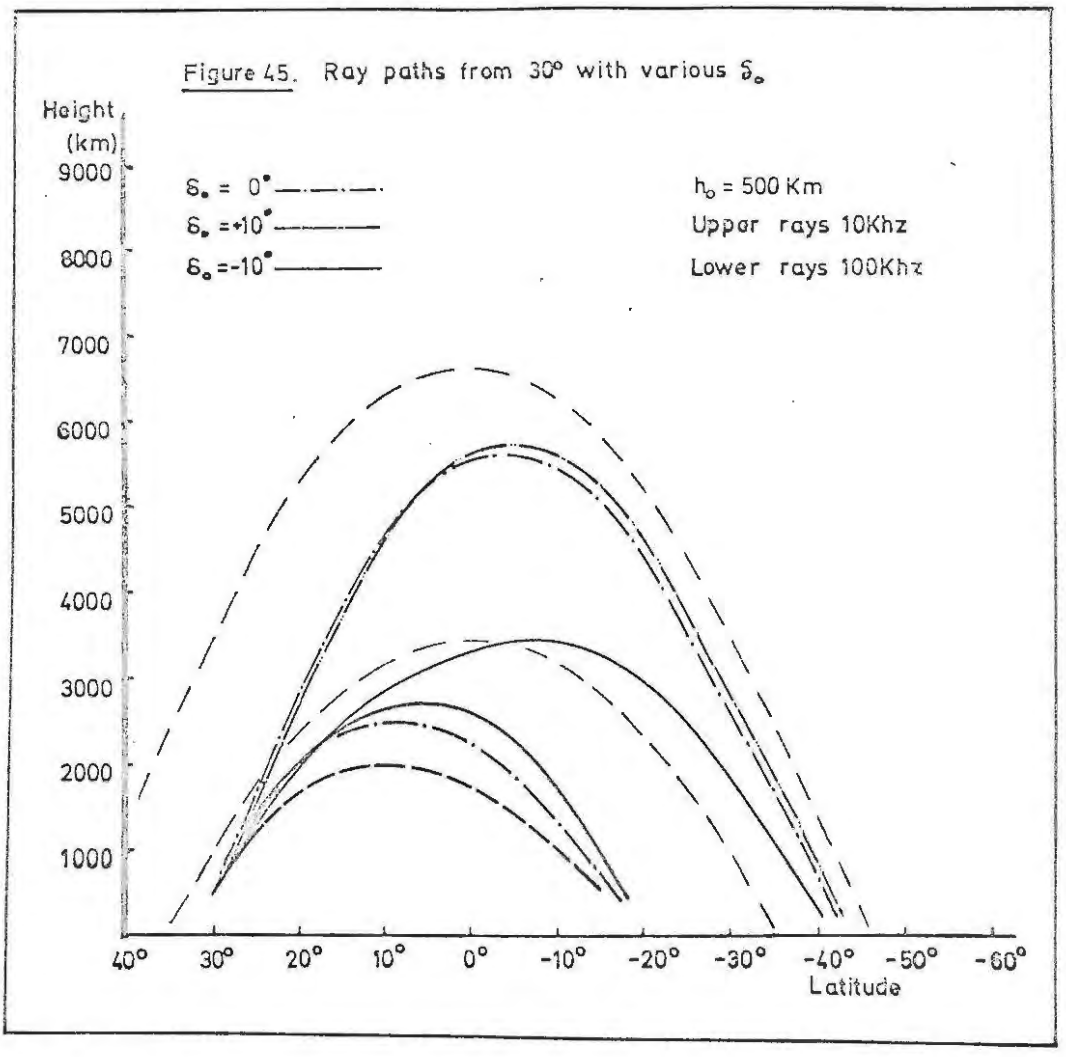

Figure 45. Ray paths from 30° with various δ_0

Figure 46. Comparison with Kimura and with Shawan.

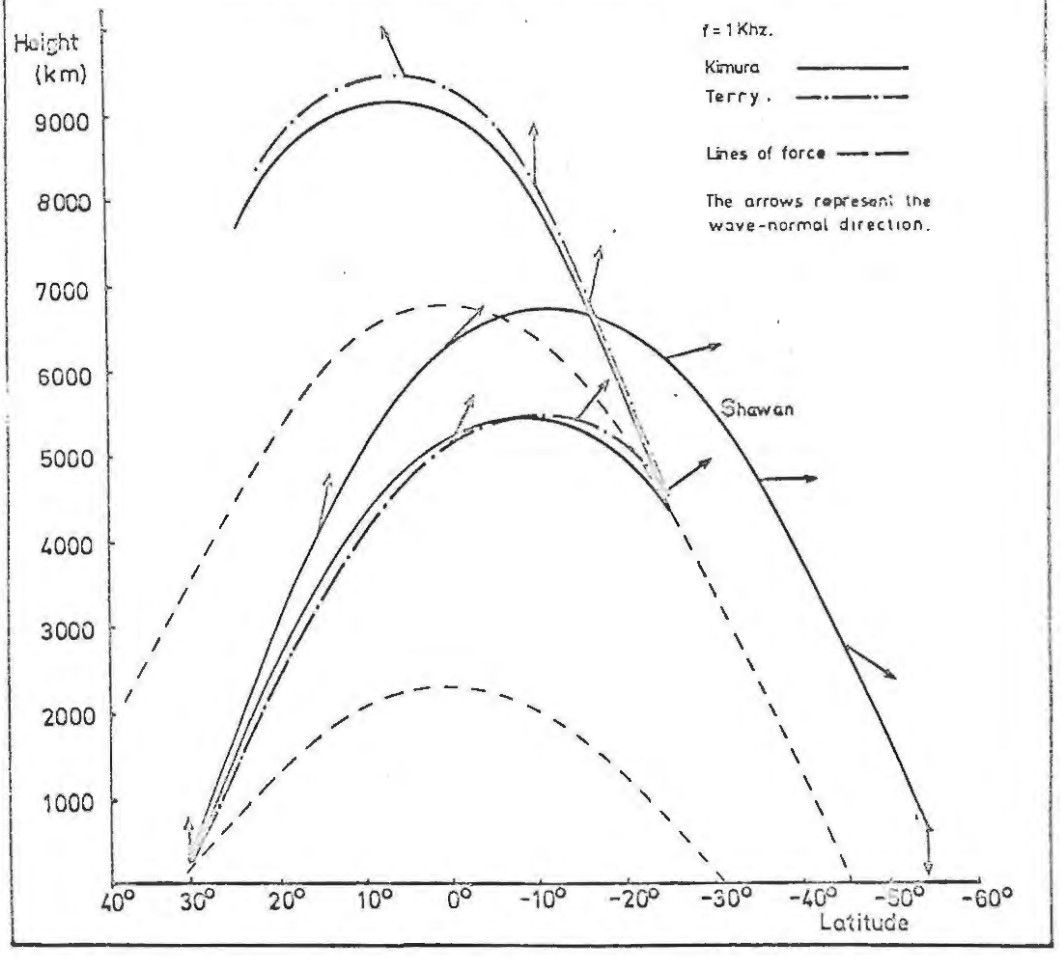

Chapter 8.

Ray-tracing through the topside ionosphere.

8.1. Introduction.

As has been stated previously, the greatest changes in the behaviour of a ray can be observed in the ionosphere proper, where the gradients of refractive index are most severe. It is therefore of interest to perform some ray-tracing studies confined to this region alone. In the following sections we present the results of such studies for the two opposing cases of starting integration down from the top of the ionosphere, and of starting integration up from the bottom of the ionosphere; investigating in particular the effects of different initial wave-normal directions. For this purpose the program was modified to include the effect of the F bulge using KIMURA'S[1] simple formula as given in Chapter 5. Integration was confined between height limits of 100 Km and 1000 Km.

8.2. Integration down from the top of the ionosphere.

Since it is known that exospheric whistler paths follow the field lines closely - presumably in the light of evidence from this and similar studies along field-aligned ducts - it was deemed sufficient to investigate the behaviour of rays coming down from a

/height....

height of 1000 Km (as representative of the top of the ionosphere) with wavenormals aligned, at that altitude, along or nearly along the field. The results of some of these computations are presented in Table 6, and in Figures 47,48,49 for rays traced from 1000 Km at a latitude of 30^{o}.

From Table 6 we see that the behaviour of the rays under these conditions is largely independent of whether or not we take ions into account, even for those frequencies which are well below f_{LHR} (which is of the order of 8-10 KH_z in this area). This is not surprizing; we are dealing with quasi-longitudinal propagation over much of the path, and we have seen in the last chapter how the refractive index surfaces are much the same for $\Psi \sim 0$, whether ion effects are included or not.

From Figure 47 we see that the behaviour of the wave-normal is largely independent of the frequency considered, and is interesting in that it swings from lying along the field to point almost exactly vertically downwards. In fact this behaviour is observed for quite a wide cone of values of Ψ at the starting altitude, as can be seen from Figure 48, rays with wavenormals as much as 30^{o} from the field direction being bent so that their wavenormals point downwards. It should also be noted that this implies

/that....

that the wave-normal is then at quite an angle with the field - at the latitudes considered here it is about 36^{o}, which is outside the cone of 19.5^{o} within which the anisotropy caused by the magnetic field is held responsible for accurate guiding. (STOREY[5]).

Although the wave-normal is always bent in this way, the final latitude reached at a height of 100 Km depends quite strongly on the initial wave normal angle, as can be seen from Figure 49, where we have plotted the final latitude at 100 km, as a function of the initial value of Ψ at 1000 Km for rays of 5 KH_z at an initial latitude of 30^{o}. The rays are seen to spread over a latitude range of nearly 2^{o}, which represents a great circle distance on the earth's surface of the order of 200 Km. This may help to explain simply why fixed frequency whistler-mode signals are sometimes detected at some distance from the theoretical conjugate point of the transmitter.

The behaviour of the wave normal in these circumstances is interesting in that it will be tied up with the problem of transmission of energy through the ionosphere to the point where it is to be received. It is fairly obvious that there will be preferred angles between field and wave-normal for optimum transmission, as a careful study of the reflection and transmission coefficients would reveal - a study

/which...

which would have to be undertaken on a "full-wave" theory basis.

As a first step towards this study, some preliminary work was started during the course of this project to investigate the transmission coefficient of a sharply bounded ionosphere to see what effect incidence at various alignments to the field would have, the idea being ultimately to extend the treatment to slowly varying media. Unfortunately snags developed in the method, thought to be due to instabilities in numerical processes, and these could not be solved in time for inclusion into the present thesis.

8.3. Integration up from the bottom of the ionosphere.

The results of the previous section have shown that for quasi-longitudinal rays incident on the ionosphere from above the wavenormal is bent to point almost vertically downwards by the time the bottom of the ionosphere is reached, and that this occurs for quite a wide range of values of Ψ_o. This would seem to imply that, for rays penetrating the ionosphere from beneath, the behaviour of the rays and especially of the wave normal should be strongly dependent on the initial value of wave-normal angle. Accordingly, some rays were traced to

/investigate...

investigate this behaviour, and the results are presented in Table 7 and in Figures 50,51,52 and 53, for an initial altitude of 100 Km at a latitude of 30^{o}.

From Table 7 we see that the behaviour of the rays is again largely independent of whether or not we take ions into account, even at frequencies below f_{LHR}. This is more surprising than in the previous section, since a ray with wave-normal initially vertical is already subtending an angle of about 40^{o} with the field direction, and we should expect to observe ion effects, especially if this angle were to increase (as it frequently does). The author is led to believe that coincidence more than anything else led to these effects remaining undetected, although it must also be remembered that at these altitudes H^{+} is not the predominant ion species, and hence the term X_{H+} will not have a significant effect.

From Figure 50 we see that the behaviour of the wave-normal for rays initially vertical is much the same over a wide frequency range; and, as is to be expected, is the reverse of that observed for the rays in the previous section in that the wave-normal is now bent to lie approximately along the field lines at a height of 1000 Km. Note that in this figure we have plotted $\Psi-180^{o}$ (Ψ being measured from polar axis

/along...

along $\overline{B}$) to give the acute angle between field and wave normal, measured from a polar axis along $-\overline{B}$. This has also been done in Figure 51, where we have plotted the acute angle between wave normal and field line as a function of height for a frequency of $5KH_Z$ for rays starting at various angles to the vertical. It is at once apparent that ray tracing predicts that only rays with wave-normals initially vertical will penetrate into the exosphere successfully; as little as 5^o either way from vertical initially finds the transverse propagation condition being reached within a short distance. While this may help explain sub-protonopsheric and other low altitude whistlers, it seems very restrictive on the initial conditions necessary to predict exopsheric whistlers. These results should not be regarded as too highly conclusive, however; we have used a very elementary model of ionosphere, smoothly varying and spherically symmetric. In a real ionosphere the actual penetration through to the exosphere could be considerably more complicated, especially as the effects of collisions would surely be felt. The treatment we have put forward has been done more to show what results are obtained from application of ray tracing techniques than to try to explain the observed phenomena.

/In....

In Figure 52 we have plotted the latitude reached at an altitude of 750 Km as a function of the initial wave-normal angle at 100 Km; and in Figure 53 we present actual ray paths for different initial wave-normal angles. The only real point of interest to be gleaned here is that the guiding effect along the field lines is quite pronounced in all cases, even those for which propagation is tending to become transverse; a condition which must lead to reflection and refraction effects becoming prominent further up the path. (These were not detected by our program, which was set in this case to stop when an altitude of 1000 Km had been reached.)

8.4. Conclusion.

In this chapter we have seen that the application of ray theory to the passage of "exospheric" whistlers through the ionosphere predicts that the wave-normal is bent between the two simple directions of lying along the field at the "top" and lying along the vertical at the "bottom".

We must not forget, however, that we are working in a region where the validity of a ray tracing approach may be in doubt, so that the results outlined above may have to be treated carefully. In the next chapter we have undertaken a study of whether or not we may find ray tracing through the ionosphere justifiable.

Table 6.

Comperison of "no-ion" and "with-ion" ray paths through the ionosphere, traced downwards from 1000 Km at a latitude of 30°.

Freq. (Khz)	Ψ_o	Θ_f	Ψ_f	δ_f	t	Θ_f	Ψ_f	δ_f	t
		No ions				With ions			
.5	-5	33.7	34.8	178.0	.10	33.5	35.7	178.6	.56
.5	0	33.6	35.3	178.4	.10	33.3	36.5	179.2	.52
.5	5	33.4	35.9	178.7	.10	33.2	36.7	179.3	.51
1	-5	34.1	35.7	179.2	.09	34.0	35.9	179.4	.09
1	0	33.9	36.1	179.6	.09	33.9	36.4	179.7	.09
1	5	33.7	36.5	179.6	.09	33.7	36.7	179.9	.09
3	-5	34.1	35.7	179.0	.05	34.0	35.7	179.1	.05
3	0	33.9	36.2	179.5	.05	33.9	36.1	179.3	.05
3	5	33.8	36.5	179.7	.05	33.7	36.5	179.6	.05
5	-5	34.1	35.6	179.0	.04	34.1	35.7	179.2	.04
5	0	34.0	36.0	179.3	.04	33.9	36.0	179.4	.04
5	5	33.9	36.4	180	.04	33.7	36.4	179.6	.04
10	-5	34.1	35.5	179.1	.03	34.1	35.6	179.1	.03
10	0	33.9	35.9	179.3	.03	33.9	36.0	179.4	.03
10	5	33.8	36.4	179.6	.03	33.8	36.4	179.6	.03
50	-5	33.9	33.9	177.2	.01	33.9	33.9	177.2	.01
50	0	33.7	34.5	177.6	.01	33.7	34.5	177.7	.01
50	5	33.5	35.1	178.0	.01	33.5	35.1	178.0	.01

Θ_f = final latitude at 100 Km

Ψ_f = angle between field and wave normal at 100 Km

δ_f = angle between vertical and wavenormal at 100 Km.

Table 7.

Comparison of "no-ion" and "with-ion" ray paths through the ionosphere traced upwards from 100 Km at a latitude of 30°.

Freq. KHz	δ_o	Θ_f	Ψ_f	δ_f	t	Θ_f	Ψ_f	δ_f	t
		No ions				With ions			
.5	-5	21.0	100.5	-126.9	.16	21.2	102.8	-124.9	.18
.5	0	25.0	178.9	-47.6	.14	26.0	182.5	-42.5	.18
.5	5	26.5	261.2	36.1	.13	26.5	260.7	35.6	.30
3	-5	23.0	95.1	-134.7	.06	23.0	94.4	-135.6	.06
3	0	25.6	177.3	-49.0	.06	25.6	176.2	-50.1	.06
3	5	26.8	260.3	35.7	.05	26.9	260.8	36.2	.05
5	-5	21.9	96.1	-135.1	.05	21.9	95.4	-135.7	.05
5	0	25.7	181.4	-44.7	.04	25.6	180.8	-45.3	.04
5	5	26.7	259.2	34.4	.04	26.7	259.5	34.8	.04
10	-5	21.3	97.5	-134	.04	21.3	94.3	-137	.04
10	0	25.5	180.8	-45.6	.03	25.5	180.5	-45.9	.03
10	5	26.6	258.0	33.0	.03	26.6	258.2	33.1	.03
50	-5	28.4	191.8	-31.0	.01	28.4	191.4	-31.3	.01
50	0	28.7	216.7	-5.8	.01	28.7	216.5	-5.9	.01
50	5	28.7	235.4	13.1	.01	28.7	235.4	13.1	.01

Θ_f = final latitude at 800 Km

Ψ_f - angle between field and wave normal at 800 Km

δ_f = angle between vertical and wave normal at 800 Km.

Figure 47 Wave normal against height for rays coming into the ionosphere along a field line at $\theta = 30°$

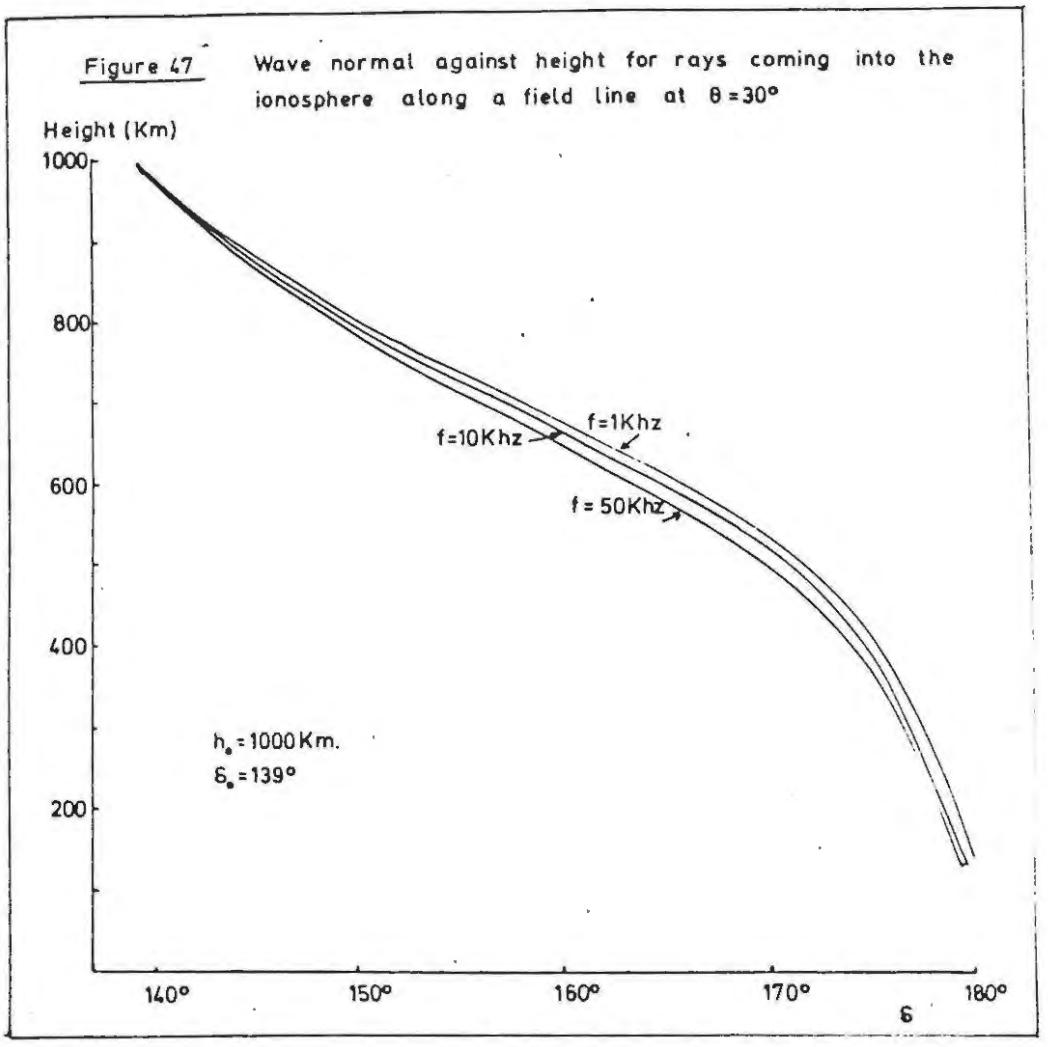

Figure 48 Wave normal angle against height for 5Khz rays coming into the ionosphere from 1000Km at various angles to the field.

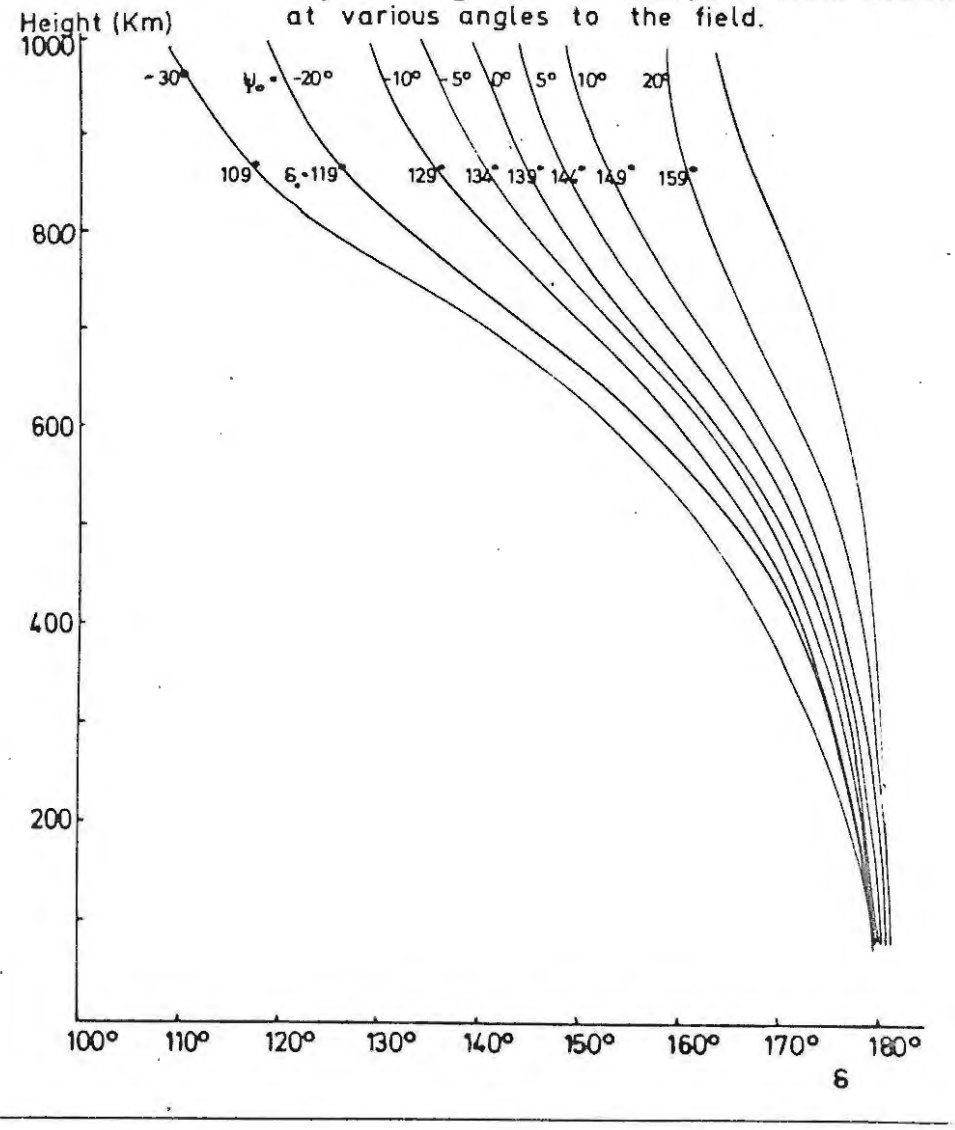

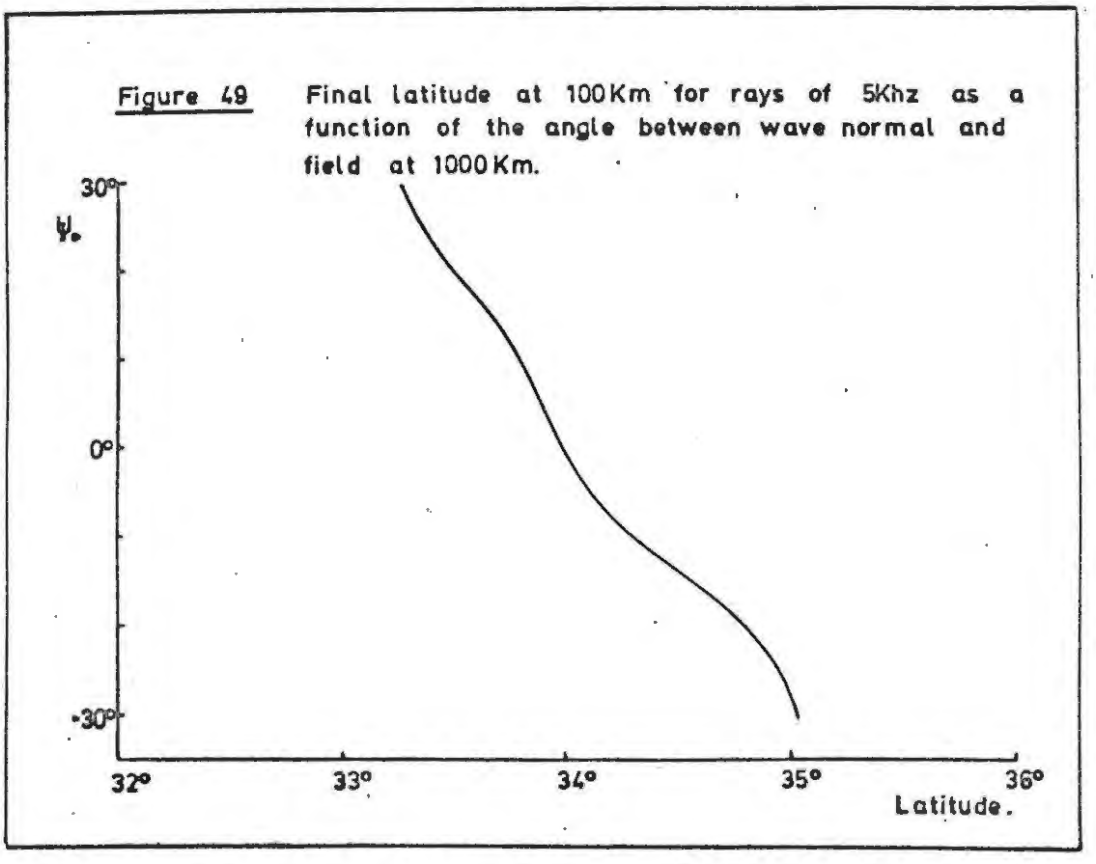

Figure 49 Final latitude at 100Km for rays of 5Khz as a function of the angle between wave normal and field at 1000Km.

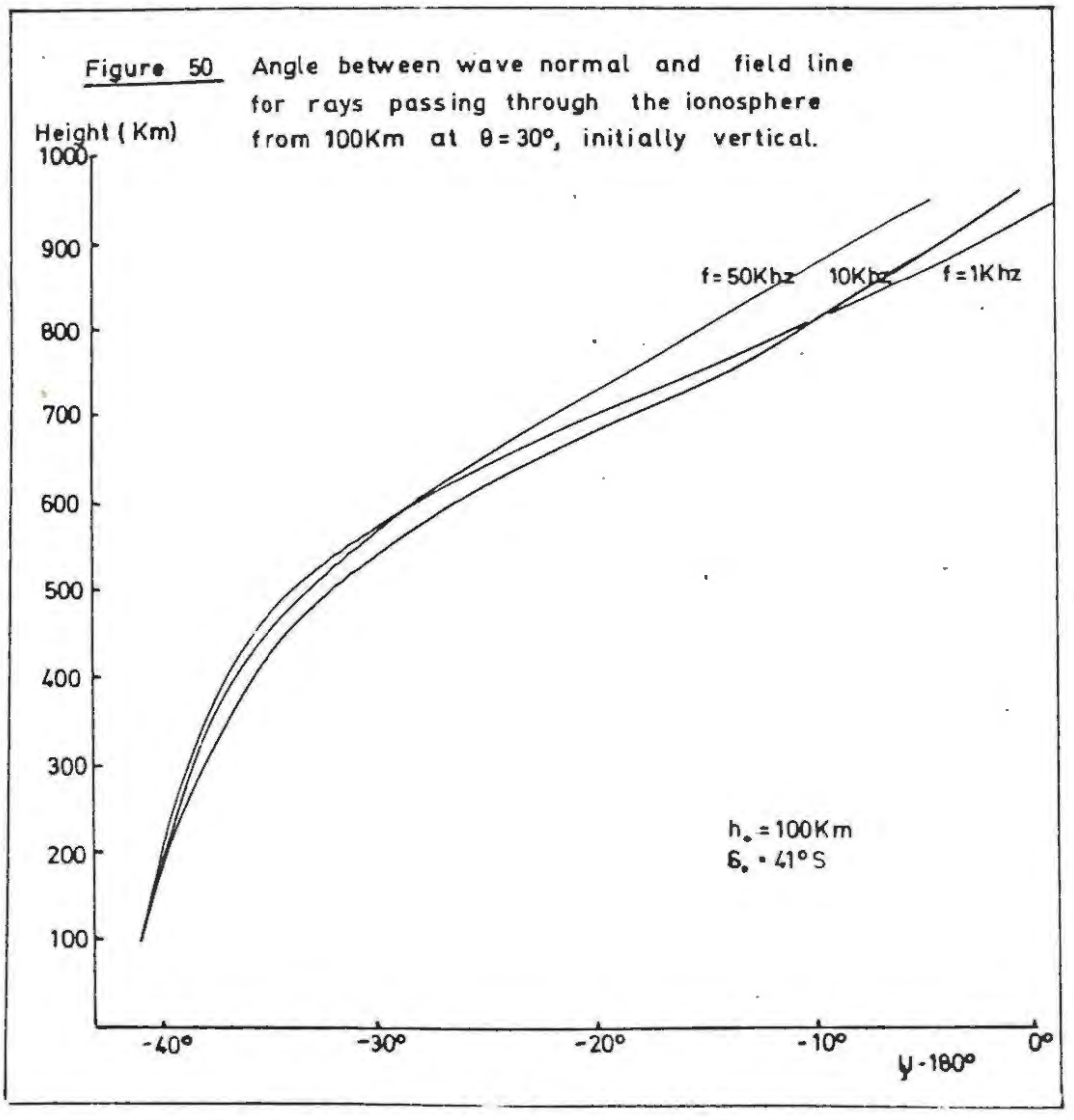

Figure 50 Angle between wave normal and field line for rays passing through the ionosphere from 100Km at θ = 30°, initially vertical.

Figure 51. Angle between wave normal and field line as a function of height for 5Khz rays starting upwards from 100 Km at various angles to the vertical.

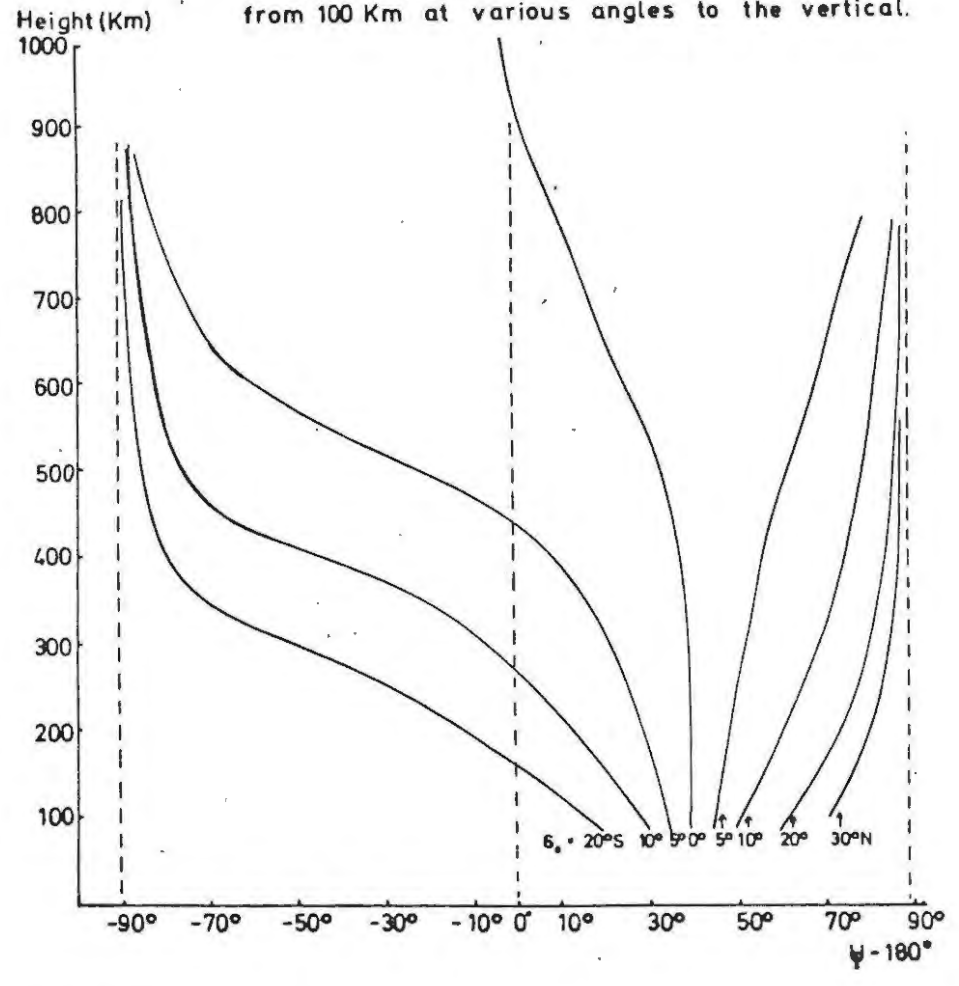

Figure 52. Final latitude at 750Km for rays of 5Khz as a function of the angle between wave normal and vertical at 100Km.

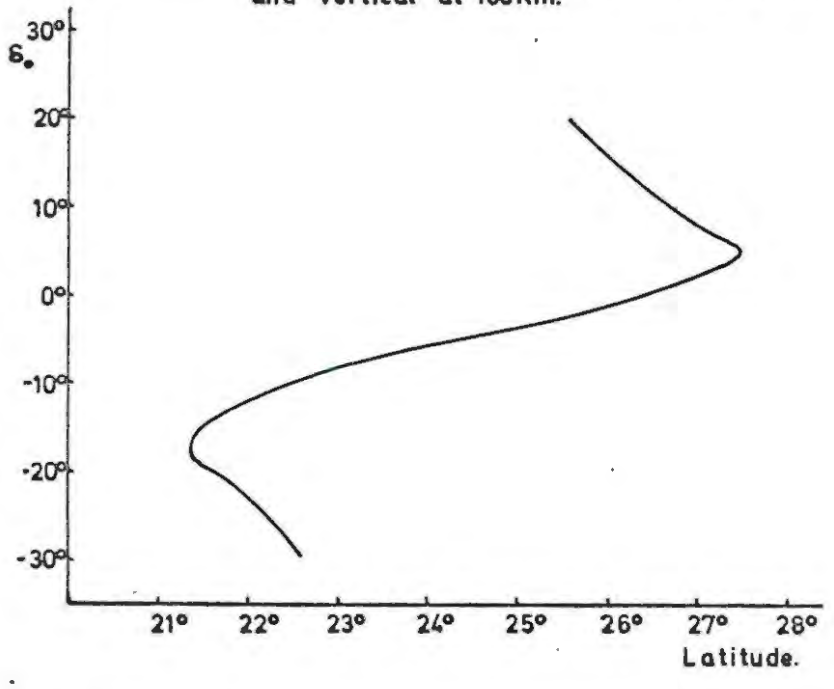

Figure 53. Ray paths through the ionosphere for f= 5Khz, starting at various angles to the vertical.

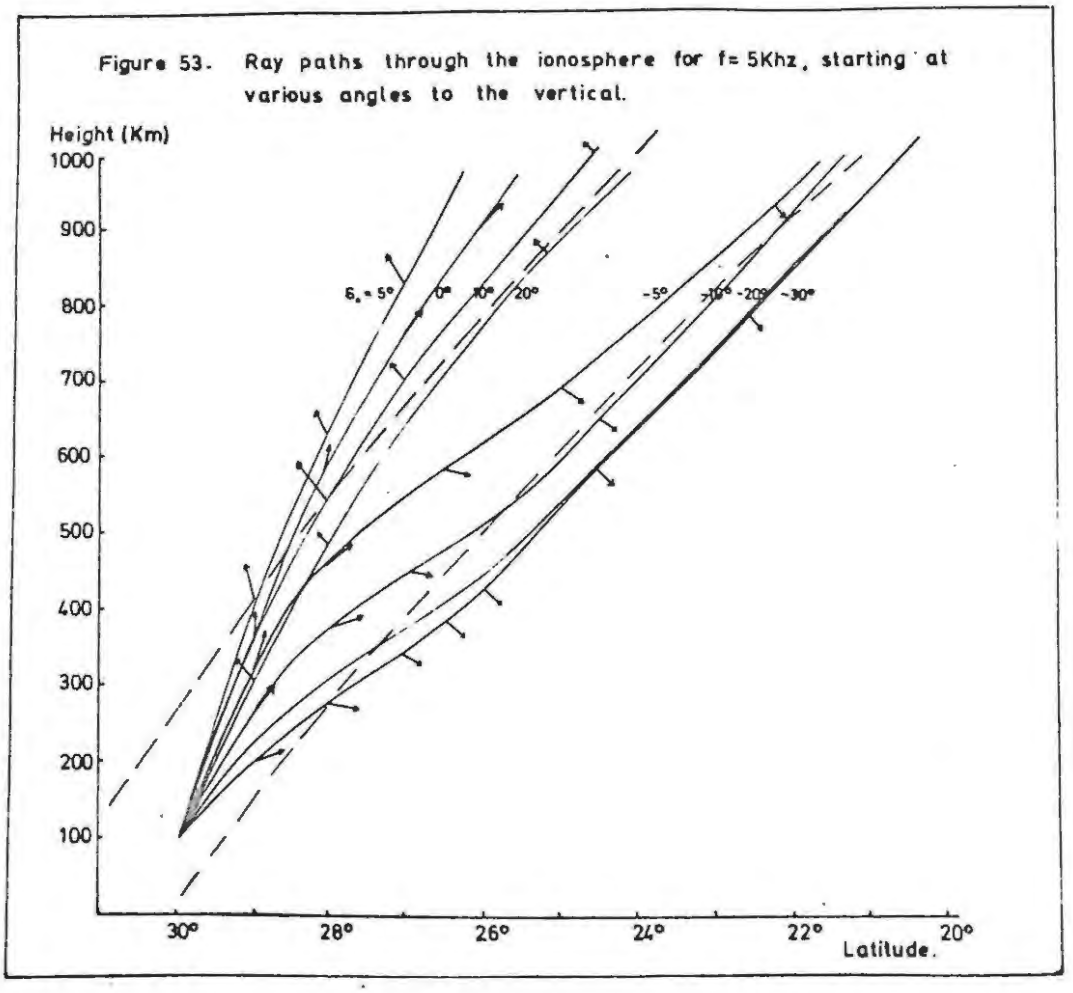

Chapter 9.

When is ray-tracing justified?

9.1. Introduction.

In the previous chapters we have presented some results of computations performed by step-by-step integration of the Haselgrove equations governing the path of a ray; equations which were derived in Chapter 3 with the fundamental assumption that the medium in which we apply them is "slowly varying" in space; a criterion for the term "slowly varying" having been presented in Chapter 2. In common with, it seems, every other ray-tracing study, we have not checked whether this criterion is met with in the ionosphere. In this chapter we present a few results of computations performed to test the criterion.

9.2. The W.K.B.J. criterion for slowly varying media.

In section 2.5 of chapter 2 we quoted two mathematical conditions for the concept of slowly-varying as applied to oblique propagation in a horizontally stratified media; these being

$$\frac{1}{k^2}\left|\frac{3}{4}\left(\frac{1}{q^2}\frac{dq}{dz}\right)^2 - \frac{1}{2q^3}\frac{d^2q}{dz^2}\right| \ll 1 \qquad 9.1$$

for the case of horizontal polarization (with respect to the plane containing the magnetic field) and

$$\left|\left(\frac{dq}{dz}\right)^2 - \frac{1}{2q^3}\frac{d^2q}{dz^2} + \frac{1}{q^2}\left\{\frac{1}{n}\frac{d^2n}{dz^2} - 2\left(\frac{1}{n}\frac{dn}{dz}\right)^2\right\}\right| \ll 1 \qquad 9.2$$

for the case of vertical polarization.

These conditions apply strictly only to a horizontally stratified medium; the ionosphere is more closely spherically symmetric, but for the local phenomenon of an almost vertical ray, as we have seen the start of an exospheric whistler to be, it may be regarded as horizontally stratified. Remembering also that $q = \mu \cos \chi$ really defines the z component of the refractive index, which in our case is integrated step-by-step as ρ_r, we see that the first of the above conditions may be rewritten

$$\frac{1}{k^2} \left| \frac{3}{4}\left(\frac{1}{\rho_r^2}\frac{d\rho_r}{dh}\right)^2 - \frac{1}{2\rho_r^3}\frac{d^2\rho_r}{dh^2} \right| \ll 1 \qquad 9.3$$

This condition is seen to have three weaknesses; it can break down for very small k, for very small ρ_r, or for very large derivatives of ρ_r. It is easy to analyse these conditions separately.

(a) A very small k is, of course, a consequence of an extremely low frequency; so that we must expect dangers here; how low we can go must thus be investigated. But if we look a little more closely at Equation 9.3 we see that we have the product $k^2\rho_r^4$ in the denominator. To some extent for quasi-longitudinal propagation the decrease in k with frequency is offset by an increase in ρ_r, as can be

the refractive index surfaces in Figure 25;

/or....

or from taking the quasi-longitudinal approximation to the Appleton-Hartree formula to the extreme for very low frequencies:

$$n^2 = 1 - \frac{X}{1-Y} \approx \frac{f_n^2}{f_H f \cos\Psi} \qquad 9.4$$

so that the product $k^2 q^4$ is approximately frequency independent, and is not too small, provided χ (the angle of incidence on the ionosphere) is not too large. In the cases we shall have to consider we are mainly interested in initially normal incidence, although we should use the criterion for oblique incidence to cater for the departures from normal. SHAWAN[24] does not seem to realise this; he quotes (without subsequent application) the criterion for normal incidence only. (b) The criterion may be violated by ρ_r approaching or going through a zero. It is hard to predict when this may occur without performing actual computations, but it is possible to examine the significance of this event. The level when $q = 0$ may be one of strong reflection, or of coupling between modes, as is discussed by BUDDEN[25][26], who points out that it is only a level of reflection if the Booker Quartic has a double root at that level. If it has only one root at the critical level the W.K.B.J. solutions may still be good approximations; which is comforting for the users of ray tracing techniques. Anomalous ray

sults might, however, profit from further

/consideration....

consideration of the behaviour at these critical levels.
(c) The meaning of the term "large derivatives of ρ_r" must be considered with due respect to the size of units employed. Perhaps an example will clarify what is implied; if the refractive index were to change linearly from unity to 300 in the space of 30Km, this would give a value to $\frac{dn}{dz}$ of $\frac{299}{30,000} \simeq \cdot 01$ which is not a large number in the ordinary sense, although we would say that the refractive index had changed rapidly. For a subjective glance at this question it would probably be better to examine the product $\lambda \frac{dq}{dz}$, giving the change in refractive index occurring in a free space wavelength.

The effect of a large change in refractive index will frequently be masked out by the ρ_r^4 term in the denominator, for if the refractive index changes appreciably without passing through zero, the effective value of ρ_r^4 will also be large.

We have not yet mentioned the effect of the term in the second derivative. It is however reasonable to expect that this will be of second order in almost every instance.

9.3. Results of computations.

It would appear from the results of the previous discussion that we will not have much success in trying

/to....

to violate the W.K.B.J. criterion in physical situations, as the effects of various singularities frequently tend to cancel one another. However such a statement is open to attack, and it is of interest to check with numerical examples.

It is perhaps useful to decide how much less than unity we should demand the criterion to be before we accept the idea of ray-tracing, as we have seen the units to be deceptive. Suppose, for example, we have a wave frequency of 100 H_Z in a region where $n = 200$ and $\frac{dn}{dz}$ is as in the previous example. Then $k \sim 2 \times 10^{-6}$ and the criterion is of the order of $\frac{10^{12}}{4} \cdot \frac{3}{4} \cdot \frac{1}{16.10^8} \cdot 10^{-4} \sim \cdot 01$. Let us therefore (somewhat arbitrarily) take 1% as our significance level.

The ray-tracing program was modified to prepare punched data of co-ordinates (ρ_r, h) for several rays traced through the ionosphere. This data was then used as input to a second program which fitted a second order Lagrangian polynomial

$$\rho_r (h) = Eh^2 + Fh + G \qquad 9.6$$

to the co-ordinates; this polynomial was then readily differentiated to give approximations for $\frac{d\rho_r}{dh}$ and $\frac{d^2\rho_r}{dh^2}$ which were thought sufficiently accurate for the purpose. Some typical results are presented in

It will be noted that no mention is made

/of...

of the second derivative in this table; it was however less than 10^{-6} in all cases considered. The results contained in this table were worked out for the horizontal polarization case.

It is at once apparent that the criterion is violated in the lowest regions of the ionosphere, even for frequencies as high as 10 KH_z. Yet above an altitude of about 250 Km it would appear that ray-tracing is safe even down to a frequency of 100 H_z. As is to be expected, we can venture lower into the ionosphere (viewed from above) as the frequency increases; at 10 KH_z we appear safe above the height of 150 Km. Nor does it seemingly make much difference whether propagation os longitudinal or tending to transverse, as comparison of Tables 8a and 8b shows - if anything transverse propagation os better suited. This is naively unexpected; the reason again being the presence of the term ρ_r^4 in the denominator; the increase in n for transverse propagation being effectively realised as an increase in ρ_r, since the magnetic field is at an angle to the radius of about 40^o.

In Table 8f we have performed these computations over the whole of a ray path into the opposite hemisphere. It will be seen that the criterion seemingly breaks down near the top of the path where ρ_r changes

/sign; ....

sign; a region where intuitively we expect to find ray-tracing satisfactory. It is also fair to note that in this path our intervals between points are so large that the assumption of a horizontally stratified region is not well-founded.

On the basis of these results it would appear that ray-tracing is dangerous in the lower ionosphere, but acceptable above the F region for frequencies above about 300 H_z. This also implies that the interpretations of low altitude whistlers by ray-tracing studies such as KIMURA'S[1] may not be totally adequate at the lowest frequencies.

Table 8.

Ray paths through the ionosphere at 30° latitude with the values of the W.K.B.J. criterion at each point.

a. $f = 100\ H_z$, $h_o = 100$ Km, $\delta_o = 0°$

h	ρ_r	$\frac{d\rho_r}{dh}$	Criterion	$\Psi - 180°$
100.0	86.5	.28	244.39	41.0
131.5	299.7	.25	1.370	40.7
148.9	381.5	.23	.423	40.6
163.6	432.0	.20	.204	40.5
176.9	465.1	.18	.119	40.4
189.4	486.3	.16	.075	40.3
201.5	498.7	.13	.049	40.2
213.3	504.2	.11	.034	40.1
225.1	503.9	.09	.023	40.0
236.9	499.0	.07	.015	39.9
248.9	490.0	.05	.009	39.7
261.0	477.5	.04	.005	39.6
273.6	462.1	.03	.002	39.4
286.6	444.1	.01	.001	39.2
300.2	423.8	.00	.000	39.0
314.4	401.7	-.01	.000	38.8
329.3	378.1	-.01	.001	38.5
345.3	353.2	-.02	.003	38.2
362.4	327.5	-.02	.005	37.9
380.8	301.0	-.02	.008	37.4
400.8	274.2	-.02	.011	36.9
422.8	247.1	-.02	.014	36.3
447.1	220.1	-.02	.018	35.5
474.3	193.2	-.01	.024	34.5
505.3	166.5	-.01	.031	33.2
540.9	140.4	-.01	.043	31.4
582.8	114.9	-.01	.062	28.9
633.0	90.4	-.01	.099	25.4

Table 8 (Contd)

b. $f = 100$ Hz $\quad h_o = 100$ Km $\quad \delta_o = 10^o$

h	ρ_r	$\frac{d\rho_r}{dh}$	Criterion	$\Psi - 180^o$
100.0	93.3	.29	192.471	51.0
131.4	329.1	.27	1.029	53.2
148.8	422.5	.24	.314	54.1
163.5	482.2	.22	.150	54.9
176.7	522.8	.19	.086	65.7
189.2	550.6	.17	.054	56.4
201.3	568.7	.15	.036	57.1
213.0	579.2	.13	.024	57.8
224.8	583.5	.10	.016	58.5
236.6	582.5	.08	.010	59.3
248.6	576.9	.07	.007	60.1
260.8	567.4	.05	.004	60.9
273.4	554.5	.03	.002	61.7
286.4	538.7	.02	.001	62.6
300.0	520.2	.01	.000	63.6
314.3	499.5	.00	.000.	64.6
329.5	476.9	-.00	.000.	65.7
345.8	452.8	-.01	.001	66.9
363.3	427.4	-.02	.002	68.2
382.3	401.2	-.02	.003	69.6
403.4	374.3	-.02	.003	71.1
427.0	347.1	-.02	.004	72.8
453.9	319.7	-.02	.005	74.8
485.5	292.3	-.01	.005	76.9
523.9	265.2	-.01	.004	79.2
573.6	238.5	-.01	.003	81.8
645.3	212.8	-.01	.002	84.5
773.5	192.3	-.00	.000	86.9

Table 8 (Cont).

c. $f = 300$ Hz $\quad h_o = 100$ Km $\quad \delta_o = 10^o$

h	ρ_r	$\frac{d\rho_r}{dh}$	Criterion	$\Psi - 180^o$
100.0	53.9	.16	60.409	51
140.9	222.2	.14	.155	54.3
182.9	278.7	.12	.046	55.6
181.8	310.9	.10	.021	56.7
199.4	329.2	.08	.011	57.7
216.5	337.9	.06	.006	58.8
233.5	339.4	.05	.003	59.9
250.7	335.1	.03	.002	61.1
268.6	326.2	.02	.001	62.3
287.3	313.5	.01	.000	63.6
307.3	297.7	-.00	.000	65.1
328.9	279.3	-.01	.000	66.7
352.9	259.1	-.01	.000	68.5
379.7	237.5	-.01	.001	70.5
410.7	215.1	-.01	.001	72.7
447.9	192.3	-.01	.001	75.4
494.6	169.4	-.01	.001	78.4
559.0	147.0	-.01	.002	81.9
668.3	126.9	-.00	.000	85.4

Table 8 (Cont).

d. $f = 1KH_z$ $h_o = 100$ Km $\delta_o = 10^o$

h	ρ_r	$\frac{d\rho_r}{dh}$	Criterion	$\Psi-180$
100.0	29.5	.09	19.000	51°
132.6	106.5	.08	.092	53.3
150.6	136.3	.07	.028	54.3
165.8	155.1	.06	.013	55.1
179.5	167.8	.06	.008	55.9
192.6	176.2	.05	.004	56.6
205.2	181.4	.04	.003	57.4
217.6	184.1	.04	.002	58.1
229.9	184.8	.03	.001	58.9
242.5	183.7	.02	.001	59.7
255.2	181.2	.02	.001	60.6
268.3	177.4	.01	.000	61.4
281.8	172.5	.01	.000	62.4
295.9	166.6	.00	.000	63.3
310.8	159.8	.00	.000	64.4
326.6	152.4	-.00	.000	65.5
343.5	144.5	-.00	.000	66.8
361.8	136.0	-.01	.000	68.1
381.9	127.3	-.01	.000	69.6
404.0	118.4	-.01	.000	71.2

Table 8 (Cont)

e. $f = 10KH_z$, $h_o = 100$ Km, $\delta_o = -10^o$

h	ρ_r	$\frac{d\rho_r}{dh}$	Criterion	$\Psi - 180^o$
100.0	8.1	.03	3.059	-9.9
131.1	26.9	.02	.020	-13.3
148.4	33.9	.02	.006	-14.8
162.8	38.0	.02	.003	-16.1
175.8	40.5	.02	.002	-17.4
188.0	41.9	.02	.001	-18.7
199.7	42.6	.01	.001	-19.9
211.2	42.6	.01	.001	-21.3
222.5	42.1	.01	.000	-22.7
233.7	41.2	.01	.000	-24.2
245.0	39.9	.01	.000	-25.8
256.4	38.4	.00	.000	-27.5
267.9	36.6	.00	.000	-29.4
279.8	34.6	.00	.000	-31.4
291.8	32.4	.00	.000	-33.7
304.2	30.0	.00	.000	-36.1
385.3	14.5	-.00	.000	-57.6
429.4	6.5	-.00	.000	-74.1
442.4	3.9	-.00	.029	-80.3
456.3	1.3	-.00	20.935	-86.8
470.0	-1.3	-.01	75.965	-93.2

Table 8 (Contd)

f. $f = 100\ H_z$ $h_o = 100$ Km $\delta_o = 0$

h	ρ_r	$\frac{d\rho_r}{dh}$	Criterion	Ψ-180°
100.0	86.5	.28	244.39	41.0
131.5	299.7	.25	1.37	40.7
148.9	381.4	.23	.42	40.6
163.6	432.0	.20	.20	40.5
176.9	465.0	.18	.12	40.4
189.4	486.3	.02	.00	40.3
201.5	498.7	-.01	.00	40.2
860.1	34.7	-.00	.02	4.4
1275.4	11.1	-.00	1.11	-17.7
1567.8	3.4	-.00	159.74	-25.3
1740.0	1.7	.00	10^3	-23.1
1894.4	2.33	.00	10^5	-14.8
2036.2	1.47	.06	10^6	-10.1
2099.8	-10.2	.25	10^6	-30.1
2112.3	-19.3	-.01	56.88	-40.5
2071.2	-25.0	-.00	.10	-45.6
1966.0	-27.1	.00	.02	-47.3
1509.3	-31.7	.00	.38	-47.2
1102.2	-45.4	.01	2.44	-48.4
571.8	-160.6	-.03	.31	-51.9
208.7	-593.7	-.19	.04	-54.7
198.3	-584.9	-.21	.06	-52.9
187.6	-569.4	-.23	.09	-52.9
176.6	-545.9	-.26	.13	-52.8
165.0	-511.6	-.29	.20	-52.7
152.4	-462.4	-.31	.36	-52.7
138.1	-389.4	-.16	.20	-52.6

Chapter 10.

Suggestions for further research.

Two major questions seem to arise from the results of the work described in this thesis; both of which strain the usefulness of ray-tracing techniques somewhat.

In the first place, we have seen in Chapter 7 that numerical integration with finite step lengths may result in resonance and reflection effects remaining unobserved through being stepped over. Future ray-tracing studies should be "tuned up" to a greater efficiency if possible to cope with this problem; an effort should be made to decide conclusively whether and how reflection of the type predicted in this work does occur.

Secondly, we must repeat MAEDA and KIMURA's[17] request for a more detailed investigation of the propagation through the ionosphere proper; which, as the results of Chapter 9 show, will have to be done on the basis of "full wave" theory. Comparison of these results with those obtained from ray-tracing could be profitable. In addition, the computations could be extended to include the effects of collisions, which KIMURA[1] claims will be important at these low frequencies.

/we....

We have seen that ray theory predicts that the anisotropy introduced by the presence of the earth's field is insufficient to explain the accurate guiding along the field lines which experiment supports, except at frequencies so low that ion effects cause reflection before the ionosphere is reached. It would not be difficult to introduce a field-aligned enhancement to the exospheric plasma model, and then to vary this until results more consistent with experiment are observed. The extent of the enhancement might then be profitably compared with results obtained from full wave theories such as those of WALKER[27].

REFERENCES.

1.	Kimura I.	Effects of ions on whistler-mode ray-tracing Rad. Sci. 1(3), 269-283,	(1966)
2.	Barkhausen H.	Physik Z. 20, 401-403	(1919)
3.	Eckersley T.L.	Phil Mag 49(6), 1250-1259	(1925)
4.	Burton E.T. and Boardman E.M.	Proc I.R.E. 21(10), 1476-1494	(1933)
5.	Storey L.R.O.	Phil. Trans. Roy. Soc. 246A, 113-141	(1953)
6.	Appleton E.V.	U.R.S.I. Proc. Washington Assembly	(1927)
7.	Hartree D.R.	Proc. Camb. Phil. Soc. 27, 143	(1931)
8.	Budden K.G.	"Radio Waves in the Ionosphere" Chapter 3	(1961)
9.	Stix T.H.	"Theory of Plasma Waves" Chapter 1.	(1962)
10.	Booker H.G.	Proc. Roy. Soc. 155A, 235	(1936)
11.	Poeverlein	Sity. Bayerischen. Akad. Wiss 1, 175-201	(1948)
12.	Budden K.G.	"Radio Waves in the Ionosphere" Chapter 14-2,3	(1961)
13.	Haselgrove J.	Proc. Phys. Soc. 70A(7), 653-662	(1957)
14.	Budden K.G.	"Radio Waves in the Ionosphere" Chapter 14.6	(1961)
15.	Yabroff	J. Res N.B.S. 65D(5), 485-505	(1961)
16.	Gill	Proc. Camb. Phil. Soc. 47, 96	(1951)
17.	Maeda K and Kimura I.	R.I.S.R.J. 10, 105-123	(1956)
18.	Shawan S.D.	"V.L.F. Ray Tracing in a Model Ionosphere" (Doctoral Thesis) (Iowa)	(1966)
19.	Angerami J.J. and Thomas J.O.	J.G.R. 69, 4537-4560	(1964)
20.	Shawan S.D. and Gurnett D.A.	J.G.R. 71, 741-754.	(1966)
21.	Smith R.L.	J.G.R. 65, 815-823	(1960)
22.	Hines C.O.	J.A.T.P. 11(2), 36-42	(1957)
23.	Smith R.L. and Brice N.M.	J.G.R. 69, 5029-5039	(1964)
24.	Shawan S.D.	"A computer program for VLF ray tracing in a model ionospher"	(Iowa)
25.	Budden K.G.	"Radio Waves in the Ionosphere" Chapter 9	(1961)
26.	Budden K.G.	"Radio Waves in the Ionosphere" Chapter 18	(1961)
27.	Walker A.D.M.	J.A.T.P. 28, 807-822.	(1966)

APPENDICES.

Appendix A.

Derivation of the canonical equations 3.16, 3.17, 3.18.

From curl $\bar{\rho} = \bar{0}$ we get

$$\frac{\partial \rho_\Theta}{\partial \Phi} = \cos\Theta \frac{\partial \rho_\Phi}{\partial \Theta} - \sin\Theta\, \rho_\Phi \qquad A$$

$$\frac{\partial \rho_r}{\partial \Phi} = r\cos\Theta \frac{\partial \rho_\Phi}{\partial r} + \cos\Theta\, \rho_\phi \qquad B$$

$$\frac{\partial \rho_r}{\partial \Theta} = r\frac{\partial \rho_\Theta}{\partial r} + \rho_\Theta \qquad C$$

Now from equations 3.9 we have

$$\frac{dG}{dr} = \frac{\partial G}{\partial r} + \frac{\partial G}{\partial \rho_r}\cdot\frac{\partial \rho_r}{\partial r} + \frac{\partial G}{\partial \rho_\Theta}\cdot\frac{\partial \rho_\Theta}{\partial r} + \frac{\partial G}{\partial \rho_\Phi}\cdot\frac{\partial \rho_\Phi}{\partial r} = 0$$

$$= -\frac{1}{\mu}\cdot\frac{\partial \mu}{\partial r} + \frac{dr}{ds}\cdot\frac{\partial \rho_r}{\partial r} + \frac{r}{r}\cdot\frac{d\Theta}{ds}\left\{\frac{\partial \rho_r}{\partial \Theta} - \rho_\Theta\right\} + \frac{r\cos\Theta}{r\cos\Theta}\cdot\frac{d\Phi}{ds}\left\{\frac{\partial \rho_r}{\partial \Phi} - \rho_\Phi \cos\Theta\right\}$$

From equations 3.10, B and C;

$$= -\frac{1}{\mu}\cdot\frac{\partial \mu}{\partial r} + \left\{\frac{\partial \rho_r}{\partial r}\cdot\frac{\partial r}{\partial s} + \frac{\partial \rho_r}{\partial \Theta}\cdot\frac{\partial \Theta}{\partial s} + \frac{\partial \rho_r}{\partial \Phi}\cdot\frac{\partial \Phi}{\partial s}\right\} - \rho_\Theta\frac{d\Theta}{ds} - \rho_\Phi\cos\Theta\frac{d\Phi}{ds}$$

Then, since

$$\frac{\partial \rho_r}{\partial r}\cdot\frac{\partial r}{\partial s} + \frac{\partial \rho_r}{\partial \Theta}\cdot\frac{\partial \Theta}{\partial s} + \frac{\partial \rho_r}{\partial \Phi}\cdot\frac{\partial \Phi}{\partial s} = \frac{d\rho_r}{ds}$$

$$\frac{dG}{dr} = \frac{1}{\mu}\cdot\frac{\partial \mu}{\partial r} + \rho_\Theta\frac{d\Theta}{ds} - \rho_\Phi\cos\Theta\frac{d\Phi}{ds} \qquad (3.16)$$

$$\frac{dG}{d\Theta} = \frac{\partial G}{\partial \Theta} + \frac{\partial G}{\partial \rho_r}\cdot\frac{\partial \rho_r}{\partial \Theta} + \frac{\partial G}{\partial \rho_\Theta}\cdot\frac{\partial \rho_\Theta}{\partial \Theta} + \frac{\partial G}{\partial \rho_\Phi}\cdot\frac{\partial \rho_\Phi}{\partial \Theta} = 0$$

$$= -\frac{1}{\mu}\cdot\frac{\partial \mu}{\partial \Theta} + \frac{dr}{ds}\left\{\rho_\Theta + r\frac{\partial \rho_\Theta}{\partial r}\right\} + r\frac{d\Theta}{ds}\cdot\frac{\partial \rho_\Theta}{\partial \Theta} + \frac{r\cos\Theta}{\cos\Theta}\cdot\frac{d\Phi}{ds}\left\{\frac{\partial \rho_\Theta}{\partial \Phi} + \rho_\Phi\sin\Theta\right\}$$

From equations 3.11, A and C.

$$\frac{dG}{d\phi} = -\frac{1}{\mu}\cdot\frac{\partial\mu}{\partial\phi} + r\left\{\frac{\partial\rho_\phi}{\partial r}\cdot\frac{\partial r}{\partial s} + \frac{\partial\rho_\phi}{\partial\phi}\cdot\frac{\partial\phi}{\partial s} + \frac{\partial\rho_\phi}{\partial\theta}\cdot\frac{\partial\theta}{\partial s}\right\} + \rho_\phi\frac{dr}{ds} +$$

$$r\rho_\theta \sin\phi\frac{d\theta}{ds}$$

$$\frac{d\rho_\phi}{ds} = \frac{1}{r}\left\{\frac{1}{\mu}\cdot\frac{\partial\mu}{\partial\phi} - \rho_\phi\frac{dr}{ds} - r\rho_\theta\sin\phi\frac{d\theta}{ds}\right\} \qquad (3.17)$$

$$\frac{dG}{d\phi} = \frac{\partial G}{\partial\phi} + \frac{\partial G}{\partial\rho_r}\cdot\frac{\partial\rho_r}{\partial\phi} + \frac{\partial G}{\partial\rho_\theta}\cdot\frac{\partial\rho_\theta}{\partial\phi} + \frac{\partial G}{\partial\rho_\phi}\cdot\frac{\partial\rho_\phi}{\partial\phi} = 0$$

$$= -\frac{1}{\mu}\cdot\frac{\partial\mu}{\partial\phi} + \frac{dr}{ds}\left\{\rho_\phi\cos\phi + r\cos\phi\frac{\partial\rho_\phi}{\partial r} + r\frac{d\phi}{ds}\left\{\cos\phi\frac{\partial\rho_\phi}{\partial\phi}\right.\right.$$

$$\left.\left. - \rho_\phi\sin\phi\right\} + r\cos\phi\frac{d\phi}{ds}\cdot\frac{\partial\rho_\phi}{\partial\phi}\right.$$

From equations 3.12, A, and B.

$$= -\frac{1}{\mu}\frac{\partial\mu}{\partial\phi} + r\cos\phi\left\{\frac{\partial\rho_\phi}{\partial r}\frac{\partial r}{\partial s} + \frac{\partial\rho_\phi}{\partial\phi}\frac{\partial\phi}{\partial s} + \frac{\partial\rho_\phi}{\partial\theta}\frac{\partial\theta}{\partial s}\right\} + \rho_\phi\cos\phi\frac{dr}{ds}$$

$$- r\rho_\theta\sin\phi\frac{d\theta}{ds}$$

$$\frac{\partial\rho_\theta}{\partial s} = \frac{1}{r\cos\phi}\left\{\frac{1}{\mu}\cdot\frac{\partial\mu}{\partial\theta} - \rho_\theta\cos\phi\frac{dr}{ds} + r\rho_\phi\sin\phi\frac{d\phi}{ds}\right\} \qquad (3.18)$$

Appendix B.

Derivatives of A,B,C with respect to Ψ, X_j; Y_j, and f

$$A = S \sin^2\Psi + P \cos^2\Psi$$

$$B = -[RL \sin^2\Psi + PS(1+\cos^2\Psi)] = -[(S^2-D^2)\sin^2\Psi + PS(1+\cos^2\Psi)]$$

$$C = (S^2-D^2)P = PRL$$

For no collisions $U = 1$

$$R = 1 - \sum_j \frac{X_j}{1+\epsilon_j Y_j}$$

$$L = 1 - \sum_j \frac{X_j}{1-\epsilon_j Y_j}$$

$$P = 1 - \sum_j X_j$$

$$S = 1 - \sum_j \frac{X_j}{1-Y_j^2}$$

$$D = \sum_j \frac{\epsilon_j X_j Y_j}{1-Y_j^2}$$

$$\frac{\partial X_j}{\partial f} = \frac{\partial}{\partial f}\left(\frac{f_{n_j}}{f^2}\right)^2 = -\frac{2}{f} X_j$$

$$\frac{\partial Y_j}{\partial f} = \frac{\partial}{\partial f}\left(\frac{f_{Hj}}{f}\right) = -\frac{1}{f} Y_j$$

$$\frac{\partial A}{\partial \Psi} = 2\sin\Psi \cos\Psi (S-P)$$

$$\frac{\partial B}{\partial \Psi} = 2\sin\Psi \cos\Psi (PS-RL)$$

$$\frac{\partial C}{\partial \Psi} = 0$$

$$\frac{\partial A}{\partial X_j} = \frac{\sin^2\psi}{Y_j^2-1} - \cos^2\psi$$

$$\frac{\partial B}{\partial X_j} = -\left((1+\cos^2\psi)\left\{\frac{P}{Y_j^2-1} - S\right\} + \sin^2\psi\left\{\frac{2S}{Y_j^2-1} + \frac{2\epsilon_j Y_j D}{Y_j^2-1}\right\}\right)$$

$$\frac{\partial C}{\partial X_j} = \left\{\frac{2S}{Y_j^2-1} + \frac{2\epsilon_j Y_j D}{Y_j^2-1}\right\} P - (S^2-D^2)$$

$$\frac{\partial A}{\partial Y_j} = \frac{2X_j Y_j \epsilon_j}{(Y_j^2-1)^2} \sin^2\psi$$

$$\frac{\partial B}{\partial Y_j} = -\left\{\frac{2P(1+\cos^2\psi)\,\epsilon_j X_j Y_j}{(Y_j^2-1)^2} + \sin^2\psi\left(\frac{\Sigma \epsilon_j X_j Y_j}{(Y_j^2-1)^2} + \frac{2DX_j(Y_j^2+1)}{(Y_j^2-1)^2}\right)\right\}$$

$$\frac{\partial C}{\partial Y_j} = \left\{\frac{2DX_j(Y_j^2+1)}{(Y_j^2-1)^2} + \frac{4SX_j Y_j \epsilon_j}{(Y_j^2-1)^2}\right\} P$$

$$\frac{\partial A}{\partial f} = \frac{\partial P}{\partial f}\cos^2\psi + \frac{\partial S}{\partial f}\sin^2\psi$$

$$\frac{\partial B}{\partial f} = -(1+\cos^2\psi)\left(P\frac{\partial S}{\partial f} + S\frac{\partial P}{\partial f}\right) + \sin^2\psi\left\{2S\frac{\partial S}{\partial f} - 2D\frac{\partial D}{\partial f}\right\}$$

$$\frac{\partial C}{\partial f} = \left(2S\frac{\partial S}{\partial f} - 2D\frac{\partial D}{\partial f}\right) P + (S^2-D^2)\frac{\partial P}{\partial f}$$

where

$$\frac{\partial P}{\partial f} = \frac{2}{f}\sum_j X_j$$

$$\frac{\partial S}{\partial f} = \frac{2}{f} \sum_j \frac{X_j}{(Y_j^2-1)^2}$$

$$\frac{\partial D}{\partial f} = \frac{1}{f} \sum_j \frac{X_j Y_j (3-Y_j^2)}{(Y_j^2-1)^2}$$

Appendix C.

Modifications to the autocode facilities offered by MAC (Manchester Autocode).

MAC is a simple scientific autocode devised in its original form by Dr. R.A. Brooker and his colleagues at the Computing Machine Laboratory, Manchester University, and is used on the I.C.L. 1300 series of digital computers. In common with all autocodes, its flexibility makes for loss in efficiency, a factor aggravated on the computer at Rhodes University by the limited I.A.S. storage which causes much program segmentation and use of the backing store; a magnetic drum store with access time three orders of magnitude greater than for the core store. Further, standard library subroutines such as "exponential" have to be called off the backing store every time they are to be used.

The machine coding for the I.C.L. 1301 is very simple, being single address coding, and it was early decided to modify the autocode compiler to accept segments of machine coded object program within the source program, a system which can combine the usefulness of autocoding with the efficiency of machine coding, without too many of the difficult addressing problems usually encountered in the latter.

/Of....

Of course, such a system has to be completely compatible with the existing autocode facilities, which means that the compiler has to be fairly well understood. The original flow-charts and coding were unavailable, but some preliminary work had been done on decoding by Mr. M.A. Lawrie, and with his experience the basic compiler operations were quickly grasped, so that new statements were easily devised.

Besides the feature of incorporating object language directly, several other autocode facilities were incorporated, including a crude form of "time-sharing". Two compilers were generated, and a program compiled and executing on the one could be manually interrupted so that testing or running of a short program could be performed on the other; subsequently control could be manually returned to the original task. This facility has been of immense use in the present and similar projects, where the running time may be of the order of several hours.

The rest of this appendix contains a specification of the new facilities introduced by the author, with a brief list of the more efficient subroutines which have been written, and will be understood only by those familiar both with MAC and with 1301 machine language.

/1. Instructions...

1. Instructions for introduction of machine coded segments.

There are two instructions for this purpose.

(a) The directive

INSERT m/n,

Where m and n are integers, indicates to the compiler that m halfwords of instructions are to follow, and then n words of associated constants. Either m or n may be zero; m may not be greater than 400 and n may not be greater than 125. The m halfwords of instructions are entered into the next available words of chapter space, beginning at the next complete words, and the n words of constants are stored in the usual MAC way, starting at the end of available chapter space and working backwards. The directive INSERT m/n, should be prefixed by a label if jumps are intended to the routine from without.

(b) The directive

CLEAR n

Where n is a non zero positive integer has the effect of zeroizing the next n words in the chapter, starting with the next available full word. This space may then be filled with standard machine code routines without transforming them to the format needed by the INSERT directive. The location of the space thus cleared may be found by means of the new PSA directive.

2. Format for instructions.

The m halfwords of instructions are punched as 6 digit numbers separated by commas. Zeros other than the first need not be punched, and binary digits '0 to '5 are allowed. The instructions must be in absolute form, the same function coding as for normal machine code being used. [illegible] amount of relativizing is allowed; this is explained below.

3. Format for constants.

The n words of constants are punched as 12 digit numbers, the same rules as for instructions applying. Constants to be used in floating-point arithmetic must be entered in floating-point form.

/4. ....

4. Punching instructions.

The number of instructions or constants on each card may vary, provided

(a) INSERT m/n, need not be on a separate card, although it is suggested that this be done for ease of modification

(b) The last column on each card must be blank - no carry over between cards is allowed.

(c) The n constants must start on a new card.

(d) Punching commences on all cards from column 9.

(e) Zeros other than the first need not be punched.

5. Designations and Indicators.

Designations are entered in the third digit. Designations 4,8,9 have their usual significance; and there are two special designations.

(a) Designation 7 : Test indicator, if successful, jump to the label indicated in the following 3 digits e.g. 007001, = JUMP 1
217062, = JUMP 62, 21 SET

(b) Designation 6: Indicates that the next 3 digits are a label and not an LAS address. The designation is removed at the end of compilation and the label replaced with the LAS address

e.g. 416127, == Store link on label 127

With INSERT coding access is allowed to all indicators available. However care must be exercised as indicators 10-19 and 25-29 are used in standard MAC routines.

Indicators 10,11 may be used provided no floating point arithmetic or reading is attempted between setting/testing

Indicators 16,17 may be used provided no Φ functions are used between setting/testing

Indicators 14,18,19 should not be used without "preserving" first.

6. Relativizers.

(a) It is possible to refer to other blocks or to standard MAC statements by means of labels and the 6 and 7 designations.

/(b).....

6. (b) Within an INSERT routine the place of relativizer B is taken by relativizer "I", after the relevant instruction

e.g. 004001,I, Jump to word 1 of this block
The first word of each routine is regarded as "Word 0" of its block.

(c) Within an INSERT routine, constants used must be referred to with the relativizer "J". Constants used are stored in a block and referred to by their address in that block punched as the last three digits of the instruction.

e.g. 370002,J, bring word 2 of the block of constants for this routine to B register.

Blocks of constants also start with Word 0. The constants are in fact stored backwards, but may be thought of as stored forwards in nearly all cases except when using the 45 instruction or when the address is to be modified by program, e.g. to bring word M of the constant block to B register we have to code

```
0/I  37   33,
     65   1,I

1/I  64   1,I
     37   0,J
```

(d) Main variables may be referred to by punching the appropriate variable name as though it were a relativizer

e.g. 37 9,π, Transfer π9 to B register

Variables of the form A(I+5) may be dealt with as follows

```
0/I  37   29,
     64   1,I,

1/I  65   1,I
     37   5,I
```

(e) Fixed point constants may be negated on compilation by use of relativizer "M," This cannot be used with floating-point constants or with instructions.

(f) Negative relativizing may be used with the above relationizers, by punching the 3 digit address in complimentary form by subtracting from 1000

/e.g. ....

```
e.g.  41  999,I,   Store A reg on word - 1 of block
      37  997,J,   Transfer the constant read in
                   three constants before the first
                   of this block to B register.
```

(Note that every constant detected by MAC other than 0 or fixed point I is stored separately)

In a similar way it is possible to locate the main variable A(I-5) as follows

```
37   29,
64   1,I,
65   1,I,
37   995, A,
```

It should be noted that the negative relativizing used in INSERT coding is different from that used in standard machine code.

7. Error Conditions

There are four stops possible as a result of mistakes

11	11	67	Relativizers A to H or U to Z encountered with no A → n directive
11	11	70	Label not set (at CLOSE) This could be due to relativizing an instruction with a 6 or 7 designation. The unset label appears in B reg
11	11	75	Label > 127
11	11	74	Invalid INSERT coding, as a result of one of the following (a) Incorrect format (b) Incorrect length (c) m and n incorrect (d) Column 80 punched (e) Invalid relativizer (f) not starting the constants on a new card.

8. Using INSERT coding

Programmers using INSERT coding will have to have an idea of how MAC uses LAS space; and must also bear in mind that floating-point arithmetic must employ the MAC floating-point routines. A pamphlet is available explaining these points, and giving some examples of coding.

A number of standard INSERT routines have been written, including equivalents of most of the Φ functions, quadratic and differential equation solution etc. A list of those written by the author appears below; specifications are available

/from.....

from the Computer Centre.

1. Print B register and space I
2. Floating point square root
3. Floating point exponential
4. Floating point sine/cosine
5. Floating point logarithm
6. Floating point arctangent
7. Preserve and restore indicators 10-19
8. Quadratic equations
9. Quadratic equations with iterative correction
10. Complex multiplication and division
11. Complex Square root
12. Random Index
13. Round up floating point variable
14. Round down floating point variable
15. Print 3 bank and Space
16. Booker Quartic Routine.
17. Graph plotting subroutine

9. Instruction for automatic print out of 1.A.S.

The statement DUMP n where n = 1,2,3 or 4 causes n blocks of 200 words of 1.A.S. to be printed out during execution; whereafter the original program is resumed.

10. Instruction for manual timesharing

The statement TEA enables a long program to be temporarily interrupted, when the computer may be switched off and left, or other programs run which do not use the same drum storage as the program at TEA. Later control may be returned to the first program, when it will take up where it left off.

The statement is used in conjunction with M.I.27. If the statement is encountered during execution with M.I.27 inset, no action is taken. If M.I.27 is set, appropriate preservation routines are entered, and the computer stops with 11 1150 in CR3. Re-entry to the program is accomplished through Initial Orders with MI 25 and 22 (and 21 if using compiler 2).

11. Subroutine facilities.

A number of statements have been developed to provide an analogy to the SUBROUTINE facility of FORTRAN and to make for easier programming of subroutines which are to be used several times in one chapter.

Such subroutines are introduced by the statement

SUB(n)

/which.....

which may be followed by any name for the programmer's reference. n is an integer in the range 0-127 which is to be interpreted as a label.

A subroutine is completed by the statement

RETURN

A subroutine is entered by the statement CALL n, where n is the number of the subroutine. When this statement is encountered during execution, control is transferred to the subroutine beginning SUB(n). When RETURN is encountered, control is transferred back to the statement immediately following CALL n. Standard INSERT routines are all entered in this way too.

More than one entry point may be gained to a subroutine having only one RETURN statement as in the example below

```
SUB (1)          Entry at SUB(1) reads A and B
READ (A)
SUB (2)          Entry at SUB(2) reads B only
READ (B)
RETURN
```

Note that subroutines like this must all be contained within one chapter. While it is possible to leave the routine temporarily within the same chapter, the use of DOWN and ACROSS is forbidden. One subroutine may call an independent one, but may not call subsequent entry points to itself. It may jump to any other statements within itself other than SUB(n).

e.g.

```
SUB (1)                    SUB (1)
READ (A)                   READ (A)
CALL 3                     JUMP 4
SUB (2)                    SUB (2)
READ (B)   is invalid      READ (B)     is valid
SUB (3)                    SUB (3)
READ (C)                   4)READ (C)
RETURN                     RETURN
```

Two error stops may be encountered

```
11  11  97    RETURN before SUB(n)
11  11  98    NO RETURN for previous SUB(n) (At CLOSE)
```

12. Equivalence facilities

The directives A → B and/or A → Bn, where A and B are any main variables and n is a positive integer, allot spaces for the A; in common with the B; so

/that....

that A0 and B0 have the same LAS address, or A0 and Bn if n is specified. Subsequent main variables follow suit.
Thus

A → 10	places	A0,B0	in LAS	41	
B → A		A1,B1	" "	42	
C → A2		A2,B2,C0	" "	43	etc.

This facility is of use in changing the names of main variables used in standard subroutines without repunching the cards.

Appendix D.

Flow chart of Ray-Tracing Program.

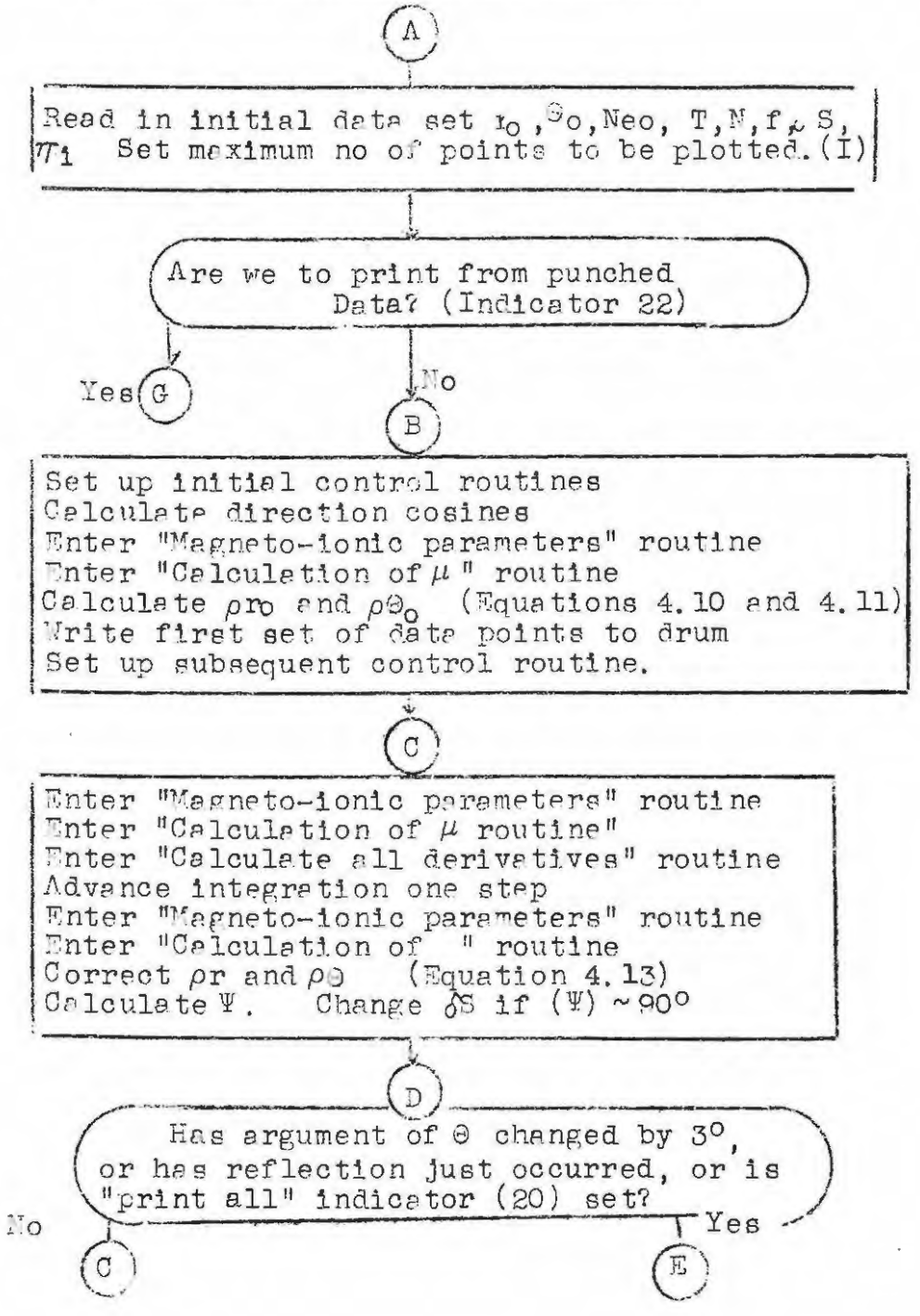

Flow chart of Ray-Tracing Program (contd)

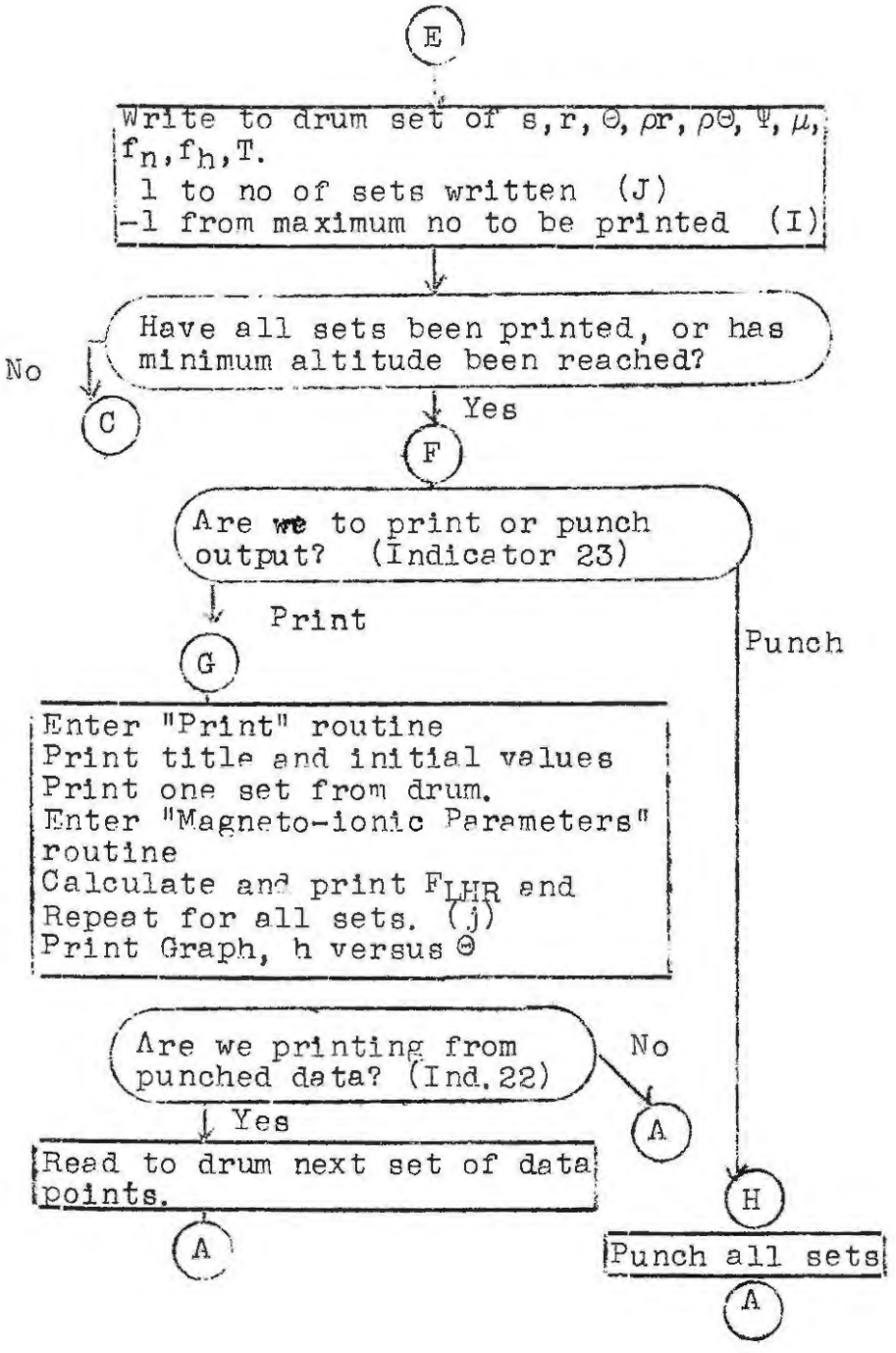

Flow chart of Ray Tracing Program (contd)

"Magneto-ionic parameters" routine

Calculate $Y, Yr, Y\Theta, \frac{\partial Y_j}{\partial r}, \frac{\partial Y_j}{\partial \Theta}, X_j, N_j, \frac{\partial X_j}{\partial r}$, (Chapter 5)
Calculate $\sin\Psi$ and $\cos\Psi$ (Equations 4.2, 4.3)

"Calculation of μ" routine

Calculate R L P S D and A B C (Chapter 2.3)
Solve $A\mu^4 + B\mu^2 + C = 0$
Select correct root and check non-negative μ^2

"Calculate all derivatives" routine

Calculate derivatives of A B C w.r.to Ψ, X_j, Y_j, f (Appendix B)
Calculate derivatives of P S D w.r.to f (Appendix B)
Calculate $\frac{\partial\mu}{\partial\Psi}\ \frac{\partial\mu}{\partial\rho r}\ \frac{\partial\mu}{\partial Y_j}\ \frac{\partial\mu}{\partial f}\ \frac{\partial\mu}{\partial r}\ \frac{\partial\mu}{\partial\Theta}$ (Chapter 4.2)
Calculate $\frac{dr}{ds}\ \frac{d\Theta}{ds}\ \frac{\partial\rho r}{\partial s}\ \frac{d\rho\Theta}{ds}\ \frac{dT}{ds}$ (Chapter 3.6, 3.7)

Appendix D.

The final draft of the program used to perform the ray tracing described in this thesis followed the flow-chart depicted above. As well as being unorthodox in its coding, the program was loaded and operated in a singular manner. A copy of the program with instructions and specifications has been filed in the computer centre at Rhodes University.

Appendix B.

List of symbols used in the text.

a	Reference radius (=6370 Km) for Ionosphere Model
c	Speed of light in vacuo
f	Wave frequency
f_n	Plasma frequency
f_H	Gyro-frequency
h	Height above surface of earth
j	$\sqrt{-1}$
k	Wave number ω/c
n	Complex Refractive Index
q	$= \mu \cos \chi$
r	Radius in spherical polars
s	Integration parameter
t	Time
u,v,w	Generalized co-ordinates
x,y,z,	Cartesian co-ordinates
A,B,C,P,R.L,S,D	Coefficients in Astrom Hines formulation of refractive index.
S	$= \mu \sin \chi$
T	Time of travel of a ray
U	$= 1-jZ$
X	$= f_n^2/f^2$ with subscripts refer to the term for that species of ion.
Y	$= f_H/f$
Z	$= \nu/f$
$\alpha,\beta,\gamma,\delta,\epsilon$	Coefficients of Booker Quartic Equation
η	
λ	Latitude of foot of a field line
μ	Real part of refractive index
ν	Collision frequency
$\bar{\rho}$	Refractive index vector
φ	Polar co-ordinate, measured West of Greenwich
Θ	Polar co-ordinate = latitude; measured from equator
Ψ	Angle between $\bar{B}$ and ρ, measured from B axis

δ	Angle between $\bar{r}$ and $\bar{\rho}$, measured from $\bar{r}$ axis
ω	$= 2\Pi f$
D	Eckersley Dispersion $= +\sqrt{f}$
χ	Angle of incidence on plane stratified medium

In addition, the following symbols are understood to have their usual meanings:

$\bar{E}$, $\bar{B}$, $\bar{D}$, $\bar{H}$, $\bar{P}$, $\bar{J}$, μ_o, ϵ_o